
University of Copenhagen

Faculty of Science


Thesis submitted for the degree of Master in Physics

# Cotunneling spectroscopy of coupled spin systems


*Author:*
Chiara Stevanato

*Supervisor:*
Prof. Jens Paaske


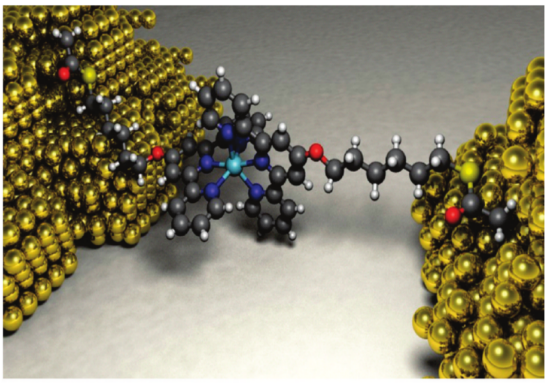

## Abstract

Over the past few years, experiments on three-terminal molecular junctions gave new insights in the understanding of a variety of quantum electron transport effects. In this work, we model a molecular junction as a few-spin system tunnel coupled to two electrodes. We calculate the differential conductance due to cotunneling and study the behavior of the Kondo temperature of the system, which in general depends on the internal exchange couplings between the interacting spins. A proposal for the experimental study of the two-channel Kondo model is sketched. Moreover we demonstrate that a simple two-spin model allows to reproduce a peculiar, not previously explained, feature characterising the differential conductance of a Mn complex in the neighborhood of a singlet to triplet ground-state transition [5]. We come to the conclusion that such a feature, contrary to what stated in [5], must be due to the non-equlibirum rearrangement of the occupation probability of the different two-spin states.

## Abstract italiano

I risultati sperimentali degli ultimi anni nel campo dell'elettronica molecolare hanno fornito importanti dati per la comprensione degli effetti quantistici nel trasporto degli elettroni attraverso una singola molecola o un complesso molecolare. In questo lavoro abbiamo modellizzato una giunzione molecolare attraverso un sistema di pochi spin interagenti ed accoppiati a due elettrodi metallici. Abbiamo calcolato la conduttanza differenziale dovuta agli effetti di cotunneling e abbiamo studiato il comportamento della temperatura di Kondo del sistema, che dipende in generale dagli accoppiamenti interni al sistema di spin interagenti. Abbiamo inoltre suggerito una proposta per la realizzazione sperimentale dell'effetto Kondo a due canali. Abbiamo inoltre dimostrato che un semplice modello a due spin ci permette di riprodurre una certa caratteristica, mai spiegata prima, che appare in [5] nelle misure della conduttanza differenziale attraverso un complesso di Mn nelle vicinanze di una transizione dello stato fondamentale da singoletto a tripletto. Siamo arrivati alla conclusione che questa caratteristica, contrariamente a quanto affermato in [5], sia dovuta agli effetti di non-equilibrio nel riarrangiamento delle probabilitá di riempimento dei diversi stati di spin.

## Indledning

Inden for det sidste årti har eksperimenter med tre-terminal molekylære transistorer givet ny indsigt en række kvante-elektrontransport effekter. I dette arbejde beskrives en molekylær transistor under Coulombblokade som et få-spin-system, cotunnelkoblet til to elektroder med en påtrykt spændingsforskel. Den differentielle ledningsevne beregnes og systemets Kondo temperatur studeres som function af de interne exchangekoblinger i molekylet. Der gives endvidere et forslag til en realisering af den såkaldet to-kanal Kondo effekt. Endelig demonstreres det, at en simpel to-spin-model er nok til at forklare en særlig cotunneleringslinje, som tidligere er observeret i et Mn-komplex i nærheden af en gate-induceret overgang fra singlet, til triplet grundtilstand[5]. I modsætning til den ufuldstændige forklaring givet i [5], konkluderes det her, at den karakteristiske linjeform, som observeres experimentelt, kun kan forklares ved at indrage uligevægtsbesætning af de forskellige spin-tilstande.

# Contents

# 1. Introduction

The demand for device miniaturization is nowadays pushing the size of electronic components toward their natural limit and this challenges our ability to manipulate and exert control over the nanometer scale, where quantum phenomena typically play a fundamental role. Combining the advantages of high chemical versatility and small length scale, single-molecule devices set apart as particularly suitable systems for studies on this topic.
Over the past few years single molecule devices have been regarded as interesting systems, both from a theoretical point of view and for the promising envisioned applications. The fields of molecular electronic and spintronics have developed to meet the need of full control over the electronic and spin degrees of freedom of single-molecule devices and numerous achievements have already been reached, proving transistor effects and information storage properties [8, 9, 10]. Nevertheless there is still a wide variety of not understood properties arising in the study of a single molecule coupled to two metallic electrodes. This is the elementary structure behind all electrical devices and therefore a deep understanding of the physical phenomena taking place in it is required to exert full control over its properties.

From a theoretical point of view single-molecule junctions can be studied by identifying the interesting molecular orbitals with a number of single-level quantum dots. In order for this to be a sensible approximation, a careful study is needed that takes into account the renormalization effects of the molecular levels due to the internal electron-electron interactions and the effect of the coupling to the lead electrodes (tunneling coupling, localization effects of the spin degrees of freedom etc...).
The motivation for the present work comes from the experimental data of the conductance properties of a Mn-complex [5] (Figure 1.1) and a thiol and-capped $\pi$-conjugated molecular junctions [6]. We take our move from the interesting features of their conductance spectrum in order to develop a more general theoretical framework for the study of molecular junctions. The treatment of the internal molecular interactions are out of the scope of this work, while we

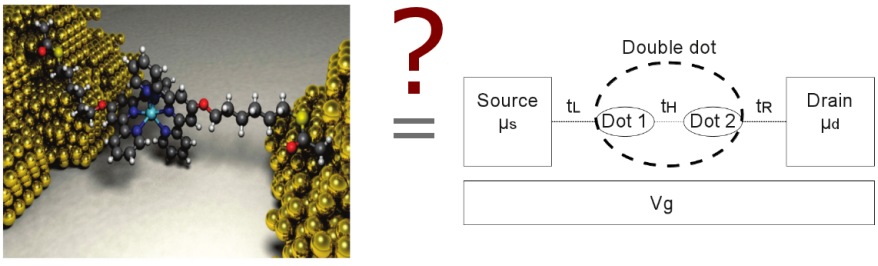


Figure 1.1.: Schematic representation of the Mn-complex junction studied in [5] and sketch of the simplified model we deal with. Part of the scope of this thesis is to check the validity of such a model for describing the differential conductance spectrum of the Mn-junction of [5].

focus, instead, on the electronic transport properties of these devices. We discuss a two-spin and a three-spin system in a three terminal junction, where two metallic leads act as source and drain electrodes and a third terminal acts as a gate voltage, allowing the shifting of the discrete energy levels of the two- or three- spin system in and out of resonance with the Fermi level of the two metallic leads. A number of features of these systems are discussed, primarily giving a description of the differential conductance: inelastic cotunneling, Kondo temperature of the system and a study of the ground-state transitions, due to the tuning of an external magnetic field, are considered.

The thesis is structured in the following way. In Chapter 2 we review the basics of electronic transport in quantum dots in the Coulomb blockaded regions, where electrostatic Coulomb repulsion between electrons prevents current to flow through the junction. Nevertheless quantum mechanics allows higher order tunneling processes between the electrodes and the dot and these give rise to a measured current (cotunneling current) even in the regions where Coulomb repulsion classically prevents electron flow. We then give a theoretical introduction to the Kondo effect. This consists of a zero-bias peak in the differential conductance when the dot has an even number of electrons in it. We will see that the two-fold spin degeneracy of the unpaired electron is at the origin of the resonance peak in the conductance spectrum. In Chapter 3 we define the basic Hamiltonians for a number of simple two- and three-dot systems coupled to two electrodes. We namely study a central region between the leads, which is not any more characterized by just one dot, but by a number of them. We study the differential conductance through the systems in the limit of big Coulomb in-site repulsion inside each dot, so that the ground state solution of our systems has one (and only one) electron in each dot.

Two- and three-charge systems, like the ones here considered, can allow energy degeneracies of the different total-spin states. Such situations can give rise to the Kondo effect, in a way analogous to the spin-degeneracy induced Kondo peak appearing in a even-occupied single quantum dot. The Kondo effect is due to the strong coupling between the dot electrons and the electrodes ones, which bind together in an entangled state. A well specific energy scale, called Kondo temperature, marks the temperature at which this strong coupling effect sets in.

In Chapter 4 we study the behavior of the Kondo temperature for the three-spin system. Because of the internal spin-spin interaction between pairs of electrons within the central region, the Kondo temperature depends on the strength of these internal couplings.
In the last part of the thesis (Chapter 5) we turn to the low-energy features of the double dot and we compare our results with the differential conductance spectrum of the Mn-complex of [6] inside a Coulomb diamond presenting two-charge features. A singlet-to-triplet transition is observed in the ground state of system and where this transitions occurs a very peculiar line, to our knowledge not previously observed, appears in the differential conductance maps against bias and gate voltage. We show that our double dot model accounts for this line and its characteristic shape. We conclude by giving a detailed description of this line and hypothesize that its appearance is related to the non-equilibrium rearrangement of the occupation probability of the different two-spin states.

# 2. Physics of electron transport in quantum dots

Quantum dot systems are nanometric electronic structures characterized by a strong confinement potential in all three spatial directions. Confinement in real space makes these structures effectively zero-dimensional giving a discrete energy spectrum, in many ways similar to that of real atoms. For this reason, quantum dots are often regarded as "artificial atoms".
From a theoretical point of view, quantum dots stand out as the simplest systems allowing the study of low-energy electronic transport in break junctions and STM devices. The basic model includes a central region (which can be either described as a single quantum dot or a number of them) tunnel-coupled to two metallic junctions.
In this Chapter we first (2.1) review the basic physics of electronic transport in quantum dots. Then we will discuss the Kondo effect (2.2) and extend the basic theory to more complicated situations (2.3), involving more then one quantum dot.

## 2.1. Basics of electronic transport in quantum dots

The typical setup allowing the study of electronic transport through a quantum dot is represented in Figure 2.1. The right and left leads serve as a double barrier junction, while the gate voltage allows the discrete energy levels of the dot to be shifted on and off resonance with the Fermi energy of the leads.
Classically, current can flow from one lead to the other if the addition energy, i.e. the energy required to add an electron to the dot, is overcome by the thermal energy of the conduction electrons. However at low enough temperatures current flow is not allowed and the system is said to be Coulomb blockaded. This regime can be described by a so-called "constant interaction model", which relies on two assumptions. The first is that interactions among electrons can be characterized by a constant capacitance $C = C_g + C_s + C_d$, where $C_g$ is the capacitive coupling to the gate and $C_s$, $C_d$ is the capacitive coupling to source and drain electrode, respectively. The second is that the dot's energy spectrum is independent of electron-electron interactions. The ground state energy $U(N)$ of the system with $N$ electrons in the dot can then be approximated by:

$$U(N) = \frac{[e(N - N_0) - C_g V_g]^2}{2C} \tag{2.1}$$

where $C_g V_g$ is the charge induced in the dot by the shifting of the gate voltage $V_g$ and $N_0$ is the number of electrons in the dot at zero gate voltage. $C$ is the total capacitance between dot and electrodes and gate: $C = C_s + C_d + C_g$. The chemical potential of the dot with $N$ elecftrodes $\mu_{dot}(N)$ is defined by the difference between the energy of the dot with $N$ electrons and $N - 1$ electrons:

$$\mu_{dot}(N) = U(N) - U(N-1) = E_c \left( N - N_0 - \frac{1}{2} - \frac{C_g V_g}{e} \right) \tag{2.2}$$

where $E_c = \frac{e^2}{C}$ is the charging energy. Notice that for $\frac{C_g V_g}{e} = N - N_0 + \frac{1}{2}$ the charge states $N$ and $N + 1$ become degenerate. This means that no energy is required to add an electron to

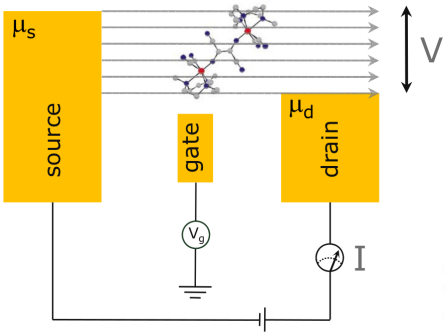


Figure 2.1.: Schematic representation of the typical nanostructure allowing electronic transport measurements through a quantum dot or a molecular system. The molecular/dot system is placed between two lead electrodes, which we define source and drain. Each electrode is characterized by a chemical potenitial $\mu$ and the difference between source and drain chemical potenitial gives the bias voltage $eV = \mu_s - \mu_d$ ($e$ is the electron charge). A third electrode, called gate, is characterized by a voltage $V_g$ and it allows to shift the energy levels of the molecule/dot. [17].

the dot and therefore the probabilities of finding $N$ or $N+1$ electrons in the dot is equal. This regime is called "mixed valence regime".
The transition amplitude $\Gamma^{\alpha}_{N+1,N}$ for an electron to jump from a lead $\alpha$ ($\alpha$ can be either the source or the drain electrode) to the dot is given by:

$$\Gamma^{\alpha}_{N+1,N} = \Gamma_{\alpha}(U(N+1) - U(N) - \mu_{dot}(N) + \mu_{\alpha}) n_B \left[U(N+1) - U(N) - \mu_{dot}(N) + \mu_{\alpha}\right] \quad (2.3)$$

which depends on the alignment of the chemical potential of the dot $\mu_{dot}(N)$ with the chemical potential $\mu_{\alpha}$ of the lead $\alpha$. Notice that we have introduced the combined tunneling density of states $\Gamma_{\alpha} = 2\pi|t_{\alpha}|^2 \nu_{dot} \nu_{\alpha}$, where $t_{\alpha}$ is the tunneling amplitude from the electrode $\alpha$ to the dot, $\nu_{\alpha}$ is the density of states in the electrode, and $\nu_{dot}$ is the density of states in the dot.
If the gate voltage $V_g$ is tuned in such a way that the two energy states $U(N+1)$ and $U(N)$ become degenerate, $\Gamma^{\alpha}_{N+1,N} \approx (\mu_{dot}(N) - \mu_{\alpha})\Theta(\mu_{dot}(N) - \mu_{\alpha})$ and one electron can jump on the dot for $\mu_{\alpha} = \mu_{dot}(N)$ (Figure 2.2 (a) and (b)).
Away from the mixed valence regions the energy gap between the different charge states prevent charge changing in the dot. Shifting the gate voltage one can gradually scan regions with a fixed number of electrons in the dot (Figure 2.2 (c)). At each energy degeneracy (mixed valence region) a single electron is added to the dot. By shifting the gate voltage one can then gradually charge the dot in a sequence of single-electron additions. This regime is called "sequential tunneling", being characterized by a sequence of tunneling processes, each separating two equilibrium conditions of the system.
The application of a bias voltage $V$ between the leads opens an energy window $eV = \mu_s - \mu_d$. If this is large enough current can flow for values of the gate voltage where it was previously not allowed. When $V$ is larger then the addition energy $E_c$ required to add one electron to the dot, $|eV| > \mu_{dot}(N+1) - \mu_{dot}(N) = E_c$, high conductance regions arise. Plotting the differential conductance dependence on $V_g$ and $V$, diamond-like zones of high conductance are outlined (Figure 2.2 (d), (e) and (f)).
If the bias voltage is turned on, also excited states may be involved in electronic transport between the leads. In fact, when the bias voltage is high enough to allow the occupation of an excited state, transitions between the excited state, with e.g. $N$ charges, and the ground state

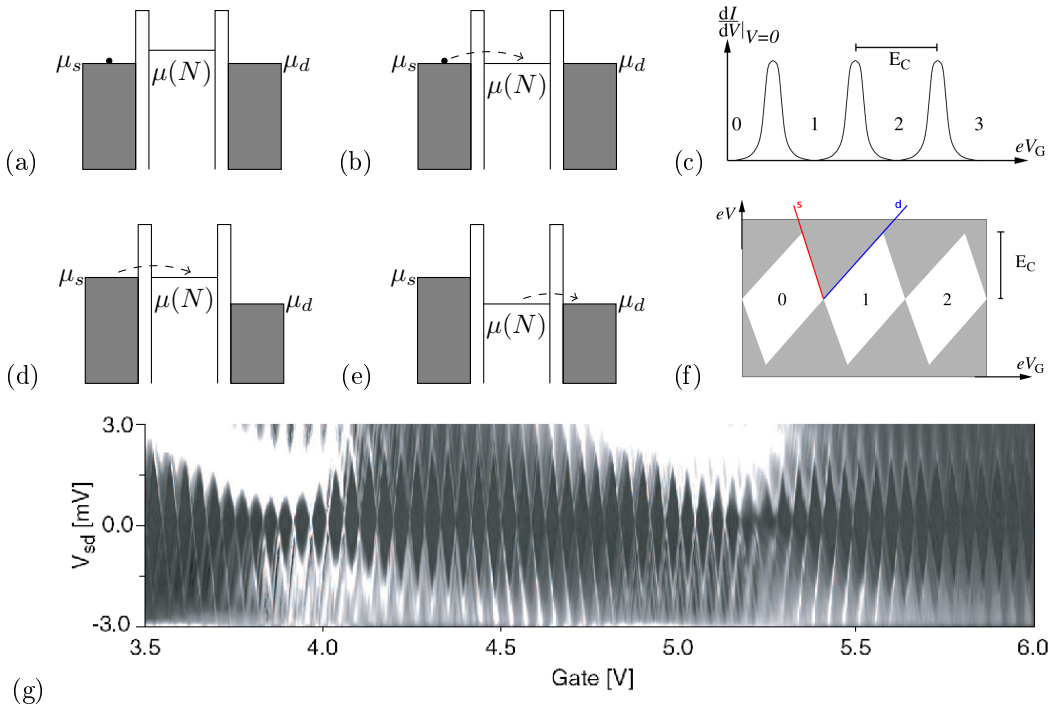


Figure 2.2.: Sequential tunneling regime. (a) No transport is allowed if the chemical potential of the dot is not aligned with the chemical potential of the leads. (b) When the gate voltage shifts the chemical potential of the dot to the level of one of the leads, one electron can jump from the lead to the dot, changing the charge of the dot by one unit. (c) The gradual change of the gate voltage periodically brings the dot's available energy level in resonance with the leads, allowing the measurement of an increased current and therefore periodical peaks in the differential conductance. (d and f) If a bias voltage is applied to the leads, an energy window $eV = \mu_s - \mu_d$ opens up. (f) This allows a finite value of the differential conductance (gray in (f)) for all the values of $Vg$ for which a dot energy level falls within the window. Allowing both the bias $V$ and the gate $Vg$ to change, we obtain the sketch in (f), which outlines diamond-like regions of zero conductance (Coulomb blockade), characterized by a specific charge state (written inside the diamonds in (f)). The edges of the diamond (two of them in colour in (f)) are obtained by setting $\mu_{dot} = \mu_s/\mu_{dot} = \mu_d$ and solving fot $V$ and $V_g$ through (2.2). (g) A typical measurement of a Coulomb blockaded spectrum (measurements on a InAs-wire based Quantum Dot, T.Sand Jespersen, NBI).

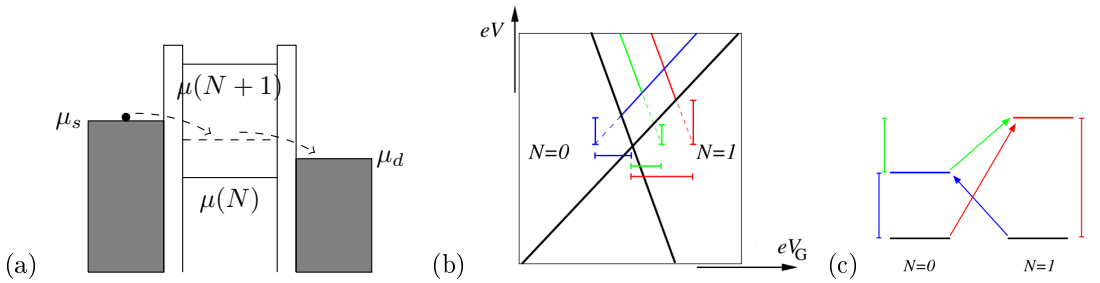


Figure 2.3.: Sequential tunneling through an excited state. (a) Schematic representation of the process and (c) of the energy levels involved. (b) Differential conductance against bias $V$ and gate voltage $V_g$, where black lines represent the edges of the two Coulomb diamonds corresponding to charge states 0 and 1, and colored lines (only shown at positive bias for simplicity) correspond to the sequential tunneling events involving the corresponding high energy states in (c). (b) and (c) have been reproduced from [14].

with $N+1$ charges may occur. This possibility shows up in the high-conductance lines running parallel to the Coulomb diamonds (Figure 2.3).

Let us now consider a well defined charge state, i.e. a specific Coulomb diamond. Inside this region no charge fluctuation is classically possible and the dot contains a well specific number of electrons. In this regime quantum mechanics allows energetically forbidden transitions to different charge states within the time scale of two consecutive tunneling events. Electrons from one lead can jump into energetically forbidden states and then jump out into the other lead leaving the dot either in the initial state ("elastic cotunneling")or in a different final state ("inelastic cotunneling"). In this second case, the electron jumping off the dot belongs to an energy level different from the one occupied by the incoming electron. The central region is then left in an excited state. For a schematic representation of cotunneling, see Figure 2.4.
The physics of cotunneling can be described by an Anderson Hamiltonian $H_A$:

$$H_A = H_d + H_{leads} + H_t \tag{2.4}$$

which includes the Hamiltonian of a single-level quantum dot $H_d$, the leads $H_{leads}$ and the tunneling coupling between the dot and the leads $H_t$.
The non-interacting dot is described by $H_d$:

$$H_d = \sum_\sigma \varepsilon_d d_\sigma^\dagger d_\sigma + U n_{d\uparrow} n_{d\downarrow} \tag{2.5}$$

where $\varepsilon_d$ is the single electron energy, $d_\sigma^\dagger$ and $d_\sigma$ are the creation and annihilation operators, respectively, of the dot, i.e. $d_\sigma^\dagger$ creates an electron with spin $\sigma$ on the dot, $d_\sigma$ annihilates an electron with spin $\sigma$ from the dot. $n_{d\sigma}$ is the number operator, which counts the number of electrons with spin $\sigma$ in the dot and $U$ is an on-site Coulomb repulsion, which penalizes double occupation in the dot.
The Hamiltonian of the lead electrodes $H_{leads}$ is:

$$H_{leads} = \sum_{\alpha=\{R,L\},k,\sigma} \varepsilon_k c_{\alpha k\sigma}^\dagger c_{\alpha k\sigma}, \tag{2.6}$$

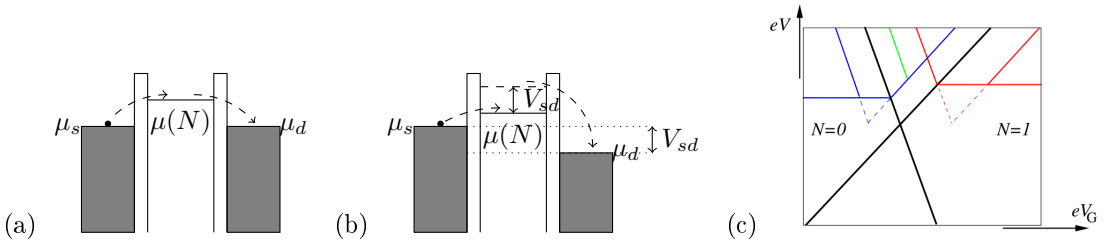


Figure 2.4.: (a)Elastic cotunneling. (b) Inelastic cotunneling. Inelastic cotunneling can only occur when the bias voltage exceeds the excitation energy (i.e. the energy difference between the final excited state and the initial one). Elastic cotunneling gives a finite background conductance inside the classically blocked regions, while inelastic cotunneling gives a step-like increase of the differential conductance for bias voltages corresponding to the excitation energy (the step is shown in (c) as a schematic line running parallel to the gate voltage). If the life-time of the excited state left by an inelastic cotunneling process is long enough, a single-electron tunneling process can take its move from there. Such a combined process is called cotunneling-assisted single-electron-tunneling (COSET) and can occur only for bias allowing the population of the starting excited state. The COSET high-conductance lines are represented in (c) as lines running parallel to the diamond edges and starting above the cotunneling steps. (c) has been reproduced from [14].

where $\alpha = \{R, L\}$ keeps track of the leads (labeled as right, R, or left, L) and $c^\dagger_{\alpha k\sigma}$ and $c_{\alpha k\sigma}$ are the creation and annihilation of the electrodes electrons. Notice that each electron is characterized by a label $\alpha$, keeping track of which electrode it belongs to, and $k$ and $\sigma$ are the electron momentum and spin projection, respectively. The electrodes are described as Fermi seas with Fermi energy equal to their chemical potential.
The tunneling part of the Hamiltonian $H_t$ allows an electron to jump from one lead to the dot or vice versa with probability $\sim |t|^2$:

$$H_t = \sum_{\alpha,k,\sigma} \left( t_{\alpha,k} d^\dagger_\sigma c_{\alpha,k\sigma} + t^*_{\alpha,k} c^\dagger_{\alpha,k\sigma} d_\sigma \right). \tag{2.7}$$

Applying perturbation theory to the Anderson Hamiltonian one can obtain a description of all the weak-coupling features of the differential conductance inside a specific Coulomb diamond.

Using second order perturbation theory one can calculate the amplitude $\Gamma_{RL}$ of the cotunneling processes involving transport from the left to the right lead.

$$\Gamma_{RL} \approx \frac{\Gamma^L \Gamma^R}{2\pi} \frac{1}{\varepsilon_d^2} \sum_{\sigma\sigma'} (\Delta_{\sigma'\sigma} - eV) n_B(\Delta_{\sigma'\sigma} - eV) n_\sigma \approx \frac{\Gamma^L \Gamma^R}{2\pi} \frac{1}{\varepsilon_d^2} \sum_{\sigma\sigma'} (eV - \Delta_{\sigma'\sigma}) \Theta(eV - \Delta_{\sigma'\sigma}) n_\sigma \tag{2.8}$$

where $\Gamma^\alpha = 2\pi |t_\alpha|^2 \nu_\alpha$, $n_\sigma$ is the probability for the dot level considered to be in spin state $\sigma$, $n_B(E) = \frac{1}{e^{\frac{E}{k_B T}} - 1}$ is thew Bose function ($k_B \approx 8.6 \times 10^5$ eV/K being the Boltzmann constant and $T$ being the temperature) and $\Delta_{\sigma'\sigma}$ is the energy difference between the two spin states $\sigma'$ and $\sigma$. If no external magnetic field is applied to the system, the energy levels of the dot will in general not depend on the spin degree of freedom and the occupation probabilities of the two spin states $|\uparrow\rangle$ and $|\downarrow\rangle$ will be equal. In this case $\Delta_{\sigma'\sigma} = 0$ and the last equation gives the elastic cotunneling contribution to the current, which is linear in $V$ and is present for any bias

voltage, therefore leading to a non-zero (classically absent) back-ground conductance inside the Coulomb diamonds. On the contrary, inelastic cotunneling can occur when different spin states have different energies, e.g. when an external magnetic field is applied to the system. In this case a non-zero tunneling probability through the dot appears when the bias voltage is high enough to let an excited state to be filled. For all the bias voltages higher then a certain threshold, required to fill the excited state, the current is increased, giving a step in the differential conductance vs. bias. These inelastic cotunneling events are represented by two high conductance lines running at finite (positive and negative) bias inside the Coulomb diamond (Figure 2.4 (c)).

When even stronger coupling between the dot and the leads is allowed, the perturbative treatment used above breaks down. In strongly correlated systems the hypothesis of perturbation theory are not valid any more and non-perturbative treatments have to be found. Physically speaking the failure of perturbative methods is due to the presence of other effects, and therefore other energy scales, taking over when the many body system is highly correlated. A typical example of strong-coupling regime is the Kondo effect. Let us consider a quantum dot with average occupation equal to an odd integer, we are then inside a Coulomb diamond characterized by an odd number of electrons, e.g. one. Because of the spin degeneracy, there are two states with the same energy (in absence of an external magnetic field) and this opens more possibilities for electrons to cotribute by virtual processes to the cotunneling current. The degeneracy thus gives rise to a peak in the zero-bias differential conductance. A physical picture for this phenomenon exploits a screening effect of the conduction electrons over the dot spin. In fact if we consider a single 1/2-spin in the dot, virtual processes allow the spin to jump off the dot while an electron from the leads replaces it inside the dot. The new electron can have either spin up or spin down. Taking all such processes together then produces a resonance. The ground state of the total system (dot plus conduction electrons) becomes a many-body entangled state, with effective total spin zero (effective singlet). This effect leads to a rise in the scattering processes between lead and dot electrons, thus allowing an enhancement of the differential conductance.
The Kondo effect is controlled by a well defined energy scale, called Kondo temperature. For temperatures below the Kondo temperature, the strong-coupling regime is entered and the zero-bias peak appears. For temperatures above the Kondo temperature the dot and electrodes spins remain independent and no Kondo peak is present in the zero-bias differential conductance spectrum.
The study of Kondo physics requires the condition of odd charge occupation in the dot, i.e. a single electron in the highest occupied level. We thus need a Hamiltonian intrinsically satisfying this condition. This can't be the Anderson Hamiltonian (2.4) defined above, which allows in principle double occupation of each dot level, but we can nevertheless start from there and assume that the energy cost for setting two electrons in the dot is extremely high. This is what we are going to do in the next section. The procedure outlined below will eventually lead to a Hamiltonian describing exactly singly-occupied dots.

## 2.2. From the Anderson model to the Kondo model

In introducing the Kondo effect, we said that it can occur when the average dot occupation is odd. Let us then start by treating the case of average occupation equal to 1. We are then considering a single level system, which can in principle contain zero, one or two (spin-antiparallel) electrons. For the assumption of average occupation equal to 1 to be valid, we must find a way of excluding the double-occupied and zero-occupied states by making them "unlikely", namely energetically inconvenient. This assumption is formalized by the following statement on the energy scales of

the Anderson model system (2.4):

$$\varepsilon_d \ll U$$

where $\varepsilon_d$ is the single-electron energy and $U$ is the energy cost for having two electrons inside the dot.

The goal of the following calculation is to write a Hamiltonian describing a single-occupied dot, i.e. the inside of the Coulomb diamond with one charge inside the dot. Thanks to the coupling to the electrodes (2.6), the single-occupied dot can still experience tunneling (energetically forbidden) processes to different charge states, i.e. to the high energy states with zero or two electrons in the dot, but such transitions only occur as cotunneling processes and any charge state different from one is not allowed as ground state of the system.

Let us for a moment forget about the presence of two different leads and assume the dot is coupled to a single lead. The procedure outlined in the following part, can then be easily generalized to the two-lead case. In order to restrict to the 1-occupation region, we need to project out the zero and double-occupied states by effectively going to a single-electron Hilbert space. This is done by writing the Schrödinger equation for the system in the following way:

$$\begin{pmatrix} H_{00} & H_{01} & 0 \\ H_{10} & H_{11} & H_{12} \\ 0 & H_{21} & H_{22} \end{pmatrix} \begin{pmatrix} \psi_0 \\ \psi_1 \\ \psi_2 \end{pmatrix} = E \begin{pmatrix} \psi_0 \\ \psi_1 \\ \psi_2 \end{pmatrix} \tag{2.9}$$

where the terms in the diagonal $H_{nn}$ describe the energy of the system with $n$ electrons in the dot and the off-diagonal terms $H_{n'n}$ represent the tunneling Hamiltonians allowing to change the number of electrons in the dot from $n$ to $n'$. $\psi_n$ is the state of the system with $n$ electrons in the dot.

The off-diagonal terms of (2.9) can be rewritten as tunneling events occuring when the system is its ground state (i.e. single occupation in the dot):

$$\begin{aligned} H_{10} &= \sum_{k,\sigma} t_k d_\sigma^\dagger (1 - n_{d-\sigma}) c_{k\sigma} \\ H_{01} &= H_{10}^\dagger = \sum_{k,\sigma} t_k^* c_{k\sigma}^\dagger (1 - n_{d-\sigma}) d_\sigma \\ H_{21} &= \sum_{k,\sigma} t_k d_\sigma^\dagger n_{d-\sigma} c_{k\sigma} \\ H_{12} &= H_{21}^\dagger = \sum_{k,\sigma} t_k^* c_{k\sigma}^\dagger n_{d-\sigma} d_\sigma. \end{aligned} \tag{2.10}$$

Formally these expressions are obtained by projecting the total Hamiltonian of the system appearing in (2.9) in different subspaces: $H_{nn'} = P_n H P_{n'}$ where $P_n$ is the projector operator on to the subspace with $n$ electrons in the dot, i.e.

$$\begin{aligned} P_0 &= (1 - n_{d,\uparrow})(1 - n_{d,\downarrow}) \\ P_1 &= n_{d,\uparrow} + n_{d,\downarrow} - 2 n_{d,\uparrow} n_{d,\downarrow} \\ P_2 &= n_{d,\uparrow} n_{d,\downarrow}. \end{aligned} \tag{2.11}$$

Physically speaking, the projections (2.10) describe tunneling process occuring when the dot has only one electron on it (the number operators $n_{d\sigma}$ actually make sure that each tunneling process is only allowed when the dot is singly occupied with an electron with the proper spin.) When we eliminate the double and zero occupied states in the dot, we obtain from (2.9):

$$[H_{11} + H_{12}(E - H_{22})^{-1} H_{21} + H_{10}(E - H_{00})^{-1} H_{01}]\psi_1 = E\psi_1. \tag{2.12}$$

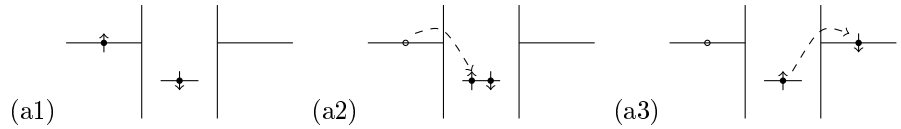


Figure 2.5.: Figure representing one of the second order processes in $H_{12}(E-H_{22})^{-1}H_{21}$ where the dot goes through a cotunneling process involving one more chrage state, i.e. an electron jumps into the dot, making it double occupied, and then out of the dot again, restoring the single-occupation ground state of the dot. This process gives a contribution equal to $\sum_{k,k'} \frac{-t_k^* t_{k'}}{U+\varepsilon_d-\varepsilon_{k'}} S^+ c^\dagger_{Rk\downarrow} c_{Lk'\uparrow}$, i.e. the final electron inside the dot has spin up, while the initial electron had spin down, a spin flip process has namely occured which has increased the z-spin component (from which the factor $S^+$ describing the increase of the dot spin). At the same time the conduction electron (the electron going from one lead to the other) has decreased its spin in the process ($c^\dagger_{Rk\downarrow} c_{Lk'\uparrow}$, i.e. an electron with spin down has been annhilited in the left electrode and an electron with spin up has been created in the right one). The denominator of $\frac{-t_k^* t_{k'}}{U+\varepsilon_d-\varepsilon_{k'}}$ gives the total energy cost of this virtual process ($U+\varepsilon_d$ is the energy required to add an electron to the dot, while $-\varepsilon_{k'}$ is the energy cost of having annihilated an electron in the left lead), while the numerator gives the probability of this process in terms of tunneling amplitudes to the left and the right lead. More detailed on the study of these terms can be found in Appendix .

A One can calculate the terms in round brackets and obtain:

$$H_{10}(E-H_{00})^{-1}H_{01} = \sum_{k,k',\sigma,\sigma'} \frac{-t_k^* t_{k'}}{\varepsilon_k-\varepsilon_d}\left(1-\frac{E-H_k}{\varepsilon_k-\varepsilon_d}\right)^{-1} c_{k'\sigma'} c^\dagger_{k\sigma} d^\dagger_{\sigma'} d_\sigma (1-n_{d-\sigma'})(1-n_{d-\sigma}) \tag{2.13}$$

$$H_{12}(E-H_{22})^{-1}H_{21} = \sum_{k,k',\sigma,\sigma'} \frac{-t_k^* t_{k'}}{U+\varepsilon_d-\varepsilon_{k'}}\left(1-\frac{E-\varepsilon_d-H_k}{U+\varepsilon_d-\varepsilon_{k'}}\right)^{-1} c^\dagger_{k\sigma} c_{k'\sigma'} d_\sigma d^\dagger_{\sigma'} n_{d-\sigma} n_{d-\sigma'} \tag{2.14}$$

where $H_k$ is the Hamiltonian of the conduction electrons. To lowest order one can forget about the second term in brackets.

Before going further on, let us just notice that each term of (2.13) and (2.14) can be represented like in Figure 2.5. Moreover, one should remember that in the $n_d = 1$ subspace the following relations are valid:

$$\begin{aligned} &n_{d\uparrow} + n_{d\downarrow} = 1 \\ &n_{d\uparrow} n_{d\downarrow} = 0 \\ &d^\dagger_\uparrow d_\downarrow (1-n_{d\uparrow}-n_{d\downarrow}) = S^+ \\ &d^\dagger_\downarrow d_\uparrow (1-n_{d\uparrow}-n_{d\downarrow}) = S^- \\ &\frac{1}{2}(n_{d\uparrow}-n_{d\downarrow}) = S^z. \end{aligned} \tag{2.15}$$

One can then calculate the different terms in (2.13):

$$\begin{cases} \text{if } \sigma' = \uparrow, \sigma = \downarrow & c_{k'\uparrow} c^\dagger_{k\downarrow} d^\dagger_\uparrow d_\downarrow (1-n_{d\uparrow})(1-n_{d\downarrow}) = -S^+ c^\dagger_{k\downarrow} c_{k'\uparrow} \\ \text{if } \sigma' = \downarrow, \sigma = \uparrow & c_{k'\downarrow} c^\dagger_{k\uparrow} d^\dagger_\downarrow d_\uparrow (1-n_{d\downarrow})(1-n_{d\uparrow}) = -S^- c^\dagger_{k\uparrow} c_{k'\downarrow} \\ \text{if } \sigma' = \sigma & \begin{cases} c_{k'\uparrow} c^\dagger_{k\uparrow} d^\dagger_\uparrow d_\uparrow (1-n_{d\downarrow})(1-n_{d\downarrow}) + c_{k'\downarrow} c^\dagger_{k\downarrow} d^\dagger_\downarrow d_\downarrow (1-n_{d\uparrow})(1-n_{d\uparrow}) \\ = -\frac{\mathbb{I}}{2} \tau^0_{\sigma\sigma'} c^\dagger_{k\sigma} c_{k'\sigma'} - S^z \tau^0_{\sigma\sigma'} c^\dagger_{k\sigma} c_{k'\sigma'} \end{cases} \end{cases}$$

so that, all together

$$H_{10}(E - H_{00})^{-1} H_{01} = \sum_{k,k',\sigma,\sigma'} \frac{t^*_k t_{k'}}{\varepsilon_k - \varepsilon_d} \left( \frac{\mathbb{I}}{2} \tau^0_{\sigma\sigma'} c^\dagger_{k\sigma} c_{k'\sigma'} + \vec{S} \cdot \vec{\tau}_{\sigma\sigma'} c^\dagger_{k\sigma} c_{k'\sigma'} \right) \tag{2.16}$$

and analogously the terms in (2.14) give:

$$H_{12}(E - H_{22})^{-1} H_{21} = \sum_{k,k',\sigma,\sigma'} \frac{t^*_k t_{k'}}{U + \varepsilon_d - \varepsilon_{k'}} \left( -\frac{\mathbb{I}}{2} \tau^0_{\sigma\sigma'} c^\dagger_{k\sigma} c_{k'\sigma'} + \vec{S} \cdot \vec{\tau}_{\sigma\sigma'} c^\dagger_{k\sigma} c_{k'\sigma'} \right). \tag{2.17}$$

The new interaction Hamiltonian will then look

$$H' = \sum_{k,k',\sigma,\sigma'} \left( J_{kk'} \vec{S} \cdot \vec{\tau_{\sigma\sigma'}} c^\dagger_{k\sigma} c_{k'\sigma'} + W_{kk'} \frac{\mathbb{I}}{2} \tau^0_{\sigma\sigma'} c^\dagger_{k\sigma} c_{k'\sigma'} \right) \tag{2.18}$$

where

$$\begin{aligned} J_{kk'} &= t^*_k t_{k'} \left( \frac{1}{U + \varepsilon_d - \varepsilon_{k'}} + \frac{1}{\varepsilon_k - \varepsilon_d} \right) \\ W_{kk'} &= t^*_k t_{k'} \left( \frac{1}{\varepsilon_k - \varepsilon_d} - \frac{1}{U + \varepsilon_d - \varepsilon_{k'}} \right). \end{aligned} \tag{2.19}$$

When taking into account two leads, one will have to take track of the lead which is considered step after step. In order to deal with this one can introduce an index $\alpha = R, L$ and in general the coupling constants will depend on this index: $J_{\alpha k,\alpha' k'}$, $W_{\alpha k,\alpha' k'}$.
Equation (2.18) is the well known Schrieffer-Wolff Hamiltonian [13]. By performing a unitary transformation on the Anderson Hamiltonian and projecting into the single-occupied state of the dot, we have effectively got a new Hamiltonian, which is able to describe both the weak-coupling cotunneling conductance and the strong-coupling limit leading to the Kondo effect.
Using first order perturbation theory on (2.18), one recover the same expressions (2.8) for the transition probability between the leads and therefore the same result for the conductance. The Kondo Hamiltonian then lets us deal more easily with the calculations describing the single-occupied dot, because it effectively lowers the order of the problem. If the Anderson Hamiltonian includes in principle all the charge states, the Schrieffer-Wolff Hamiltonian is only valid inside the one-electron Coulomb diamond.
Equation (2.18) also let us understand what exactly goes wrong when trying to push perturbation theory beyond its range of validity. In other words, we can now specify the energy scale at which the system becomes strongly correlated, and therefore the break down of perturbation theory. As a matter of fact, when third order perturbation theory in the tunneling is performed on the Schrieffer-Wolff Hamiltonian, one obtains:

$$I \propto \Gamma_{RL} - \Gamma_{LR} = \int d\xi' \left[ n_F(\xi' - \mu_L) - n_F(\xi' - \mu_R) \right] T(\xi') \tag{2.20}$$

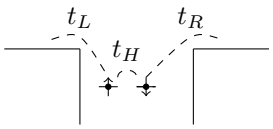


Figure 2.6.: Lateral double-dot. The only tunneling couplings considered are the ones in Figure. Therefore the lowest order processes transporting an electron from one lead to the other are second order processes, involving a transition through both the dots.

where we defined the transmission coefficient:

$$T(\xi') = \left[ \frac{3\pi}{2} (\nu_F J_{RL})^2 \left( 1 - 2 \sum_{\beta=R,L} \nu_F J_{\beta\beta} \int_{-D}^{D} d\xi n_F(\xi - \mu_\beta) \frac{1}{\xi - \xi'} \right) + 2\pi 4 (\nu_F W_{RL})^2 \right]. \tag{2.21}$$

We then see that the conductance has a logarithmically divergent peak at low temperatures:

$$\int_{-D}^{D} d\xi n_F(\xi - \mu_\beta) \frac{1}{\xi - \xi'} \approx \int_{-D}^{D} d\xi n_F(\xi) \frac{1}{\xi} \approx \int_{-D}^{-T} d\xi \frac{1}{\xi} = \ln\left(\frac{T}{D}\right) \tag{2.22}$$

where $D$ and $-D$ represent the edges of the band width of the leads and $\nu_F$ is the density of states in the leads (here assumed to be the same in both the leads). This marks the break down of perturbation theory and the transition to a strong correlated regime. A simple estimate of the energy scale at which this transition occurs is given by the energy scale at which the logarithmic temperature-dependent term in (2.21) becomes relevant, i.e. of the same order of the other term in parenthesis. This occurs for a typical temperature, called "Kondo temperature", which is then seen to be exponentially dependent on the coupling constants:

$$T_K \approx D e^{-\frac{1}{\sum_\beta 2 J_{\beta\beta} \nu_F}}. \tag{2.23}$$

At $T < T_K$ non-perturbative methods are needed in order to deal with the strong coupling regime. For calculating equilibrium properties of a Kondo system in this regime, the numerical renormalization group methods by Wilson can be used. One of the most striking result of this method is that the conductance at the Kondo resonance for symmetric coupling to the leads ($t_L = t_R$), is given by $G = 2\frac{e^2}{h}$.

## 2.3. From the extended Anderson model to the second order Kondo model

When the middle region between two leads is not a single dot, but rather a multi-dot system, transitions between different dots are allowed. In this case virtual transitions to states with one more or one less electron in the central region can be mediated by an internal transition between two dots.
We want to develop a theoretical formal description of such systems. We want to see the relation between a generalized Anderson-like model and a Kondo-like model, in cases where such new channels internal to the middle region are open and therefore higher order processes can take place.

Let us write the Anderson-like Hamiltonian for a system like the one in Figure 2.6:

$$H_A = \sum_{i=\{R,L\},\sigma} \varepsilon_{di} d^\dagger_{i\sigma} d_{i\sigma} + \sum_{\alpha=\{R,L\},k,\sigma} \varepsilon_{\alpha,k} c^\dagger_{\alpha k\sigma} c_{\alpha k\sigma} + \sum_{k,\sigma} \left( t_{Lk} d^\dagger_{L\sigma} c_{Lk\sigma} + t^*_{Lk} c^\dagger_{Lk\sigma} d_{L\sigma} \right) + \sum_{k,\sigma} \left( t_{Rk} d^\dagger_{R\sigma} c_{Rk\sigma} + t^*_{Rk} c^\dagger_{Rk\sigma} d_{R\sigma} \right) + \sum_{\sigma} \left( t_H d^\dagger_{L\sigma} d_{R\sigma} + t^*_H d^\dagger_{R\sigma} d_{L\sigma} \right) + U \sum_{i=\{R,L\}} n_{d_i\uparrow} n_{d_i\downarrow} \tag{2.24}$$

where $d_L$ and $d_R$ label the two (right and left) dots. In the same spirit as before we can then write the following Schrödinger equation:

$$\begin{pmatrix} H_{11}^{10,10} & H_{11}^{10,01} & H_{12}^{10,11} & H_{12}^{10,20} & 0 & 0 & 0 \\ H_{11}^{01,10} & H_{11}^{01,01} & H_{12}^{01,11} & 0 & H_{12}^{01,02} & 0 & 0 \\ H_{21}^{11,10} & H_{21}^{11,01} & H_{22}^{11,11} & H_{22}^{11,20} & H_{22}^{11,02} & H_{23}^{11,21} & H_{23}^{11,12} \\ H_{21}^{20,10} & 0 & H_{22}^{20,11} & H_{22}^{20,20} & 0 & H_{23}^{20,21} & 0 \\ 0 & H_{21}^{02,01} & H_{22}^{02,11} & 0 & H_{22}^{02,02} & 0 & H_{23}^{02,12} \\ 0 & 0 & H_{32}^{21,11} & H_{32}^{21,20} & 0 & H_{33}^{21,21} & H_{33}^{21,12} \\ 0 & 0 & H_{32}^{12,11} & 0 & H_{32}^{12,02} & H_{33}^{12,21} & H_{33}^{12,12} \end{pmatrix} \begin{pmatrix} \psi_1^{10} \\ \psi_1^{01} \\ \psi_2^{11} \\ \psi_2^{20} \\ \psi_2^{02} \\ \psi_3^{21} \\ \psi_3^{12} \end{pmatrix} = E \begin{pmatrix} \psi_1^{10} \\ \psi_1^{01} \\ \psi_2^{11} \\ \psi_2^{20} \\ \psi_2^{02} \\ \psi_3^{21} \\ \psi_3^{12} \end{pmatrix} \tag{2.25}$$

where the subscript gives the total number of electrons in the central region and the superscript gives the exact configuration in the two dots, so that a process that maintain two electrons in the central region and brings one of them from the left dot to the right one is represented by $H_{22}^{02,11}$. Through this notation we keep track of what dot is involved in each process.
Going through the calculation in a way similar to what has been done for a single quantum dot and keeping the lowest-order processes, one obtains terms of the following kinds:

$$\begin{cases} H_{21}^{11,10} \frac{1}{E-H_{11}^{10,10}} H_{12}^{10,11} & \longrightarrow \quad J_R \vec{S}_R \cdot \vec{s}_R + \frac{W_R}{2} \tau^0 c^\dagger_R c_R \\ H_{21}^{11,01} \frac{1}{E-H_{11}^{01,01}} H_{12}^{01,11} & \longrightarrow \quad J_L \vec{S}_L \cdot \vec{s}_L + \frac{W_L}{2} \tau^0 c^\dagger_L c_L \\ H_{21}^{11,10} \frac{1}{E-H_{11}^{10,10}} H_{11}^{10,01} \frac{1}{E-H_{11}^{01,01}} H_{12}^{01,11} & \longrightarrow \quad J_{LR} \vec{T}_{LR} \cdot \vec{s}_{LR} + W_{LR} \frac{P^0}{2} \tau^0 c^\dagger_L c_R \\ H_{21}^{11,01} \frac{1}{E-H_{11}^{01,01}} H_{11}^{01,10} \frac{1}{E-H_{11}^{10,10}} H_{12}^{10,11} & \longrightarrow \quad J_{RL} \vec{T}_{RL} \cdot \vec{s}_{RL} + W_{RL} \frac{P^0}{2} \tau^0 c^\dagger_R c_L \\ H_{22}^{11,20} \frac{1}{E-H_{22}^{20,20}} H_{22}^{20,21} & \longrightarrow \quad J_{12} \vec{S}_R \cdot \vec{S}_L \end{cases} \tag{2.26}$$

where I wrote some of the terms on the left side and the overall contribution they give on the right side. Notice that the first two terms are exactly the same of the single-dot case (which is not hard to believe if one notices that they involve just one of the two dots) and $\vec{T}$ and $P^0$ are convenient operators, whose explicit expression has to be found by looking at each single second order process connecting the left and the right lead. It is not hard to believe that similar terms involving transitions to double occupied dots will also appear when dealing with the complete Hamiltonian (2.25). The coupling coefficients $J_\alpha$, $W_\alpha$ ( and $J_{\alpha\alpha'}$ and $W_{\alpha\alpha'}$ for the second order processes) will then include a sum of terms $1/E$ (or $1/(E_1 E_2)$ in case of second order processes), where $E$ is the energy required for the virtual process involved in the transition. The complete expressions for the coupling coefficients can for example be found in [4].
The Schrieffer-Wolff transformed interaction will then look like:

$$H' = J_{12} \vec{S}_R \cdot \vec{S}_L + \sum_{\alpha=\{R,L\},k,k',\sigma,\sigma'} \left( J_{\alpha,kk'} \vec{S}_\alpha \cdot \vec{\tau}_{\sigma\sigma'} c^\dagger_{\alpha k\sigma} c_{\alpha k'\sigma'} + W_{\alpha,kk'} \frac{\mathbb{I}}{2} \tau^0_{\sigma\sigma'} c^\dagger_{\alpha k\sigma} c_{\alpha k'\sigma'} \right) + \sum_{\alpha,\alpha'=\{R,L\},k,k',\sigma,\sigma'} \left( J_{\alpha\alpha',kk'} \vec{T}_{\alpha\alpha'} \cdot \vec{\tau}_{\sigma\sigma'} c^\dagger_{\alpha k\sigma} c_{\alpha' k'\sigma'} + W_{\alpha\alpha',kk'} \frac{P^0}{2} \tau^0_{\sigma\sigma'} c^\dagger_{\alpha k\sigma} c_{\alpha' k'\sigma'} \right) \tag{2.27}$$

Our next task is to find the explicit form of the two operators $\vec{T}$ and $P^0$. This is what we are going to do in Chapter 3.

# 3. Cotunneling transport in molecular junctions

The physics of single molecule three-terminal junctions is in many ways similar to that of analogous quantum dot devices. The energy spectrum of a single molecule is characterized by discrete energy levels, which couple to the electrodes. It is often convenient to consider the highest occupied molecular orbital (HOMO) and the lowest unoccupied molecular orbital (LUMO), whose energies will in general be perturbed by the coupling to the leads. This is usually modeled as a double barrier, whose height is related to the strength of the tunneling coupling, i.e. the overlapping between the molecular wave function and the wave function of the leads. The strength of the tunneling barriers are therefore highly dependent on the specific geometry of the molecule and the interface between this and the electrodes.
The level broadening of the molecular levels given by tunneling hybridization ($\Gamma$) can be smaller then the charging energy of the molecule, $\Gamma < E_c$, leading to a weak-coupling regime, or bigger, $\Gamma > E_c$, thus giving strong-coupling effects.
In the weak coupling regime, the double barrier effectively blocks electronic transport when the molecular levels are off-resonance with the chemical potential of the leads (Coulomb blockade regime). The characteristic Coulomb diamonds described in 2.1, arising in differential conductance maps as a function of gate and bias voltage, are also observed in single molecule junctions [6, 5, 11, 12]. Inside the Coulomb blockade diamonds higher order virtual processes can occur (cotunneling) in a way analogous that described in 2.1. Signatures for these processes have also been observed in single-molecule junctions [6, 5, 11, 12].
In this chapter we focus on the weak-coupling physics of single-molecule junctions. The theoretical model describing the physics of such systems can vary a lot, depending on the molecular complex considered. Here we focus on a number of simple two-dot and three-dot models. We moreover assume a privileged single-electron occupation in each dot, thus taking into account only virtual transitions to the doubly- and zero-occupied (higher energy) states.
Thinking a molecule as a system of two or three coupled quantum dots, each of them containing a single spin, is really a huge simplification, that therefore requires a proper justification. This can only come by a careful study of the energy levels of the isolated molecule together with the understanding of the effects on them of the tunneling coupling to the leads. Such studies have been done in relation to specific molecular junctions [6], but are out of the scope of this thesis, which focus instead on a number of abstract two- and three-spin models. We should nevertheless keep in mind that, when dealing with these models, we are really describing molecules with a very specific electronic configuration. We always assume the following:

- the considered state of the molecule has a total spin 1 (two-spin model) or 3/2 (three-spin model)
- the two or three total effective spins considered happen to be localized in well specific positions inside the molecule and such positions correspond to a very specific dot configuration in relation to the leads.

As stated above, these two assumptions are not justified a priori, but they may be proven reasonable for specific molecular junctions, when the shell structure of the atoms in the molecule

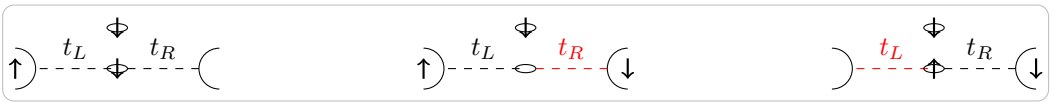


Figure 3.1.: Vertical double dot with one dot coupled to the leads. Example of a second order process coupling different total-spin states in the central region (spin-flip process). The initial state of the system (represented in the left figure) has one electron in each dot. Then a virtual process occurs (central figure) where the electron of the lowest dot is transfered out of the dot into the right electrode. An electron from the left lead is then transfered into the dot, thus replacing the electron that has gone. The final state of the system (right figure) has therefore once again one electron in each dot. Overall the process has transfered an electron from the left to the right lead while in the double dot a virtual transition to a zero-occupied (high-energy) state has occured, before the system has set back to its ground state, with one electron in each dot (single occupation). The final total spin of the two-dot system has been changed by the process, because the incoming electron (from the left lead) had a different spin from the outgoing one (that gets into the right lead). This process is then a spin-flip process and it is described by the term proportional to $J_{\alpha\alpha'}$ in (3.2). Processes that do not flip the spin can also occur (f.e. if the incoming electron had the same spin as the outgoin one) and are described by the term proportional to $W_{\alpha\alpha'}$ in (3.2). Taking into account all the processes of this kind (involving virtual transitions to zero- or double-occupied states in the lowest dot), both the spin-flip ones and the non-spin-flip, one obtains the total form of the Schrieffer-Wolff transformed Hamiltonian (3.2).

and the tunneling-coupling perturbation due to the leads are carefully studied.

In the first part of the chapter we write the Hamiltonian of the double-dot and three-dot systems considered, in the second part we focus on the cotunneling physics. We will see that the inelastic cotunneling peaks of a triangular triple dot (TTD) strongly depend on the inter-dot exchange coupling. A different inter-dot coupling between the two lowest dots and the third top electron gives an asymmetric differential conductance against bias voltage (3.2.2). This configuration breaks in fact the overall symmetry of the system, which is recovered when equal couplings are chosen, thus giving an usual symmetric dependence of the differential conductance on the bias voltage.

## 3.1. Model Hamiltonian

### 3.1.1. Vertical double dot with one dot coupled to the leads

We will first study a vertical double quantum dot, i.e. two quantum dots in parallel, as they appear in Figure 3.1. This consists of two dots, each of them we assume singly occupied. Moreover tunneling to the leads is assumed to be allowed just through one of the two dots (Figure 3.1). This very peculiar situation is then described by a standard Anderson Hamiltonian:

$$H_A = \sum_{i=\{l,u\},\sigma} \varepsilon_{di} d^\dagger_{i\sigma} d_{i\sigma} + \sum_{\alpha,k,\sigma} \varepsilon_{\alpha,k} c^\dagger_{\alpha k\sigma} c_{\alpha k\sigma} + \sum_{\alpha,k,\sigma} \left( t_{\alpha k} d^\dagger_{l\sigma} c_{\alpha k\sigma} + t^*_{\alpha k} c^\dagger_{\alpha k\sigma} d_{l\sigma} \right) + U n_{d_l\uparrow} n_{d_l\uparrow} - B(S^z_l + S^z_u) \tag{3.1}$$

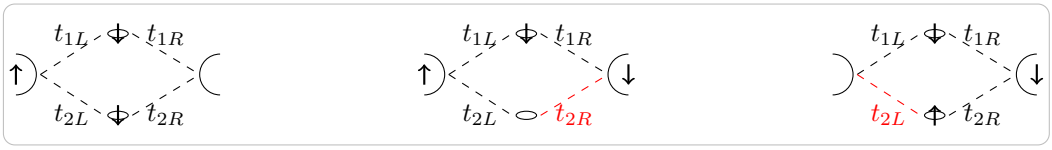


Figure 3.2.: Vertical double dot with both the dots coupled to the leads. Example of a second order process coupling different total-spin states in the central region (spin-flip process). This process is analogous to that of Figure 3.1 and it is in fact described by a similar Hamiltonian (3.3). The only difference between this system and the previous one (i.e. the one of Section 3.1.1) is that now both the quantum dots are coupled to the leads, i.e. they can both exchange electrons with the electrodes. Virtual processes can thus occur both in the uppermost and the lowermost dot. As a consequence, in the Hamiltonian (3.3) there are two similar terms added together, each of them referring to virtual transitions occurring in one of the dots. Here a virtual transition to a zero-occupied state in the lowermost dot is shown.

where $l$ and $u$ label the upper and lower dots, respectively, so that $\vec{S}_l$ and $\vec{S}_u$ are the spin operators of the two dots. Moreover we have added an external magnetic field to the system, whose effect is the addition in the Hamiltonian of a Zeeman term depending on the spin state $\approx BS^z$.
The Schrieffer-Wolff transformation of Section 2.2 allows us to transform the Anderson model (3.1) into a standard Kondo Hamiltonian:

$$H_S = J_{12}\vec{S}_l \cdot \vec{S}_u + \sum_{\substack{\alpha,\alpha' \\ k,k'}} \left( J_{\alpha\alpha'}\vec{S}_l \cdot \vec{s}_{\alpha k,\alpha' k'} + \frac{W_{\alpha\alpha'}}{2} \sum_{\sigma\sigma'} \tau^0_{\sigma\sigma'} c^\dagger_{\alpha k\sigma} c_{\alpha' k'\sigma'} \right) \tag{3.2}$$

where $\vec{s}_{\alpha k,\alpha' k'} = \sum_{\substack{\alpha\alpha' \\ kk' \\ \sigma\sigma'}} \vec{\tau}_{\sigma\sigma'} c^\dagger_{\alpha k\sigma} c_{\alpha' k'\sigma'}$ refers to the conduction electrons tunneling into and out the leads.
Notice that in this model an anti-ferromagnetic coupling $J_{12} > 0$ between the dots promotes a singlet ground state in the uncoupled central region.

### 3.1.2. Vertical double dot with both the dots coupled to the leads

If we allow for both the dots to be coupled to the leads, then transport from one lead to the other can occur through either dots (Figure 3.2). This possibility is taken into account in the following Hamiltonian:

$$H_S = J_{12}\vec{S}_u \cdot \vec{S}_l + \sum_{\substack{\alpha,\alpha' \\ k,k'}} \left[ \sum_{d=\{l,u\}} \left( J_{d,\alpha\alpha'}\vec{S}_d \cdot \vec{s}_{\alpha k,\alpha' k'} + \frac{W_{d,\alpha\alpha'}}{2} \sum_{\substack{kk' \\ \sigma\sigma'}} \tau^0_{\sigma\sigma'} c^\dagger_{\alpha k\sigma} c_{\alpha' k'\sigma'} \right) \right] \tag{3.3}$$

where $l$ stands for the lowest dot and $u$ for the uppermost.

### 3.1.3. Lateral double dot

We would now like to study yet another two-spin system. This time we consider a lateral double dot (Figure 3.4), i.e. two dots in series, whose ground state is a two-electron system.

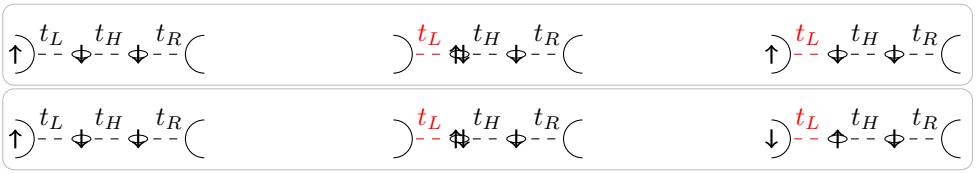


Figure 3.3.: Lateral double dot (i.e. two quantum dots in series). Example of a second order non-spin-flip (top picture) and spin-flip (bottom picture) process. The process involves a virtual transition to a double-occupied high-energy state in the left dot. Similar processes involving the electron tunneling between the right dot and the right lead can also occur. All the second order non-spin-flip (i.e. with the final total spin state equal to the initial one) processes (top picture) are described by the terms $\frac{W_\alpha}{2}\sum_{\sigma=\uparrow,\downarrow} c^\dagger_{\alpha\sigma}c_{\alpha\sigma}$ in the first line of (3.6). On the contrary, all the spin-flip (with the final total sspin state different from the initial one) second order processes (bottom picture) are described by the terms $J_\alpha \vec{S}_\alpha \cdot \vec{s}_\alpha$ in the first line of (3.6). Notice that in this system second order processes (processes involving two tunneling events) can only involve one lead at the time, each dot being coupled just to one lead.

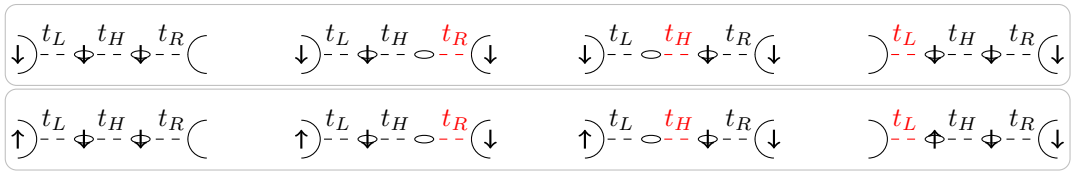


Figure 3.4.: Lateral double dot. Example of a third order non-spin-flip (top picture) and spin-flip (bottom picture) process transfering an electron from the left to the right lead. Non-spin-flip processes (top picture) couple equal total-spin states in the central region, i.e. the final two-spin state in the dot is identical to the initial one. All the processes of this kind are described by the term $\frac{W_{\alpha\alpha'}}{2}P_0\sum_{\sigma=\uparrow,\downarrow} c^\dagger_{\alpha\sigma}c_{\alpha'\sigma}$ in the second line of (3.6). Spin-flip processes (bottom picture) couple different total-spin states in the central region, i.e. the final two-spin state in the dot is different from the initial one. All the processes of this kind are described by the term $\frac{J_{\alpha\alpha'}}{2}\vec{T}_{\alpha\alpha'}\cdot\vec{s}_{\alpha\alpha'}$ in the second line of (3.6). Notice that in this system the only way of transfering an electron from one lead to the other is to tunnel through both the dots, a third order process (three tunneling events) is namely required.

Representation of a three-step (i.e. third order) process involving transport from one electrode

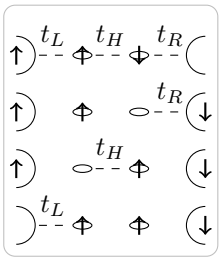


to the other in a lateral dot:

Operator $\hat{O}$ describing the process:

$$\hat{O} := \underbrace{\frac{t_L t_H t_R}{U}}_{J_{RL}} d^\dagger_{L\uparrow} c_{L\uparrow} d^\dagger_{R\uparrow} d_{L\uparrow} c^\dagger_{R\downarrow} d_{R\downarrow}$$

Matrix elements of $\hat{O}$ between all the possible initial and final states represented in the singlet-triplet basis:

$$\begin{cases} \langle T_{+1} \mid \hat{O} \mid s \rangle = \frac{1}{\sqrt{2}} c^\dagger_{R\downarrow} c_{L\uparrow} \\ \langle T_{+1} \mid \hat{O} \mid T_0 \rangle = \frac{1}{\sqrt{2}} c^\dagger_{R\downarrow} c_{L\uparrow} \end{cases}$$

Figure 3.5.: Example of a spin-flip process needed to write down the unitary transformation giving the final Schrieffer-Wolff-like Hamiltonian for a two-singly-occupied-dot system. This process involves transitions to the high-energy zero-occupied state in each dot. On the right side all the matrix elements of the transition operators between the possible initial and final state of the dot are calculated. Notice that the basis used to describe dot states is the singlet-triplet basis, namely the basis of the two combined spins, and therefore a certain state, e.g. $|\uparrow\downarrow\rangle$ might represent two different singelet-triplet states, e.g. the singlet state $\mid s\rangle$ and the triplet state $\mid T_0\rangle$.

We assume that, because of the relative distance between the dots and the leads, each dot can exchange electrons just with the nearest lead and with the other dot. This means that transport from one lead to the other must always be mediated by a virtual transition in each dot, i.e. a three-step process. The Anderson like Hamiltonian for the system is therefore:

$$\begin{aligned} H_A = & \sum_{i=\{L,R\},\sigma} \varepsilon_{di} d^\dagger_{i\sigma} d_{i\sigma} - B(S^z_L + S^z_R) + \sum_{\alpha,k,\sigma} \varepsilon_{\alpha,k} c^\dagger_{\alpha k\sigma} c_{\alpha k\sigma} + \sum_{k,\sigma} \left( t_{Lk} d^\dagger_{L\sigma} c_{Lk\sigma} + t^*_{Lk} c^\dagger_{Lk\sigma} d_{L\sigma} \right) \\ & + \sum_{k,\sigma} \left( t_{Rk} d^\dagger_{R\sigma} c_{Rk\sigma} + t^*_{Rk} c^\dagger_{Rk\sigma} d_{R\sigma} \right) + \sum_{\sigma} \left( t_H d^\dagger_{L\sigma} d_{R\sigma} + t^*_H d^\dagger_{R\sigma} d_{L\sigma} \right) + \sum_{i=\{L,R\}} U n_{d_i\uparrow} n_{d_i\downarrow} \end{aligned} \tag{3.4}$$

where $L$ and $R$ stand for the left and the right dot, respectively.
We furthermore assume that $|\varepsilon_{d_i} - \varepsilon_F| \ll U$ and $\varepsilon_{d_i} \ll \varepsilon_F$ so that the ground state configuration is the one with one electron in each dot. Then it is convenient to work in the basis generated by two coupled spins, i.e. the singlet-triplet basis:

$$\begin{cases} \text{triplet} \begin{cases} |\uparrow\uparrow\rangle = d^\dagger_{L\uparrow} d^\dagger_{R\uparrow} \mid 0\rangle :=\mid T_{+1}\rangle \\ |\downarrow\downarrow\rangle = d^\dagger_{L\downarrow} d^\dagger_{R\downarrow} \mid 0\rangle :=\mid T_{-1}\rangle \\ \frac{|\uparrow\downarrow\rangle + |\downarrow\uparrow\rangle}{\sqrt{2}} = \frac{d^\dagger_{L\uparrow} d^\dagger_{R\downarrow}|0\rangle + d^\dagger_{L\downarrow} d^\dagger_{R\uparrow}|0\rangle}{\sqrt{2}} :=\mid T_0\rangle \end{cases} \\ \text{singlet} \; \frac{|\uparrow\downarrow\rangle - |\downarrow\uparrow\rangle}{\sqrt{2}} = \frac{d^\dagger_{L\uparrow} d^\dagger_{R\downarrow}|0\rangle - d^\dagger_{L\downarrow} d^\dagger_{R\uparrow}|0\rangle}{\sqrt{2}} :=\mid s\rangle \end{cases} \tag{3.5}$$

where the notation $\mid S_L S_R\rangle =\mid S_L\rangle \otimes \mid S_R\rangle$ describes the four dimensional space of two combined spins.

We then want to project out the high energy three- and one-occupied solutions. This is done through a Shriffer-Wolff transformation, following the procedure of Section 2.3. We therefore

need to find the specific form of the operators $\vec{T}$ and $P^0$ (appearing in (2.27)) by looking at all the processes involving virtual transitions to higher energy states (see the example of Figure 3.5). We then calculate the matrix elements of each possible process in the singlet-triplet basis and write the Hamiltonian for all these processes as a sum of projection operators over the states of the dot. All the details of this somehow cumbersome calculation are shown in Appendix A. The resulting Hamiltonian for two-singly-occupied dots can then be rewritten through the usual spin operators in the following form:

$$H'_S = J_{12}\vec{S}_L \cdot \vec{S}_R + \sum_{\alpha=\{R,L\}} \left[ J_\alpha \vec{S}_\alpha \cdot \vec{s}_\alpha + \frac{W_\alpha}{2} \sum_{\sigma=\uparrow,\downarrow} c^\dagger_{\alpha\sigma} c_{\alpha\sigma} \right] + \sum_{\substack{\alpha\neq\alpha' \\ \alpha,\alpha'=\{R,L\}}} \left[ \frac{J_{\alpha\alpha'}}{2} \vec{T}_{\alpha\alpha'} \cdot \vec{s}_{\alpha\alpha'} + \frac{W_{\alpha\alpha'}}{2} P_0 \sum_{\sigma=\uparrow,\downarrow} c^\dagger_{\alpha\sigma} c_{\alpha'\sigma} \right] \tag{3.6}$$

where the exchange operator $\vec{T}$ is now found to be:

$$\vec{T}_{\alpha\alpha'} := (\vec{S}_\alpha + \vec{S}_{\alpha'}) - 2i(\vec{S}_{\alpha'} \times \vec{S}_\alpha) \tag{3.7}$$

and the potential scattering term $P_0$ is:

$$\frac{P_0}{2} := 2(\vec{S}_L \cdot \vec{S}_R) + \mid s\rangle\langle s \mid = \frac{1}{4}\mathbb{I} + \vec{S}_L \cdot \vec{S}_R. \tag{3.8}$$

The first term in (3.6) represents the internal coupling of the two dots uncoupled to the leads, i.e. the isolated two-coupled-spin system. The second and third terms, on the contrary, give the coupling between the central region (the two-dot system) and the leads. These terms represent virtual transitions involving a different charge state in the central region. Such transitions appear as virtual fluctuation given by tunneling in and out the dot. Remember, in fact, that the Schrieffer-Wolff procedure, applied to get this form of the Hamiltonian, describes singly occupied dots, effectively eliminating double and zero-occupied states. These states appear now only as non-energy conserving virtual fluctuations.
The second term of the Hamiltonians describes such virtual fluctuations in and out of the same lead, thus involving the same tunneling amplitude $t_\alpha$. The term proportional to $W_\alpha$ describes events leaving the dot in the same state as it was before the transition (Figure 3.3 top), while the term $J_\alpha \vec{S}_\alpha \cdot \vec{s}_\alpha$ represents event that flip the spin of one dot (Figure 3.3 bottom). The third term of the Hamiltonian is the only one describing electron transport from one lead to the other (i.e. it contains terms like $c^\dagger_{\alpha\sigma} c_{\alpha'\sigma}$ with $\alpha \neq \alpha'$). In this system the only way such electron transport can happen is through tunneling events involving both the dots. Once again the total spin (i.e. of the two combined electrons) of the dot can be left untouched by the transition (Figure 3.4 top) and this is described by the term $\frac{W_{\alpha\alpha'}}{2} P_0 \sum_{\sigma=\uparrow,\downarrow} c^\dagger_{\alpha\sigma} c_{\alpha'\sigma}$, involving the scalar operator $P_0$. Otherwise a spin flip (Figure 3.4 bottom) of the combined two-spin-1/2 system can occur. Such possibility is taken into account by the term $\frac{J_{\alpha\alpha'}}{2} \vec{T}_{\alpha\alpha'} \cdot \vec{s}_{\alpha\alpha'}$. This combination is still a dot product of spin operators (as it was the spin-flip term representing virtual transitions in only one dot) but the new spin operator $\vec{T}$ effectively takes into account the spin of both the dots involved in the transition and therefore it is actually a combination of the 1/2-spin operators of each dot.

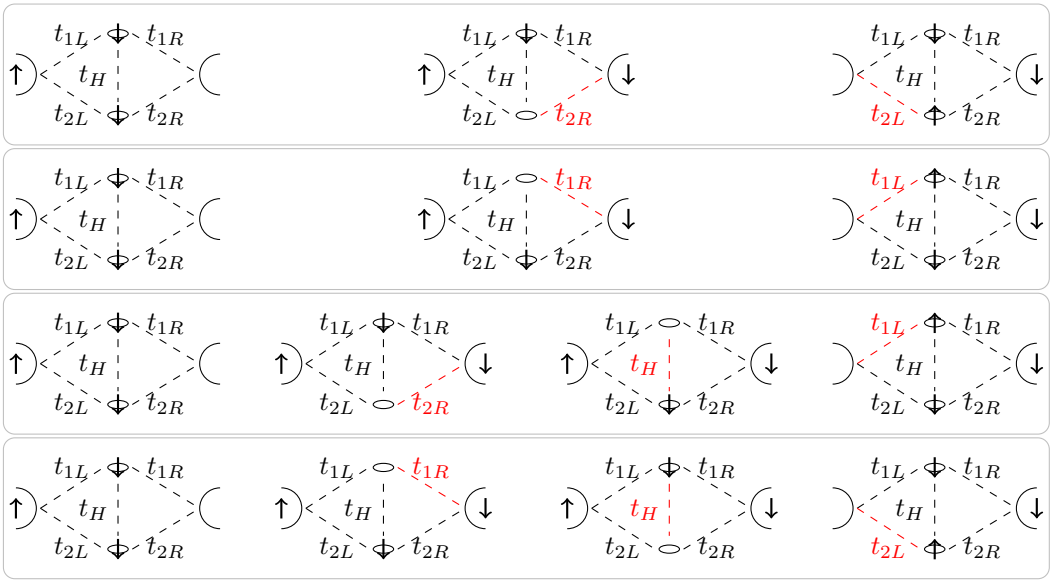

Figure 3.6.: Example of possible (second and third order) processes coupling different total-spin states in the central region. The processes involve virtual transitions to a zero-occupied state.

### 3.1.4. Vertical double dot with both the dots coupled to the leads and tunneling between the dots

We now consider the situation in which both the dots are coupled to the leads and moreover there is a tunneling probability between the two dots as well (Figure 3.6). This situation is much richer then the previous ones because many channels are open simultaneously, allowing for transport between the leads to be either a second order process (involving virtual transitions in just one of the dots just like in the systems 3.1.1 and 3.1.2) or a third order process, mediated by two virtual transitions involving both the dots, like in the lateral double dot 3.1.3.
The Hamiltonian for this system will have to keep track both of the leads and each dot involved in each transition. Moreover third order processes allow for a virtual transition to a doubly or zero-occupied states to occur in dot 1 first and dot 2 afterwards or vice versa. We thus have to keep track of the order in which the dots are driven into the higher energy virtual states. All this is taken into account in the Hamiltonian:

$$\begin{aligned} H_S = J_{12}\vec{S}_1\cdot\vec{S}_2 + \sum_{\alpha,\alpha'}\Bigg[\sum_{d=\{1,2\}}\left(J_{d,\alpha\alpha'}\vec{S}_d\cdot\vec{s}_{\alpha\alpha'} + \frac{W_{d,\alpha\alpha'}}{2}\sum_{kk'\sigma\sigma'}\tau^0_{\sigma\sigma'}c^\dagger_{\alpha k\sigma}c_{\alpha' k'\sigma'}\right) \\ + \left(\frac{J_{1\alpha,2\alpha'}}{2}\vec{T}_{1\alpha,2\alpha'}\cdot\vec{s}_{\alpha\alpha'} + \frac{W_{1\alpha,2\alpha'}}{2}P_{\alpha\alpha'}\sum_{kk'\sigma\sigma'}c^\dagger_{\alpha k\sigma}c_{\alpha' k'\sigma'}\right. \\ \left. + \frac{J_{2\alpha,1\alpha'}}{2}\vec{T}_{2\alpha,1\alpha'}\cdot\vec{s}_{\alpha\alpha'} + \frac{W_{2\alpha,1\alpha'}}{2}P_{\alpha\alpha'}\sum_{kk'\sigma\sigma'}c^\dagger_{\alpha k\sigma}c_{\alpha' k'\sigma'}\right)\Bigg] \end{aligned} \tag{3.9}$$

where $P_{RL} = P_{LR} = P_0$. Moreover $\vec{T}_{1R,2L} = \vec{S}_1 + \vec{S}_2 - 2i(\vec{S}_1 \times \vec{S}_2)$ and $\vec{T}_{2R,1L} = \vec{S}_1 + \vec{S}_2 - 2i(\vec{S}_2 \times \vec{S}_1) = \vec{S}_1 + \vec{S}_2 + 2i(\vec{S}_1 \times \vec{S}_2)$.

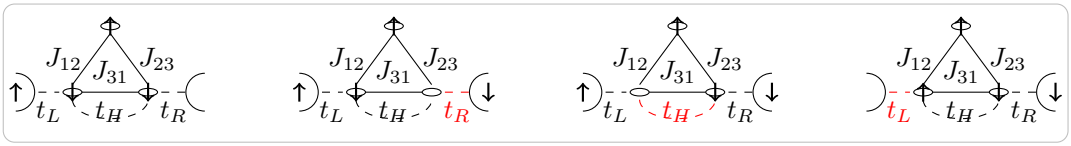


Figure 3.7.: Example of a third order process coupling different total-spin states in the central region. The process involves a virtual transition to a zero-occupied state in each dot. Studying all the processes of this kind one obtains the form of the Schrieffer-Wolff transformed Hamiltonian for the triangular triple dot. Notice that the central uppermost dot is not tunnel-coupled to the leads. We therefore expect the tunneling terms in the Hamiltonian to look the same as for the system 3.1.3.

Once again the first term in (3.9) is the internal coupling between the two spins. The second term in the first line (the parenthesis) describes processes coupling two leads through a virtual charge fluctuation in one dot. The process allows tunneling in and out of the same lead (processes with $\alpha = \alpha'$), giving processes like the ones described for the lateral double dot and represented in Figure 3.3, or coupling the two leads ($\alpha \neq \alpha'$), in which case the term contributes to the current through the system (top two pictures in Figure 3.6). The terms in the second and third line of (3.9) describe third-order processes, instead, i.e. involving virtual transitions in both the dots (two bottom pictures in Figure 3.6).

### 3.1.5. Triangular three-spin system

The last system we are going to study is similar to the lateral double dot of 3.1.3: there are still two quantum dots in a lateral configuration which are tunnel-coupled to the leads but one more dot is added to the system so that the central region is a triangular three-dot configuration (Figure 3.7). In general the new dot broadens the range of possible configurations of the system, giving the possibility for more electrons to be in the central region. Nevertheless, if we once again assume the condition (2.9), the ground state configuration has one electron in each dot. Moreover, we assume that just the two lateral dots are coupled to the leads, just like in 3.1.3, while the newly added dot is not tunnel coupled to the leads or any of the other dots. The triangular three-dot system so obtained will then have characteristics very similar to the lateral double dot previously studied. In fact, one can even guess how a Schrieffer-Wolff Hamiltonian for this system might look like. Since the central region is coupled to the leads through the same tunneling couplings as the two-dot system 3.1.3, the terms describing transport from one lead to the other will look exactly as in (3.6). Studying the processes giving the Schrieffer-Wolff transformation, we will in fact confirm this prediction.
Let us start our study by reviewing the eigenstates of three isolated spins so that later on we can use this basis. We want to find eigenstates for the total spin operator $\vec{S}^2$ and its z-component $S^z$. From the rules of addition of the angular momentum one finds that three spins $\frac{1}{2}$ combine in a quartet of total angular momentum $\vec{S}^2 = \frac{3}{4}$ and z-component $S^z = \pm\frac{3}{4}, \pm\frac{1}{2}$ and two doublets of angular momentum $\vec{S}^2 = \frac{1}{2}$ and z-component $S^z = \pm\frac{1}{2}$. We therefore have eight states with the correspondent simultaneous eigenvectors for $\vec{S}^2$ and $S^z$. In order to find these eigenstates let us write the possible combinations of the three spins in terms of eigenvectors of the single spins. We will call $\alpha$ the eigenvector of a single spin with z-component $S^z = \frac{1}{2}$ and $\beta$ the eigenvector

with z-component $S^z = -\frac{1}{2}$.

$$\begin{aligned}
\Psi_1(1,2,3) &= \alpha(1)\alpha(2)\alpha(3) \qquad |\uparrow\uparrow\uparrow\rangle \\
\Psi_2(1,2,3) &= \alpha(1)\beta(2)\alpha(3) \qquad |\uparrow\downarrow\uparrow\rangle \\
\Psi_3(1,2,3) &= \alpha(1)\alpha(2)\beta(3) \qquad |\uparrow\uparrow\downarrow\rangle \\
\Psi_4(1,2,3) &= \alpha(1)\beta(2)\beta(3) \qquad |\uparrow\downarrow\downarrow\rangle \\
\Psi_5(1,2,3) &= \beta(1)\alpha(2)\alpha(3) \qquad |\downarrow\uparrow\uparrow\rangle \\
\Psi_6(1,2,3) &= \beta(1)\beta(2)\alpha(3) \qquad |\downarrow\downarrow\uparrow\rangle \\
\Psi_7(1,2,3) &= \beta(1)\alpha(2)\beta(3) \qquad |\downarrow\uparrow\downarrow\rangle \\
\Psi_8(1,2,3) &= \beta(1)\beta(2)\beta(3) \qquad |\downarrow\downarrow\downarrow\rangle
\end{aligned} \tag{3.10}$$

Now let us apply the $S^z = (S^z(1) + S^z(2) + S^z(3))$ operator to each of these states. We obtain:

$$\begin{aligned}
&S^z\Psi_1 = \frac{3}{2}\Psi_1 \qquad S^z\Psi_2 = \frac{1}{2}\Psi_2 \qquad S^z\Psi_3 = \frac{1}{2}\Psi_3 \qquad S^z\Psi_4 = -\frac{1}{2}\Psi_4 \\
&S^z\Psi_5 = \frac{1}{2}\Psi_5 \qquad S^z\Psi_6 = -\frac{1}{2}\Psi_6 \qquad S^z\Psi_7 = -\frac{1}{2}\Psi_7 \qquad S^z\Psi_8 = -\frac{3}{2}\Psi_8
\end{aligned} \tag{3.11}$$

and the $\vec{S}^2 = (\vec{S}(1)+\vec{S}(2)+\vec{S}(3))^\dagger(\vec{S}(1)+\vec{S}(2)+\vec{S}(3)) = \frac{9}{4}+2\vec{S}(1)\cdot\vec{S}(2)+2\vec{S}(1)\cdot\vec{S}(3)+2\vec{S}(2)\cdot\vec{S}(3)$ operator applied to the states (3.10) gives:

$$\begin{aligned}
&\vec{S}^2\Psi_1 = \frac{15}{4}\Psi_1 \qquad \vec{S}^2\Psi_2 = \frac{7}{4}\Psi_2 + \Psi_3 + \Psi_5 \qquad \vec{S}^2\Psi_3 = \frac{7}{4}\Psi_3 + \Psi_2 + \Psi_5 \\
&\vec{S}^2\Psi_4 = \frac{7}{4}\Psi_4 + \Psi_6 + \Psi_7 \qquad \vec{S}^2\Psi_5 = \frac{7}{4}\Psi_5 + \Psi_2 + \Psi_3 \qquad \vec{S}^2\Psi_6 = \frac{7}{4}\Psi_6 + \Psi_4 + \Psi_7 \\
&\vec{S}^2\Psi_7 = \frac{7}{4}\Psi_7 + \Psi_4 + \Psi_6 \qquad \vec{S}^2\Psi_8 = \frac{15}{4}\Psi_8.
\end{aligned} \tag{3.12}$$

Diagonalizing the system above one finds the following simultaneous eigenstates of $\vec{S}^2$ and $S^z$:

$$\{\Psi_1, \Psi_8, \Psi_4 + \Psi_6 + \Psi_7, \Psi_2 + \Psi_3 + \Psi_5, -\Psi_4 + \Psi_7, -\Psi_2 + \Psi_5, -\Psi_2 + \Psi_3\} \tag{3.13}$$

corresponding to the following eigenvalues for $\vec{S}^2$:

$$\{\frac{15}{4}, \frac{15}{4}, \frac{15}{4}, \frac{15}{4}, \frac{7}{4}, \frac{7}{4}, \frac{7}{4}, \frac{7}{4}\}. \tag{3.14}$$

Let us finally couple the three-spin system to the two metallic leads. We want to find the Schrieffer-Wolff-like Hamiltonian describing such coupling. As previously stated, we assume that no tunneling can occur between the central dot and the lateral ones, so that transport from one lead to the other effectively occurs as in 3.1.3. The only difference between the lateral dot of Section 3.1.3 and the present case is the basis states of the uncoupled dot Hamiltonian which is used to represent the transport operators. Having at hand a three-spin system, the basis we are going to use is the one found above, which we now rewrite assigning a name at each state. We

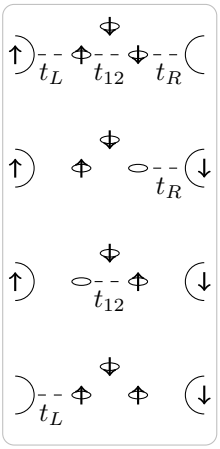


$$\propto J_H d^\dagger_{L\uparrow} d_{L\uparrow} d^\dagger_{R\uparrow} d_{R\downarrow} c^\dagger_{R\downarrow} c_{L\uparrow} := \hat{O}$$

$$\begin{cases} \langle +q \mid \hat{O} \mid -q \rangle = \frac{1}{3} c^\dagger_{R\downarrow} c_{L\uparrow} \\ \langle +q \mid \hat{O} \mid -d \rangle = -\frac{1}{\sqrt{6}} c^\dagger_{R\downarrow} c_{L\uparrow} \\ \langle +q \mid \hat{O} \mid -d' \rangle = -\frac{1}{\sqrt{6}} c^\dagger_{R\downarrow} c_{L\uparrow} \\ \langle +d \mid \hat{O} \mid -q \rangle = -\frac{1}{\sqrt{6}} c^\dagger_{R\downarrow} c_{L\uparrow} \\ \langle +d \mid \hat{O} \mid -d \rangle = \frac{1}{2} c^\dagger_{R\downarrow} c_{L\uparrow} \\ \langle +d \mid \hat{O} \mid -d' \rangle = \frac{1}{2} c^\dagger_{R\downarrow} c_{L\uparrow} \\ \langle +d' \mid \hat{O} \mid -q \rangle = -\frac{1}{\sqrt{6}} c^\dagger_{R\downarrow} c_{L\uparrow} \\ \langle +d' \mid \hat{O} \mid -d \rangle = \frac{1}{2} c^\dagger_{R\downarrow} c_{L\uparrow} \\ \langle +d' \mid \hat{O} \mid -d' \rangle = \frac{1}{2} c^\dagger_{R\downarrow} c_{L\uparrow} \end{cases}$$

Figure 3.8.: Example of a spin-flip process needed to write down the unitary transformation giving the final Schrieffer-Wolff-like Hamiltonian for a three-spin system in a triangular configuration. This process involves transitions to the high-energy zero-occupied state in each dot. On the right side the matrix elements of the transition operators are shown. Notice that the basis used is the doublet-quartet-doublet basis given by combining three spins.

here rewrite the normalized states of three combined spins:

$$\begin{cases} \text{quartet} \begin{cases} |+\frac{3}{2}\rangle := d^\dagger_{L\uparrow} d^\dagger_{C\uparrow} d^\dagger_{R\uparrow} \mid 0\rangle \\ |-\frac{3}{2}\rangle := d^\dagger_{L\downarrow} d^\dagger_{C\downarrow} d^\dagger_{R\downarrow} \mid 0\rangle \\ |+q\rangle := \frac{d^\dagger_{L\uparrow} d^\dagger_{C\downarrow} d^\dagger_{R\uparrow}|0\rangle + d^\dagger_{L\uparrow} d^\dagger_{C\uparrow} d^\dagger_{R\downarrow}|0\rangle + d^\dagger_{L\downarrow} d^\dagger_{C\uparrow} d^\dagger_{R\uparrow}|0\rangle}{\sqrt{3}} = \frac{|\uparrow\downarrow\uparrow\rangle + |\uparrow\uparrow\downarrow\rangle + |\downarrow\uparrow\uparrow\rangle}{\sqrt{3}} \\ |-q\rangle := \frac{d^\dagger_{L\uparrow} d^\dagger_{C\downarrow} d^\dagger_{R\downarrow}|0\rangle + d^\dagger_{L\downarrow} d^\dagger_{C\downarrow} d^\dagger_{R\uparrow}|0\rangle + d^\dagger_{L\downarrow} d^\dagger_{C\uparrow} d^\dagger_{R\downarrow}|0\rangle}{\sqrt{3}} = \frac{|\uparrow\downarrow\downarrow\rangle + |\downarrow\downarrow\uparrow\rangle + |\downarrow\uparrow\downarrow\rangle}{\sqrt{3}} \end{cases} \\ \text{doublet1} \begin{cases} |+d\rangle := \frac{d^\dagger_{L\downarrow} d^\dagger_{C\uparrow} d^\dagger_{R\uparrow}|0\rangle - d^\dagger_{L\uparrow} d^\dagger_{C\downarrow} d^\dagger_{R\uparrow}|0\rangle}{\sqrt{2}} = \frac{|\downarrow\uparrow\uparrow\rangle - |\uparrow\downarrow\uparrow\rangle}{\sqrt{2}} \\ |-d\rangle := \frac{d^\dagger_{L\downarrow} d^\dagger_{C\uparrow} d^\dagger_{R\downarrow}|0\rangle - d^\dagger_{L\uparrow} d^\dagger_{C\downarrow} d^\dagger_{R\downarrow}|0\rangle}{\sqrt{2}} = \frac{|\downarrow\uparrow\downarrow\rangle - |\uparrow\downarrow\downarrow\rangle}{\sqrt{2}} \end{cases} \\ \text{doublet2} \begin{cases} |+d'\rangle := \frac{d^\dagger_{L\uparrow} d^\dagger_{C\uparrow} d^\dagger_{R\downarrow}|0\rangle - d^\dagger_{L\uparrow} d^\dagger_{C\downarrow} d^\dagger_{R\uparrow}|0\rangle}{\sqrt{2}} = \frac{|\uparrow\uparrow\downarrow\rangle - |\uparrow\downarrow\uparrow\rangle}{\sqrt{2}} \\ |-d'\rangle := \frac{d^\dagger_{L\downarrow} d^\dagger_{C\downarrow} d^\dagger_{R\uparrow}|0\rangle - d^\dagger_{L\uparrow} d^\dagger_{C\downarrow} d^\dagger_{R\downarrow}|0\rangle}{\sqrt{2}} = \frac{|\downarrow\downarrow\uparrow\rangle - |\uparrow\downarrow\downarrow\rangle}{\sqrt{2}} \end{cases} \end{cases} \tag{3.15}$$

The generalized procedure 2.3 applied to this three-spin system exploits the same ideas of Section 3.1.3 (Figure 3.8) and is reported in Appendix B. The following Schrieffer-Wolff-like Hamiltonian is found:

$$H_S = J_{12}\vec{S}_L \cdot \vec{S}_C + J_{23}\vec{S}_C \cdot \vec{S}_R + J_{13}\vec{S}_L \cdot \vec{S}_R + \sum_{\alpha=\{R,L\}} \left[ J_\alpha \vec{S}_\alpha \cdot \vec{s}_\alpha + \frac{W_\alpha}{2} \sum_{\substack{\sigma=\{\uparrow,\downarrow\} \\ k,k'}} c^\dagger_{\alpha k\sigma} c_{\alpha k\sigma} \right]$$
$$+ \sum_{\substack{\alpha\neq\alpha' \\ \alpha,\alpha'=\{R,L\}}} \left[ \frac{J_{\alpha\alpha'}}{2} \vec{T}_{\alpha\alpha'} \cdot \vec{s}_{\alpha\alpha'} + \frac{W_{\alpha\alpha'}}{2} P_0 \sum_{\substack{\sigma=\{\uparrow,\downarrow\} \\ k,k'}} c^\dagger_{\alpha k\sigma} c_{\alpha' k'\sigma} \right] - \vec{B} \cdot (\vec{S}_L + \vec{S}_C + \vec{S}_R) \tag{3.16}$$

where

$$\begin{aligned} \vec{T}_{RL} &= \vec{S}_L + \vec{S}_R - 2i\vec{S}_L \times \vec{S}_R \\ \vec{T}_{LR} &= \vec{S}_L + \vec{S}_R - 2i\vec{S}_R \times \vec{S}_L \\ P_0 = P_0^\dagger &= 2\left[\vec{S_L} \cdot \vec{S_R} + \frac{\mathbb{I}}{4}\right] \end{aligned} \tag{3.17}$$

and the conduction electron operators are: $\vec{s}_{RL} = \vec{\tau}_{\sigma\sigma'} c^\dagger_{Rk\sigma} c_{Lk'\sigma'}$ and $\vec{s}_{LR} = \vec{\tau}_{\sigma\sigma'} c^\dagger_{Lk\sigma} c_{Rk'\sigma'}$.
Notice that, as we expected, in 3.16 we find the same operators $\vec{T}$ and $P$ that also appeared in the two-spin lateral system treated in 3.1.3. Using the procedure outlined in Appendix B these operators show up in the form of matrix elements of an $8 \times 8$ matrix written in the three-spin basis 3.15.
From the procedure outlined in Section 2.3, the values of the inter-dot couplings $J_{12}$, $J_{23}$ and $J_{31}$ appear to be fixed by the values of the tunneling coupling between the dots $t_H$ and with the leads $t_L$, $t_R$. However we should remember that we are trying to describe a molecular system, where interactions taking place among electrons inside the molecule are in general complicated. In particular we can expect an interplay between a ferromagnetic Hund's rule and an antiferromagnetic spin-spin interaction between electrons belonging to the same orbital. The full treatment of electron-electron interactions occurring in specific molecular systems is out of the scope of this thesis. We nevertheless account for such interplay by allowing the inter-dot couplings $J_{12}$, $J_{23}$ and $J_{31}$ to be either ferromagnetic or antiferromagnetic. We then don't set any sign to the spin-spin inter-dot interactions a priori. Instead we reserve the right of choosing a specific character for these couplings when we confront our data with a real molecular system. In that case we will refer to specific studies on the lectron-electron interactions in the isolated molecule in order to decide the ferromagnetic or anitferromagnetic character of the coupling coefficients.

## 3.2. Differential conductance

In this section we will finally study cotunneling transport through the different systems considered. For each configuration we will first describe the unperturbed Hamiltonian basis states and then apply first order perturbation theory in the tunneling Hamiltonian. The basic equation giving the transport amplitude between the left and the right lead, approximated at first order in the tunneling parameter, is given by Fermi Golden Rule:

$$\Gamma_{RL} = 2\pi \sum_{f,i} |\langle f \mid H \mid i \rangle|^2 W_i \delta(E_f - E_i). \tag{3.18}$$

where $W_i$ is the occupation probability of the initial state of the system and $E_i$, $E_f$ are the total initial and final energies, respectively. Written in this form, 3.18 gives the probability for transport to occur from the left lead $L$ to the right lead $R$, no matter what the initial and final states of the dots are. Only the terms proportional to $c^\dagger_{Rk\sigma} c_{Lk'\sigma'}$ will then give a contribution to this amplitude while we will have to sum over all the possible initial and final configurations of the dot system.
The current is then calculated as the neat difference between the charge transported from the left to the right lead and that transported from right to left:

$$I = e\left[\Gamma_{RL} - \Gamma_{LR}\right]. \tag{3.19}$$

The crucial quantity to be studied is the differential conductance, which is given by the derivative of the current with respect to the bias voltage $\frac{dI}{dV}$. The study of a differential quantity, rather then the classical ratio $G = \frac{I}{V}$, allows the study of the highly non-linear effects entering cotunneling. At the end of this section we will be able to plot the differential conductance dependence on bias voltage for the different systems previously considered. We will see that a rich physics arise in the most complicated case of a triple dot.

### 3.2.1. Double dots

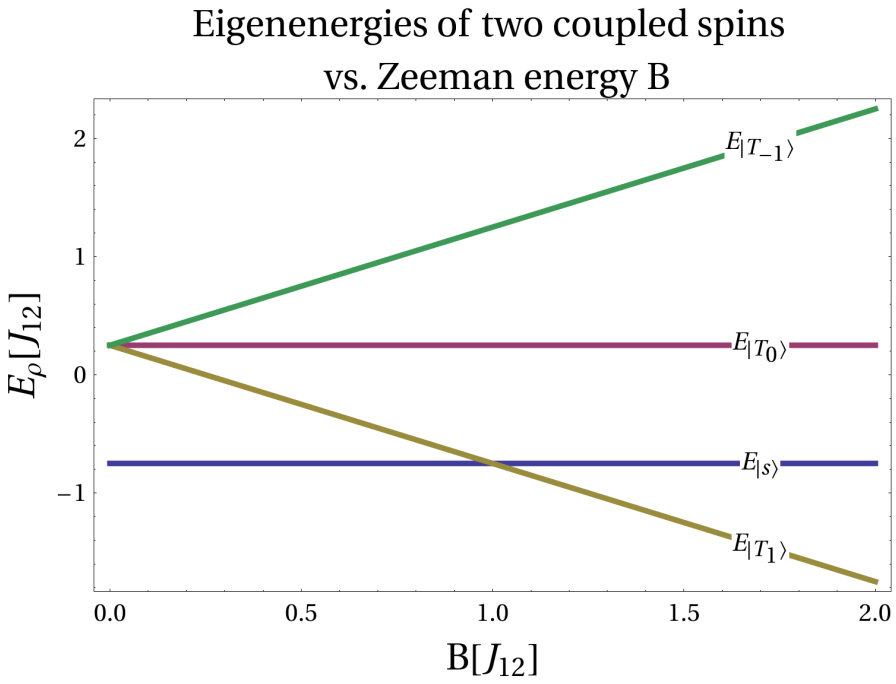


Figure 3.9.: Eigenvalues of the bare Hamiltonian of a double dot (singlet and triplet energies) plotted against the the Zeeman energy $B$. Both the Zeeman term $B$ and the eigenenergies $E_\rho$ of the singlet and the triplet states are in unit of $J_{12}$. At $\frac{B}{J_{12}} = 1$ a crossing from a singlet to a triplet ground state can be observed.

For the vertical double dot systems of Subsections 3.1.1, 3.1.2, 3.1.4 and the lateral double dot

of 3.1.3 the unperturbed Hamiltonian has the same form:

$$H_0 = \sum_{i=\{1,2\},\sigma} \varepsilon_{di} d^\dagger_{i\sigma} d_{i\sigma} + J_{12}\vec{S}_1 \cdot \vec{S}_2 - \vec{B} \cdot (\vec{S}_1 + \vec{S}_2) \tag{3.20}$$

where we have called $\vec{S}_1$ what is called $\vec{S}_u$ in the vertical dot and $\vec{S}_L$ in the lateral dot and $\vec{S}_2$ what is $\vec{S}_l$ in the vertical dot and $\vec{S}_R$ in the lateral one. Notice that this change in the name assigned to the dots does not carry any physical meaning. All the operators mentioned are simply spin operators, which have been labeled in different ways to distinguish them inside the central region.
In 3.20 an external magnetic field is present. The effect of such field is to change the single-particle energy of the electrons because of the interaction between the field and the electron spin (Zeeman term). If the field is strong enough, it can allow a transition to a different ground state in the double-dot (Figure 3.9).
By rewriting

$$\vec{S}_1 \cdot \vec{S}_2 = \frac{S_1^+ S_2^- + S_1^- S_2^+}{2} + S_1^z S_2^z \tag{3.21}$$

and assuming the magnetic field to point in the $z$-direction, one can rewrite the Hamiltonian in matrix form in the single-spin basis $\{|\uparrow\uparrow\rangle, |\uparrow\downarrow\rangle, |\downarrow\uparrow\rangle, |\downarrow\downarrow\rangle\}$:

$$H_0 = \sum_{i=\{1,2\},\sigma} \varepsilon_{di} d^\dagger_{i\sigma} d_{i\sigma} + \begin{pmatrix} \frac{1}{4}(-4B + J_{12}) & 0 & 0 & 0 \\ 0 & -\frac{J_{12}}{4} & \frac{J_{12}}{2} & 0 \\ 0 & \frac{J_{12}}{2} & -\frac{J_{12}}{4} & 0 \\ 0 & 0 & 0 & \frac{1}{4}(4B + J_{12}) \end{pmatrix}. \tag{3.22}$$

This is diagonalized by the same basis that also diagonalizes the total spin, namely the eigenvectors

$$\begin{cases} |\, s\rangle = \frac{|\uparrow\downarrow\rangle - |\downarrow\uparrow\rangle}{2} \\ |\, T_0\rangle \\ |\, T_{+1}\rangle \\ |\, T_{-1}\rangle \end{cases} \tag{3.23}$$

which have eigenenergies $\{-\frac{3J_{12}}{4}, \frac{J_{12}}{4}, \frac{1}{4}(-4B + J_{12}), \frac{1}{4}(4B + J_{12})\}$, respectively.

The current can now be calculated. We start by evaluating the transition amplitude from the left to the right lead through (3.18). The final state of the leads is then given by $|\, f_{leads}\rangle = c^\dagger_{Rk'\sigma'} c_{Lk\sigma} |\, i_{leads}\rangle$, so that the transition amplitude can be rewritten as follows:

$$\Gamma_{RL} = 2\pi \sum_{k,k',\sigma,\sigma',\rho,\rho'} |\langle i_{leads}; \rho' |\, c^\dagger_{Lk\sigma} c_{Rk'\sigma'} h_{RL} |\, i_{leads}; \rho\rangle|^2 W_{i_{leads}} n_\rho \delta(\varepsilon_{k'} + E_{\rho'} - \varepsilon_k - E_\rho) \tag{3.24}$$

where $h_{RL}$ is the part of the Hamiltonian contributing to electron transport from the left to the right lead, $\rho, \rho'$ describe the initial and final states of the central region as given in the eigenstate basis of the unperturbed Hamiltonian, (3.23), and the occupation distribution of the initial states of the leads $W_{i_{leads}}$ and the central region $n_\rho$ have to be considered.

Let us consider the vertical double dot with both the dots coupled to the leads and tunneling between the dots (Subsection 3.1.4). All the other two-dots systems considered in Section 3.1 can then be obtained from this one by taking some of the tunneling couplings to be zero.
For the considered system transport from one lead to the other can either be obtained by a

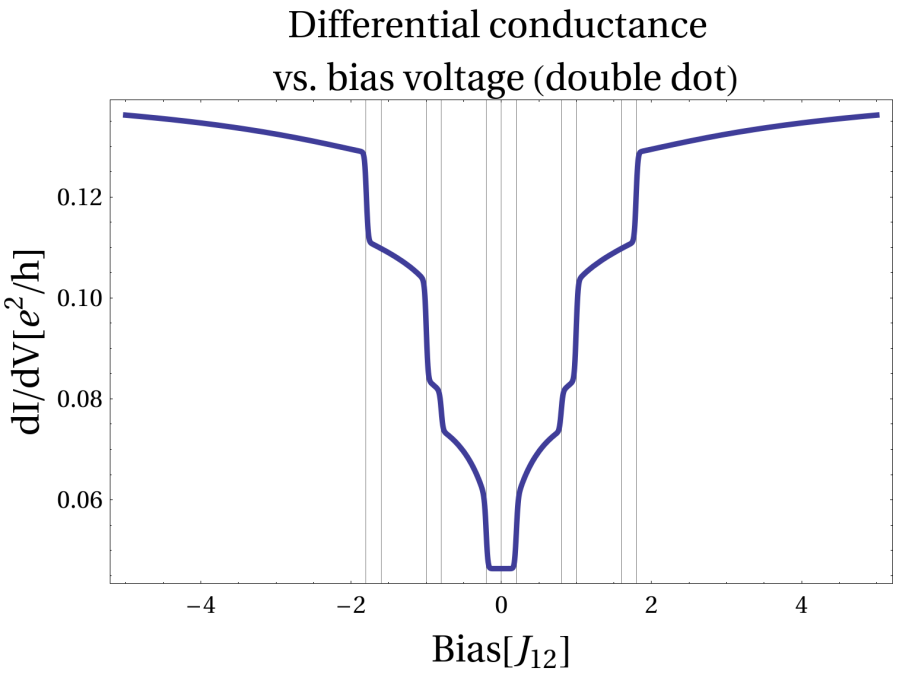


(a)

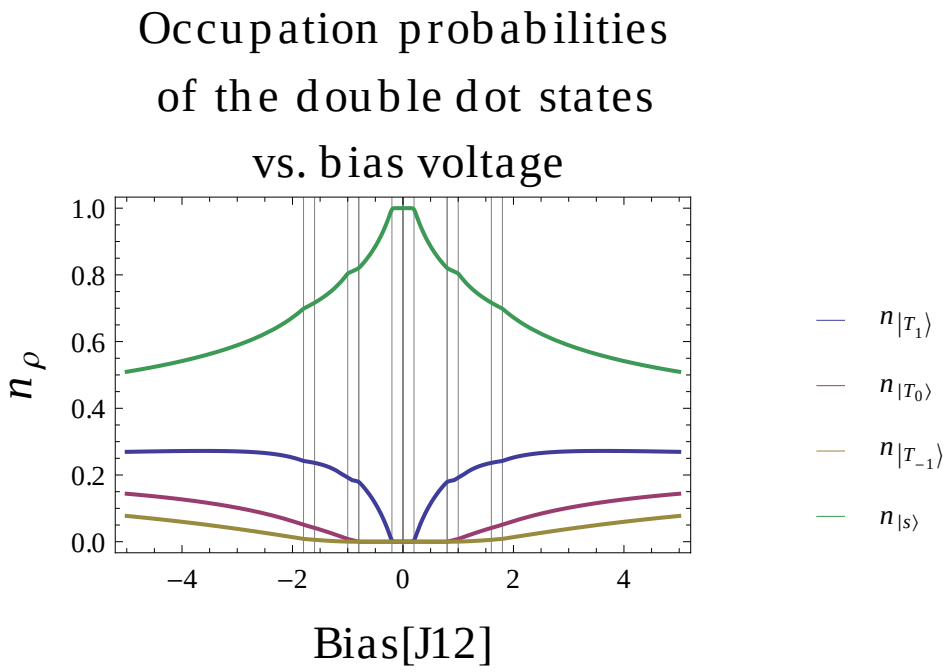


(b)

Figure 3.10.: (a)Typical cotunneling differential conductance for a double quantum dot. At values of the bias voltage corresponding to the excitation energies (marked as vertical lines in the plot), inelastic cotunneling peaks appear in the differential conductance. (b) Occupation probabilities of the different two-spin states of the double dot. Once again the vertical lines correpond to the excitation energies (i.e. the energy differences) between the different two-spin states of the double dot system. Here we used $B = 0.8$, $t = 0.008$, $t_{1R} = 0.8$, $t_{1L} = 0.57$, $t_{2R} = 0.34$, $t_{2L} = 0.68$, $t_H = 0.5$, $U = 10$, all in units of $J_{12}$. The differential conductance $dI/dV$ is expressed as a ratio $dI/dV \to \frac{dI/dV}{2\pi\nu t_{1R} t_{1L}/U}$ and it is in units of $e^2/h$.

second-order process involving just one of the dots or through an intermediate virtual transition between the dots (third-order process). For a sketch of these two possibilities see Figure 3.6. The operators describing the second order spin-flip processes are the usual spin operators of the dots ($\vec{S}_1$ and $\vec{S}_2$), while the potential scattering term, which leaves the total spin of the central region invariant must be proportional to the identity matrix ($\delta_{\rho\rho'}$). The third-order process are given by the the exchange operator $\vec{T}_{RL}$ and the potential scattering term $P$. $\Gamma_{RL}$ then becomes:

$$\begin{aligned}\Gamma_{RL} = 2\pi \sum_{\substack{i_{leads}\\ k,k',q,q'\\ \sigma,\sigma',\eta,\eta'}} \sum_{\rho,\rho'} \Big| \langle i_{leads} \mid c^\dagger_{Lk\sigma} c_{Rk'\sigma'} c^\dagger_{Rq\eta} c_{Lq'\eta'} \mid i_{leads} \rangle \\ \left[ \sum_i \tau^i_{\eta\eta'} \left( \sum_d J_{d,RL} S^i_{d,\rho'\rho} + \frac{J_{1R,2L}}{2} (T^i_{1R,2L})_{\rho'\rho} + \frac{J_{2R,1L}}{2} (T^i_{2R,1L})_{\rho'\rho} \right) \right. \\ \left. + \tau^0_{\eta\eta'} \left( \sum_d \frac{W_{d,RL}}{2} \delta_{\rho'\rho} + \frac{W_{1R,2L}}{2} P_{\rho'\rho} + \frac{W_{2R,1L}}{2} P_{\rho'\rho} \right) \right] \Big|^2 W_{i_{leads}} n_\rho \delta(\varepsilon_{k'} + E_{\rho'} - \varepsilon_k - E_\rho).\end{aligned} \tag{3.25}$$

Looking just at the conduction-electron part of the equation, one then ends up with:

$$\begin{aligned}&\sum_{\substack{i_{leads}\\ q,q',k,k'\\ \sigma,\sigma'}} \left| \langle i_{leads} \mid c^\dagger_{Lk\sigma} c_{Rk'\sigma'} c^\dagger_{Rq\eta} c_{Lq'\eta'} \mid i_{leads} \rangle \right|^2 W_{i_{leads}} \delta(\varepsilon_{k'} + E_{\rho'} - \varepsilon_k - E_\rho) = \\ &= \sum_{\substack{i_{leads}\\ q,q',k,k'\\ \sigma,\sigma'}} \left| \delta_{k'q} \delta_{\sigma'\eta} \delta_{kq'} \delta_{\sigma\eta'} n_{Lq'\eta'} \left(1 - n_{Rq\eta}\right) \right|^2 W_{i_{leads}} \delta(\varepsilon_{k'} + E_{\rho'} - \varepsilon_k - E_\rho) \\ &= \sum_{\substack{i_{leads}\\ q,q'}} n_{Lq'\eta'} \left(1 - n_{Rq\eta}\right) W_{i_{leads}} \delta(\varepsilon_q + E_{\rho'} - \varepsilon_{q'} - E_\rho) \\ &= \sum_{q,q'} n_F(\varepsilon_q - \mu_L) \left(1 - n_F(\varepsilon_{q'} - \mu_R)\right) \delta(\varepsilon_q + E_{\rho'} - \varepsilon_{q'} - E_\rho) \\ &= \nu_L \nu_R \int d\varepsilon \int d\varepsilon' n_F(\varepsilon - \mu_L) \left(1 - n_F(\varepsilon' - \mu_R)\right) \delta(\varepsilon' + E_{\rho'} - \varepsilon - E_\rho) \\ &= \nu_L \nu_R \int d\varepsilon \int d\varepsilon' n_F(\varepsilon - \mu_L) \left(1 - n_F(\varepsilon + E_\rho - E_{\rho'} - \mu_R)\right)\end{aligned} \tag{3.26}$$

where I defined the density of states in the two leads as $\nu_L$ and $\nu_R$ and I assumed them to be uniform in the energy range of interest. I now use the following two relations:

$$\begin{aligned}&n_F(e_1)(1 - n_F(e_2)) = n_B(e_1 - e_2)[n_F(e_2) - n_F(e_1)] \\ &\int de (n_F(e) - n_F(e + \omega)) = \omega\end{aligned} \tag{3.27}$$

with $e_1 = \varepsilon - \mu_L$ and $e_2 = \varepsilon + E_\rho - E_{\rho'} - \mu_R$ so that my $\omega$ becomes $\omega = E_{\rho'} - E_\rho - (\mu_L - \mu_R)$. The lead part of the transition amplitudes then becomes $n_B(\Delta_{\rho'\rho} - eV)(\Delta_{\rho'\rho} - eV)$, where the bias voltage is defined as $eV := \mu_L - \mu_R$ and the energy difference between two states of the total spin, e.g. $\mid s\rangle$ and $\mid T_{+1}\rangle$, is called $\Delta_{\rho'\rho} = E_{\rho'} - E_\rho$.

Defining:

$$(\mathbf{T}^{RL}_{\rho'\rho})^i := \sum_d J_{d,RL} S^i_{d,\rho'\rho} + \frac{J_{1R,2L}}{2}(T^i_{1R,2L})_{\rho'\rho} + \frac{J_{2R,1L}}{2}(T^i_{2R,1L})_{\rho'\rho}$$
$$\mathbf{P}^{RL}_{\rho'\rho} := \sum_d \frac{W_{d,RL}}{2}\delta_{\rho'\rho} + \frac{W_{1R,2L}}{2}P_{\rho'\rho} + \frac{W_{2R,1L}}{2}P_{\rho'\rho} \tag{3.28}$$

the transition amplitude then becomes:

$$\begin{aligned}\Gamma_{RL} &= 2\pi\nu_L\nu_R \sum_{\rho,\rho'}\sum_{\eta,\eta'} n_B(\Delta_{\rho'\rho}-eV)(\Delta_{\rho'\rho}-eV)\left|\sum_i \tau^i_{\eta\eta'}(\mathbf{T}^{RL}_{\rho'\rho})^i + \tau^0_{\eta\eta'}\mathbf{P}^{RL}_{\rho'\rho}\right|^2 n_\rho \\ &= 2\pi\nu_L\nu_R \sum_{\rho,\rho'} n_B(\Delta_{\rho'\rho}-eV)(\Delta_{\rho'\rho}-eV)\left\{2\sum_i (\mathbf{T}^{RL}_{\rho'\rho})^{i*}(\mathbf{T}^{RL}_{\rho'\rho})^i + 2\left|\mathbf{P}^{RL}_{\rho'\rho}\right|^2\right\} n_\rho \end{aligned} \tag{3.29}$$

where I used $\tau^*_{\eta\eta'} = \tau_{\eta'\eta}$ because of the hermitianity of the Pauli matrices. Notice that the sum $\sum_{\eta,\eta'}|\tau^0_{\eta\eta'}\mathbf{P}^{RL}_{\rho'\rho}|^2$ gives $\sum_{\eta,\eta'}\delta_{\eta\eta'}|\mathbf{P}^{RL}_{\rho'\rho}|^2 = \sum_{\eta=\uparrow,\downarrow}|\mathbf{P}^{RL}_{\rho'\rho}|^2 = 2|\mathbf{P}^{RL}_{\rho'\rho}|^2$ (because there are 2 possible spin states) and $Tr[\tau^j\tau^i] = Tr[i\varepsilon_{jik}\tau^k + \delta_{ji}] = 2\delta_{ji}$. In a similar way the expression for the transition amplitude from the right to the left lead is seen to be:

$$\Gamma_{LR} = 2\pi\nu_L\nu_R \sum_{\rho,\rho'} n_B(\Delta_{\rho'\rho}+eV)(\Delta_{\rho'\rho}+eV)\left\{2\sum_i (\mathbf{T}^{LR}_{\rho'\rho})^{i*}(\mathbf{T}^{LR}_{\rho'\rho})^i + 2\left|\mathbf{P}^{LR}_{\rho'\rho}\right|^2\right\} n_\rho \tag{3.30}$$

where we have defined $\mathbf{T}^{LR}_{\rho'\rho}$ and $\mathbf{P}^{LR}_{\rho'\rho}$ as the matrix elements obtained by $\mathbf{T}^{RL}_{\rho'\rho}$ and $\mathbf{P}^{RL}_{\rho'\rho}$ respectively, through the substitution $L \leftrightarrow R$. It is worth notice that $\mathbf{T}^{LR}_{\rho'\rho} = \mathbf{T}^{RL}_{\rho'\rho}$, being the following relations valid:

$$\begin{aligned} T_{1R,2L} &= \vec{S}_1 + \vec{S}_2 - 2i(\vec{S}_1 \times \vec{S}_2) = T_{1L,2R} \\ T_{2R,1L} &= \vec{S}_1 + \vec{S}_2 + 2i(\vec{S}_1 \times \vec{S}_2) = T_{2L,1R} \end{aligned} \tag{3.31}$$

as observed in Subsection 3.1.4.
The current can then be written in the following way:

$$\begin{aligned} I &= e(\Gamma_{RL} - \Gamma_{LR}) \\ &= e2\pi\nu_L\nu_R \sum_{\substack{k,k' \\ \sigma,\sigma',\rho,\rho'}} \Big[|\langle i_{leads};\rho' \mid c^\dagger_{Lk\sigma}c_{Rk'\sigma'}h_{RL} \mid i_{leads};\rho\rangle|^2 W_{i_{leads}} n_\rho \delta(\varepsilon_{k'} + E_{\rho'} - \varepsilon_k - E_\rho) \\ &\quad - |\langle i_{leads};\rho \mid c^\dagger_{Rk'\sigma'}c_{Lk\sigma}h_{LR} \mid i_{leads};\rho'\rangle|^2 W_{i_{leads}} n_{\rho'} \delta(\varepsilon_k + E_\rho - \varepsilon_{k'} - E_{\rho'})\Big] \\ &= e2\pi\nu_L\nu_R \sum_{\rho,\rho'} (\Delta_{\rho'\rho} - eV)\left[n_B(\Delta_{\rho'\rho} - eV)n_\rho + n_B(-\Delta_{\rho'\rho} + eV)n_{\rho'}\right]\left|\mathbf{M}^{RL}_{\rho'\rho}\right|^2 \\ &= e2\pi\nu_L\nu_R \sum_{\rho,\rho'} (\Delta_{\rho'\rho} - eV)\left[n_B(\Delta_{\rho'\rho} - eV)n_\rho - (1 + n_B(\Delta_{\rho'\rho} - eV))n_{\rho'}\right]\left|\mathbf{M}^{RL}_{\rho'\rho}\right|^2 \end{aligned} \tag{3.32}$$

where I defined

$$\left|\mathbf{M}^{RL}_{\rho'\rho}\right|^2 := 2\sum_i (\mathbf{T}^{RL}_{\rho'\rho})^{i*}(\mathbf{T}^{RL}_{\rho'\rho})^i + 2\left|\mathbf{P}^{RL}_{\rho'\rho}\right|^2 \tag{3.33}$$

and I used that $h_{LR} = h_{RL}^{\dagger}$ and the fact that when I look at the processes from the right to the left leads the initial state corresponds to the final states of the opposite processes (from left to right).
In order to calculate explicitly the final expression one needs to know the occupation probabilities $n_\rho$ for the different dot states. Following a standard rate equation approach one can write the following:

$$\begin{aligned}
\dot{n}_{+1} &= \Gamma_{+1,0} n_0 + \Gamma_{+1,s} n_s - \Gamma_{0,+1} n_{+1} - \Gamma_{s,+1} n_{+1} \\
\dot{n}_{-1} &= \Gamma_{-1,0} n_0 + \Gamma_{-1,s} n_s - \Gamma_{0,-1} n_{-1} - \Gamma_{s,-1} n_{-1} \\
\dot{n}_0 &= \Gamma_{0,+1} n_{+1} + \Gamma_{0,-1} n_{-1} + \Gamma_{0,s} n_s - \Gamma_{+1,0} n_0 - \Gamma_{-1,0} n_0 - \Gamma_{s,0} n_0 \\
\dot{n}_s &= \Gamma_{s,+1} n_{+1} + \Gamma_{s,-1} n_{-1} + \Gamma_{s,0} n_0 - \Gamma_{+1,s} n_s - \Gamma_{-1,s} n_s - \Gamma_{0,s} n_s.
\end{aligned} \tag{3.34}$$

(3.34) can be rewritten in a more compact form:

$$\dot{n}_\rho = \sum_{\rho'} \left( \Gamma_{\rho\rho'} n_{\rho'} - \Gamma_{\rho'\rho} n_\rho \right) \tag{3.35}$$

which basically states that the change in the occupation of state $\rho$ is given by the difference between the filling (i.e. $\sum_{\rho'} \Gamma_{\rho\rho'} n_{\rho'}$) and the emptying (i.e. $\sum_{\rho'} \Gamma_{\rho'\rho} n_\rho$) of that state. Looking for stationary solutions, i.e. setting $\dot{n}_\rho = 0$, and imposing the normalization condition:

$$\sum_\rho n_\rho = n_{+1} + n_{-1} + n_0 + n_s = 1. \tag{3.36}$$

one can solve the rate equations and get the bias dependence of the occupation of each state.
The coefficients $\Gamma_{\rho'\rho}$ can again be calculated using Fermi Golden Rule. This time the initial and final states of the central region will be fixed, while jumping to any lead will be allowed:

$$\Gamma_{\rho'\rho} = \sum_{\alpha\alpha'} \Gamma_{\rho'\rho}^{\alpha\alpha'} = \Gamma_{\rho'\rho}^{RL} + \Gamma_{\rho'\rho}^{LR} + \Gamma_{\rho'\rho}^{RR} + \Gamma_{\rho'\rho}^{LL}. \tag{3.37}$$

The following is found for the transition coefficients:

$$\Gamma_{\rho'\rho}^{RL} = 2\pi\nu_L\nu_R \sum_{\substack{i_{leads} \\ f_{leads}}} |\langle f_{leads}; \rho' \mid H \mid i_{leads}; \rho \rangle|^2 W_{i_{leads}} \delta(E_f - E_i). \tag{3.38}$$

In a way similar to the above calculation for $\Gamma^{RL}$ and $\Gamma^{LR}$, one finds the following expression:

$$\begin{aligned}
\Gamma_{RL}^{\rho'\rho} &= 2\pi\nu_L\nu_R n_B(\Delta_{\rho'\rho} - eV)(\Delta_{\rho'\rho} - eV) \left| \mathbf{M}_{\rho'\rho}^{RL} \right|^2 \\
\Gamma_{LR}^{\rho'\rho} &= 2\pi\nu_L\nu_R n_B(\Delta_{\rho'\rho} + eV)(\Delta_{\rho'\rho} + eV) \left| \mathbf{M}_{\rho'\rho}^{LR} \right|^2 \\
\Gamma_{\alpha\alpha}^{\rho'\rho} &= 2\pi\nu_\alpha\nu_\alpha n_B(\Delta_{\rho'\rho})(\Delta_{\rho'\rho}) \left| \mathbf{M}_{\rho'\rho}^{\alpha\alpha} \right|^2.
\end{aligned} \tag{3.39}$$

Solving numerically the Master equations (3.34) one obtains solutions of the kind in Figure 3.10. Note that the differential conductance is always symmetric in the bias voltage, with step-like increasing at values of the bias corresponding to the energy required to fill the higher-energy states. These steps correspond to inelastic cotunneling processes. The cusp at the threshold energies is due to the effect of the non-equilibrium ridistribution of the occupation probabilities before the saturation value is reached at larger bias. This effect can also show up as a monotonous increasing after the inelastic step up to the saturation value. The appearence of either a cusp or a an increase really depends on the details of the non-equilibrium occupation probability. More details on this can be found in [1].

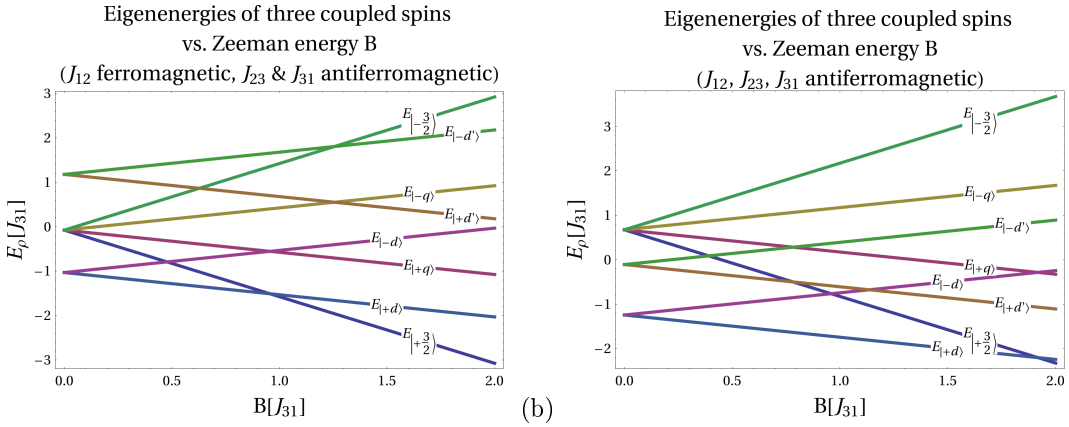


(a) (b)

Figure 3.11.: Eigenvalues of the bare Hamiltonian of a triangular triple dot plotted against the Zeeman energy $B$. This and the eigenenergies are in units of $J_{31}$. In (a) all the inter-dot couplings $J_{12}$, $J_{23}$ and $J_{31}$ are antiferromagnetic ($J_{12} = 1.5J_{31}$ and $J_{23} = 0.2J_{31}$), in (b) $J_{12}$ is ferromagnetic and $J_{31}$, $J_{23}$ are antiferromagnetic ($J_{12} = -1.5J_{31}$ and $J_{23} = 0.2J_{31}$). Notice that in (a), where one of the couplings is ferromagnetic, the low energy states at zero magnetic field ($B = 0$) are a degenerate doublet and a degenerate quartet, while in (b), where all the couplings are anitferromagnetic, the low energy states at zero field are two degenerate doublets.

### 3.2.2. Triangular triple dot

Let us now turn to the case of the triangular triple dot (TTD) of Subsection 3.1.5. The unperturbed Hamiltonian now depends on the three inter-dot couplings $J_{12}$, $J_{23}$ and $J_{31}$:

$$H_0 = \sum_{\alpha k\sigma} \xi_{\alpha k} c^\dagger_{\alpha k\sigma} c_{\alpha k\sigma} + J_{12}\vec{S}_L \cdot \vec{S}_C + J_{23}\vec{S}_C \cdot \vec{S}_R + J_{13}\vec{S}_L \cdot \vec{S}_R - \vec{B} \cdot (\vec{S}_L + \vec{S}_C + \vec{S}_R). \quad (3.40)$$

This is diagonalized by the eigenvectors:

$$\begin{cases} |+\tfrac{3}{2}\rangle \\ |+q\rangle \\ |-q\rangle \\ |-\tfrac{3}{2}\rangle \\ |+d\rangle := a\,|\uparrow\downarrow\uparrow\rangle + b\,|\uparrow\uparrow\downarrow\rangle + c\,|\downarrow\uparrow\uparrow\rangle \\ |+d'\rangle := d\,|\uparrow\downarrow\uparrow\rangle + f\,|\uparrow\uparrow\downarrow\rangle + g\,|\downarrow\uparrow\uparrow\rangle \\ |-d\rangle := l\,|\uparrow\downarrow\downarrow\rangle + m\,|\downarrow\downarrow\uparrow\rangle + n\,|\downarrow\uparrow\downarrow\rangle \\ |-d'\rangle := o\,|\uparrow\downarrow\downarrow\rangle + p\,|\downarrow\downarrow\uparrow\rangle + q\,|\downarrow\uparrow\downarrow\rangle \end{cases} \quad (3.41)$$

where the last four are some linear combinations, with appropriate coefficients $a, b, c, d, f, g, l, m, n, o, p, q$, of the states with spin z-component $1/2$ and $-1/2$ of three combined spins. These coefficients are in general some complicated functions of the internal couplings $J_{12}$, $J_{23}$ and $J_{31}$. With some abuse of notation I call $|+d\rangle$, $|-d\rangle$, $|+d'\rangle$, $|-d'\rangle$ the last states, meaning that $|+d\rangle$ and $|-d\rangle$ have lower energies then $|+d'\rangle$ and $|-d'\rangle$. From now on these names will refer to the combinations of total spin eigenstates that diagonalize the bare Hamiltonian.

The respective eigenvalues are given by:

$$\begin{cases} \frac{1}{4}(-6B + J_{12} + J_{23} + J_{31}) \\ \frac{1}{4}(-2B + J_{12} + J_{23} + J_{31}) \\ \frac{1}{4}(2B + J_{12} + J_{23} + J_{31}) \\ \frac{1}{4}(6B + J_{12} + J_{23} + J_{31}) \\ \frac{1}{4}\left(-2B - J_{12} - J_{23} - J_{31} - 2\sqrt{J_{12}^2 - J_{12}J_{23} + J_{23}^2 - J_{12}J_{31} - J_{23}J_{31} + J_{31}^2}\right) \\ \frac{1}{4}\left(2B - J_{12} - J_{23} - J_{31} - 2\sqrt{J_{12}^2 - J_{12}J_{23} + J_{23}^2 - J_{12}J_{31} - J_{23}J_{31} + J_{31}^2}\right) \\ \frac{1}{4}\left(-2B - J_{12} - J_{23} - J_{31} + 2\sqrt{J_{12}^2 - J_{12}J_{23} + J_{23}^2 - J_{12}J_{31} - J_{23}J_{31} + J_{31}^2}\right) \\ \frac{1}{4}\left(2B - J_{12} - J_{23} - J_{31} + 2\sqrt{J_{12}^2 - J_{12}J_{23} + J_{23}^2 - J_{12}J_{31} - J_{23}J_{31} + J_{31}^2}\right) \end{cases} \tag{3.42}$$

The eigenvalues of the bare Hamiltonian (3.42) are plotted in Figure 3.11 as a function of the applied magnetic field. Notice that, being the bare Hamiltonian dependent on the three inter-dot couplings $J_{12}$, $J_{23}$ and $J_{31}$, the ground state depends on the relative values of these couplings. When all the three couplings are antiferromagnetic (i.e. positive), the zero-field spectrum has two low-energy doublets and a high-energy quartet. On the contrary, choosing $J_{12}$ to be ferromagnetic, the spectrum at $B = 0$ is composed of a low-energy doublet, followed by the quartet at higher energies and the second doublet at even higher energies.

Notice that the choice $J_{31} = J_{23}$ allows us to rewrite the eigenvectors of (3.40) in a much simpler way:

$$\begin{cases} |+\tfrac{3}{2}\rangle \\ |+q\rangle \\ |-q\rangle \\ |-\tfrac{3}{2}\rangle \\ |+d\rangle := \frac{1}{\sqrt{2}}\left(-|\uparrow\downarrow\uparrow\rangle + |\downarrow\uparrow\uparrow\rangle\right) \\ |+d'\rangle := \frac{1}{\sqrt{3}}\left(\frac{1}{\sqrt{2}}|\uparrow\downarrow\uparrow\rangle - \sqrt{2}\,|\uparrow\uparrow\downarrow\rangle + \frac{1}{\sqrt{2}}|\downarrow\uparrow\uparrow\rangle\right) \\ |-d\rangle := \frac{1}{\sqrt{2}}\left(|\uparrow\downarrow\downarrow\rangle + |\downarrow\uparrow\downarrow\rangle\right) \\ |-d'\rangle := \frac{1}{\sqrt{3}}\left(\frac{1}{\sqrt{2}}|\uparrow\downarrow\downarrow\rangle - \sqrt{2}\,|\downarrow\downarrow\uparrow\rangle + \frac{1}{\sqrt{2}}|\downarrow\uparrow\downarrow\rangle\right). \end{cases} \tag{3.43}$$

Observe that the coefficients are now independent of the internal couplings $J_{12}$, $J_{23}$ and $J_{31}$. The respective eigenvalues now simplify to:

$$\begin{cases} \frac{1}{4}(-6B + J_{12} + 2J_{23}) \\ \frac{1}{4}(-2B + J_{12} + 2J_{23}) \\ \frac{1}{4}(2B + J_{12} + 2J_{23}) \\ \frac{1}{4}(6B + J_{12} + 2J_{23}) \\ \frac{1}{4}(-2B - 3J_{12}) \\ \frac{1}{4}(2B - 3J_{12}) \\ \frac{1}{4}(-2B + J_{12} - 4J_{23}) \\ \frac{1}{4}(2B + J_{12} - 4J_{23}) \end{cases} \tag{3.44}$$

We now study the behavior of the differential conductance against the bias voltage. Let us start by noticing that the formula (3.32) for the current and the rate equation (3.35) remain valid

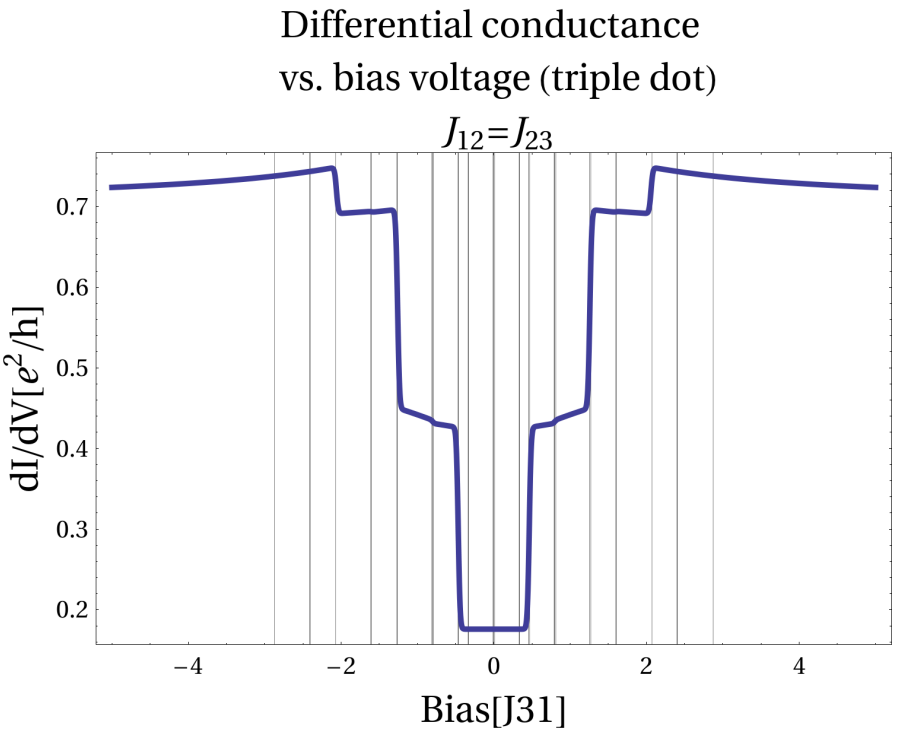


(a)

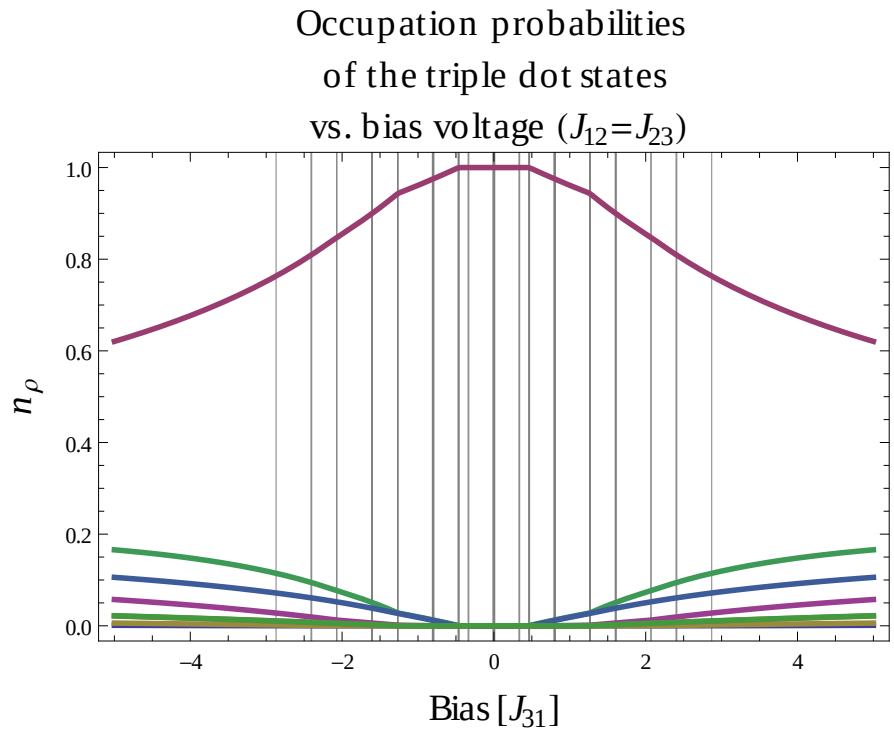


(b)

Figure 3.12.: Differential conductance and state occupation probabilities of a triangular triple dot for the specific choice of inter-dot couplings $J_{12} = J_{23}$. The differential conductance (a) is symmetric in bias. (b) shows the occupation probabilities of the different basis states.

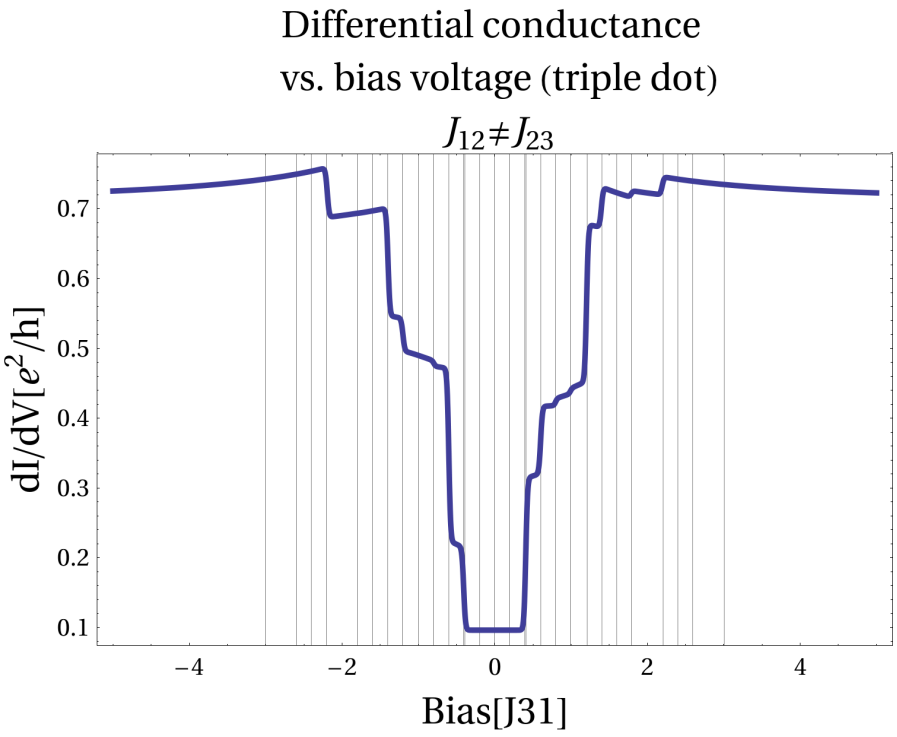


(a)

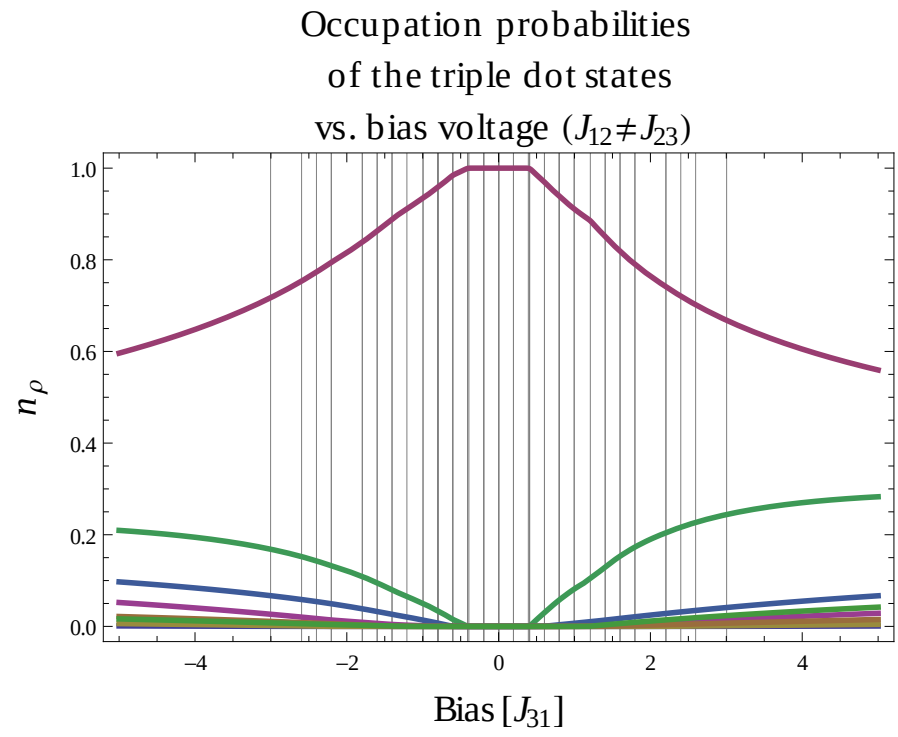


(b)

Figure 3.13.: Differential conductance and state occupation probabilities of a triangular triple dot for a generic choice of inter-dot couplings $J_{12} \neq J_{23}$. The differential conductance is asymmetric in bias (a). (b) shows the occupation probabilities of the different basis states.

for the three-dot system, the only difference being that the operators (3.33) are now written in the three-spin basis (3.41). Being this basis dependent on the inter-dot couplings $J_{12}$, $J_{23}$ and $J_{31}$, the operators (3.33) will also depend on these quantities. One can then observe that the $\sum_i T^{i*}_{RL} T^i_{RL}$ and $\sum_i T^{i*}_{LR} T^i_{LR}$ operators are not symmetric. This has some strong consequence in the calculation of the occupation probabilities and the conductance. From Figure 3.13 we see, in fact, that the differential conductance is asymmetric in bias voltage. This comes directly from the observation on the asymmetry of the $\vec{T}_{RL}$ and $\vec{T}_{LR}$ operators. When calculating the transition amplitude from the left to the right lead $\Gamma^{RL}_{\rho'\rho}$ each term of the sum on $\rho$ and $\rho'$ correspond to the term with the same fixed $\rho$ and $\rho'$ in $\Gamma^{LR}_{\rho'\rho}$, meaning that the first is the transition amplitude from a state $\rho$ to a state $\rho'$ in the dot when the bias is $V$, while the second is the amplitude between the same initial and final states in the dot when the bias is opposite, i.e. $-V$. We know that $\mathbf{T}^{RL}_{\rho'\rho} = \left[\left(\mathbf{T}^{RL}\right)^\dagger\right]^*_{\rho\rho'} = \left[\mathbf{T}^{LR}\right]^*_{\rho\rho'}$ because the Hamiltonian is hermitian, and we can rewrite the latter as $\left[\mathbf{T}^{LR}\right]^*_{\rho\rho'} = \left(\mathbf{T}^{LR}\right)^\dagger_{\rho'\rho}$. This last expression is in general different from $\left(\mathbf{T}^{LR}\right)^*_{\rho'\rho}$, being the $\vec{T}_{LR}$ operators not symmetric. As a consequence, the two symmetric points at fixed $V$ and $-V$ give different contributions to the current (and consequently also to the differential conductance). Notice that, if the operators $\mathbf{T}^{LR}$ and $\mathbf{T}^{RL}$ were symmetric, the equality $\left(\mathbf{T}^{LR}\right)^\dagger_{\rho'\rho} = \left[\left(\mathbf{T}^{LR}\right)^*\right]^T_{\rho'\rho} = \left(\mathbf{T}^{LR}\right)^*_{\rho'\rho}$ holds and consequently also $\mathbf{T}^{RL}_{\rho'\rho} = \left(\mathbf{T}^{LR}\right)^*_{\rho'\rho}$. Since in the transition amplitude what really matters is the product $\left(\mathbf{T}^{LR}_{\rho'\rho}\right)^{i*}\left(\mathbf{T}^{LR}_{\rho'\rho}\right)^i$, the fact that the last equality holds taking the complex conjugate of $\mathbf{T}^{LR}_{\rho'\rho}$ rather then $\mathbf{T}^{LR}_{\rho'\rho}$ itself does not matter. If the $\vec{T}_{RL}$ and $\vec{T}_{LR}$ operators were symmetric we would then have a symmetric plot of the differential conductance.

As a matter of fact one can see that the asymmetry of the $\sum_i T^{i*}_{RL} T^i_{RL}$ and $\sum_i T^{i*}_{LR} T^i_{LR}$ operators is due to the specific choice of basis states. If one considers the very special case $J_{12} = J_{23}$, then the last operators turn out to be symmetric and the differential conductance is also symmetric (Figure 3.12). From a physical point of view these conclusions seem reasonable, when a symmetry argument is carried out. Remember in fact that transport from one lead to the other can only occur through the right and left dots, while the central dot just assist to the process, without influencing it directly. The only way in which the latter dot plays a role, is through the internal couplings $J_{12}$ and $J_{23}$ of the unperturbed dot Hamiltonian (3.40). When we keep the symmetry of the system by choosing $J_{12} = J_{23}$ the conductance is then symmetric in bias. When we choose $J_{12} \neq J_{23}$ and thus break the symmetry, the conductance is asymmetric.

Just to better understand the form of the operators we are dealing with, let us report them here. In the double dot case the $\sum_i T^{i*}_{RL} T^i_{RL}$ operator written in the singlet-triplet states is:

$$\sum_i T^{i*}_{RL} T^i_{RL} = \begin{pmatrix} 0 & 1 & 1 & 1 \\ 1 & 0 & 1 & 1 \\ 1 & 1 & 1 & 0 \\ 1 & 1 & 0 & 1 \end{pmatrix}. \tag{3.45}$$

In the case of the triple dot, the sistuation is very different. Since the eigenvectors of the three-spin (bare) Hamiltonian (3.40) depend in general on the internal couplings $J_{12}$, $J_{23}$ and $J_{31}$, the entries of the matrix operator $\sum_i T^{i*}_{RL} T^i_{RL}$ will also depend on the internal couplings. For the specific (but completely random) choice $J_{12} = 0.86$, $J_{23} = 0.54$ and $J_{31} = 1$, $B = 0.8$ the

operator lokks like:

$$\sum_i T^{i*}_{RL} T^i_{RL} = \begin{pmatrix} 1 & 0 & 0.67 & 0 & 0 & 0.52 & 0 & 0.81 \\ 0 & 0.01 & 0.43 & 0.12 & 1.30 & 0.02 & 0.87 & 0.25 \\ 0.67 & 0.17 & 0.11 & 0.27 & 0.00 & 0.35 & 0.89 & 0.54 \\ 0 & 0.65 & 0.01 & 0.33 & 0.03 & 1.29 & 0.02 & 0.67 \\ 0 & 0.52 & 0 & 0.81 & 1 & 0 & 0.67 & 0 \\ 1.30 & 0.02 & 0.87 & 0.25 & 0 & 0.01 & 0.43 & 0.12 \\ 0 & 0.35 & 0.89 & 0.54 & 0.67 & 0.17 & 0.11 & 0.27 \\ 0.03 & 1.29 & 0.02 & 0.67 & 0 & 0.65 & 0.01 & 0.33 \end{pmatrix} \tag{3.46}$$

which is asymmetric. Choosing $J_{12} = J_{23}$, the eigenvectors of the bare Hamiltonian (3.40) happen to be independent of the internal couplings $J_{12}$, $J_{23}$ and $J_{31}$ and the operator $\sum_i T^{i*}_{RL} T^i_{RL}$ is given in this basis by:

$$\sum_i T^{i*}_{RL} T^i_{RL} = \begin{pmatrix} 1 & 0 & \frac{2}{3} & 0 & 0 & 1 & 0 & \frac{1}{3} \\ 0 & 0 & \frac{1}{3} & \frac{1}{3} & 1 & 0 & \frac{2}{3} & \frac{2}{3} \\ \frac{2}{3} & \frac{1}{3} & \frac{1}{9} & \frac{1}{9} & 0 & \frac{2}{3} & \frac{8}{9} & \frac{2}{9} \\ 0 & \frac{1}{3} & \frac{1}{9} & \frac{4}{9} & \frac{1}{3} & \frac{2}{3} & \frac{2}{9} & \frac{8}{9} \\ 0 & 1 & 0 & \frac{1}{3} & 1 & 0 & \frac{2}{3} & 0 \\ 1 & 0 & \frac{2}{3} & \frac{2}{3} & 0 & 0 & \frac{1}{3} & \frac{1}{3} \\ 0 & \frac{2}{3} & \frac{8}{9} & \frac{2}{9} & \frac{2}{3} & \frac{1}{3} & \frac{1}{9} & \frac{1}{9} \\ \frac{1}{3} & \frac{2}{3} & \frac{2}{9} & \frac{8}{9} & 0 & \frac{1}{3} & \frac{1}{9} & \frac{4}{9} \end{pmatrix}. \tag{3.47}$$

Notice that in this last case $\sum_i T^{i*}_{RL} T^i_{RL}$ is a symmetric operator. Ths is at the origin of the restored symmetry in the plot of the differential conductance in 3.12, as discussed above.

# 4. Kondo temperature in a TTD

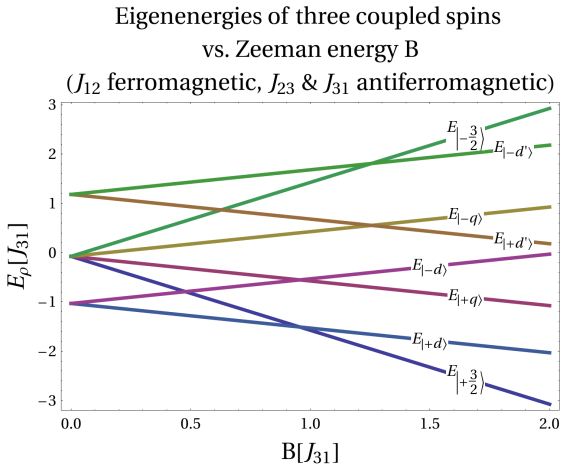


Figure 4.1.: Eigenvalues of the bare Hamiltonian of a triangular triple dot plotted against the magnetic field. The inter-dot couplings $J_{12}$, $J_{23}$ and $J_{31}$ are chosen such that $J_{12}$ is ferromagnetic and $J_{31}$, $J_{23}$ are antiferromagnetic.

As we have seen in the last chapter and again in Figure 4.1, the ground state of a triangular triple dot (TTD) system changes depending on the strength of the applied magnetic field. If we set the internal dot couplings such that $J_{12}$ is ferromagnetic and $J_{23}$, $J_{31}$ are antiferromagnetic, the spectrum of the three-spin system not coupled to the leads looks exactly like in Figure 4.1. At $B = 0$ there is a degenerate doublet, for higher values of the magnetic field $B > 0$ this splits and one of the states of the total-spin 3/2 quartet gets closer to the low-energy component of this doublet. The latter become degenerate at a well specific value of $B$ and for even bigger values the quartet state becomes the unique ground state of the system. Increasing the magnetic field we then meet two degeneracies, which we now want to study.
From a transport point of view these degeneracies are not different from the energy degeneracy of the two possible spin-states of a singly-occupied quantum dot. As we know, in such a system a strong coupling regime is entered at "low enough"temperatures. The "low enough"temperature regime here is set by the typical temperature $T_K$ characterizing the Kondo effect. For temperatures smaller then the Kondo temperature $T < T_K$, a strongly entangled many-body state is formed between the spin of the dot and that of the conduction electrons. In this situation, the dot spin is effectively screened by the conduction electrons, thus allowing for an enhanced zero-bias conductance (Kondo peak).
In this chapter we want to investigate the properties of the Kondo temperature for the more complicated degeneracies of the TTD system. We start by writing the low-energy Hamiltonians (valid in the neighborhood of the degenerate ground states) for the system. In 4.2 we then review the "Poor man's scaling"approach to Kondo physics. This allows us to take into account the strong coupling effects through a renormalization of the Hamiltonian coupling coefficients. In 4.3

we then extend the scaling procedure to a more general anisotropic Hamiltonian, so that we are able to apply the idea behind this approach to our very specific triplet dot system. We can thus investigate the presence of a possible zero-bias Kondo-like peak at the ground-state-degeneracies of our system. If any peak is present, then its relative strength when compared to the cotunneling peaks, would possibly enable actual experimental measurements of enhanced values of the conductance at the degenerate point.

## 4.1. Effective low energy TTD Hamiltonian

We start the study of the degeneracy points by projecting the perturbative Hamiltonian (3.16) for a triangular triple dot (TTD) into the subspace created by the two low energy competing ground states for each of the degenerate situations. We then want to write down an effective Hamiltonian describing the physics of the system in the neighborhood of each degeneracy. We will see that the resulting Hamiltonian turns out to be anisotropic in the different directions.

We have seen that for a choice of inter-dot coefficients where $J_{12}$ is ferromagnetic and $J_{23}$, $J_{31}$ antiferromagnetic, there exist two degeneracy points. At $B = 0$ the two doublet states $|+d\rangle$ and $|-d\rangle$ are degenerate, but when increasing the magnetic field they split and $|-d\rangle$ raises in energy, while at the same time the higher energy state $|+\frac{3}{2}\rangle$ decreases. At some point $|-d\rangle$ and $|+\frac{3}{2}\rangle$ will cross, so that the two competing low-energy states become $|+\frac{3}{2}\rangle$ and $|+d\rangle$. For a specific value of the magnetic field the respective energies will equal $E_{|+\frac{3}{2}\rangle} = E_{|+d\rangle}$ giving again a degenerate ground state. For still higher values of the external field the unique ground state becomes $|+\frac{3}{2}\rangle$.

### 4.1.1. Low energy Hamiltonian at $B = 0$

Let us begin by writing the low-energy Hamiltonian for $B = 0$. We then need to project the interaction Hamiltonian (written in the eigenstate basis (3.41)) into the subspace generated by

the low-energy doublet $\{|+d\rangle, |-d\rangle\}$. We obtain:

$$
\begin{aligned}
H_{eff} = J_L \Bigg[ & \begin{pmatrix} 0 & A \\ 0 & 0 \end{pmatrix} c^\dagger_{L\downarrow} c_{L\uparrow} + \begin{pmatrix} 0 & 0 \\ A & 0 \end{pmatrix} c^\dagger_{L\uparrow} c_{L\downarrow} + \begin{pmatrix} B1 & 0 \\ 0 & B2 \end{pmatrix} \tau^z_{\sigma\sigma'} c^\dagger_{L\sigma} c_{L\sigma'} \Bigg] \\
& + \frac{W_L}{2} \begin{pmatrix} 1 & 0 \\ 0 & 1 \end{pmatrix} \tau^0_{\sigma\sigma'} c^\dagger_{L\sigma} c_{L\sigma'} \\
& + J_R \Bigg[ \begin{pmatrix} 0 & C \\ 0 & 0 \end{pmatrix} c^\dagger_{R\downarrow} c_{R\uparrow} + \begin{pmatrix} 0 & 0 \\ C & 0 \end{pmatrix} c^\dagger_{R\uparrow} c_{R\downarrow} + \begin{pmatrix} D1 & 0 \\ 0 & D2 \end{pmatrix} \tau^z_{\sigma\sigma'} c^\dagger_{R\sigma} c_{R\sigma'} \Bigg] \\
& + \frac{W_R}{2} \begin{pmatrix} 1 & 0 \\ 0 & 1 \end{pmatrix} \tau^0_{\sigma\sigma'} c^\dagger_{R\sigma} c_{R\sigma'} \\
& + \frac{J_H^{RL}}{2} \Bigg[ \begin{pmatrix} 0 & E \\ 0 & 0 \end{pmatrix} c^\dagger_{R\downarrow} c_{L\uparrow} + \begin{pmatrix} 0 & 0 \\ E & 0 \end{pmatrix} c^\dagger_{R\uparrow} c_{L\downarrow} + \begin{pmatrix} G1 & 0 \\ 0 & G2 \end{pmatrix} \tau^z_{\sigma\sigma'} c^\dagger_{R\sigma} c_{L\sigma'} \Bigg] \\
& + \frac{W_H^{RL}}{2} \Bigg[ \begin{pmatrix} H1 & 0 \\ 0 & H2 \end{pmatrix} \sum_\sigma c^\dagger_{R\sigma} c_{L\sigma} \Bigg] \\
& + \frac{J_H^{LR}}{2} \Bigg[ \begin{pmatrix} 0 & E \\ 0 & 0 \end{pmatrix} c^\dagger_{L\downarrow} c_{R\uparrow} + \begin{pmatrix} 0 & 0 \\ E & 0 \end{pmatrix} c^\dagger_{L\uparrow} c_{R\downarrow} + \begin{pmatrix} G1 & 0 \\ 0 & G2 \end{pmatrix} \tau^z_{\sigma\sigma'} c^\dagger_{L\sigma} c_{R\sigma'} \Bigg] \\
& + \frac{W_H^{LR}}{2} \Bigg[ \begin{pmatrix} H1 & 0 \\ 0 & H2 \end{pmatrix} \sum_\sigma c^\dagger_{L\sigma} c_{R\sigma} \Bigg]
\end{aligned}
\tag{4.1}
$$

where the quantities $A, B1, B2, C, D1, D2, E, G1, G2, H1, H2$ are in general some complicated functions of the inter-dot couplings $J_{12}$, $J_{23}$ and $J_{31}$ and their exact expression is given in Appendix C.2. In the simplified case $J_{23} = J_{31}$ the eigenvectors of the bare Hamiltonian are independent of the internal couplings $J_{12}$, $J_{23}$ and $J_{31}$ (see Section 3.2.2) and therefore also the couplings appearing in (4.1) turn out to be simple numbers, namely:

$$
\begin{cases}
A = -\frac{2}{3} \\
B1 = \frac{1}{3} \\
B2 = -\frac{1}{3} \\
C = \frac{1}{3} \\
D1 = -\frac{1}{6} \\
D2 = \frac{1}{6} \\
E = -\frac{1}{3} \\
G1 = \frac{1}{6} \\
G2 = -\frac{1}{6} \\
H1 = -\frac{1}{2} \\
H2 = -\frac{1}{2}
\end{cases}
\tag{4.2}
$$

When, on the contrary, $J_{23} = J_{12}$, the couplings become:

$$\begin{cases} A = -\frac{2}{3} \\ B1 = \frac{1}{3} \\ B2 = -\frac{1}{3} \\ C = \frac{2}{3} \\ D1 = \frac{1}{3} \\ D2 = -\frac{1}{3} \\ E = \frac{4}{3} \\ G1 = \frac{2}{3} \\ G2 = -\frac{2}{3} \\ H1 = 1 \\ H2 = 1 \end{cases} \tag{4.3}$$

so that the Hamiltonian becomes isotropic.

### 4.1.2. Low energy Hamiltonian at $B > 0$

In order to study the second degeneracy at finite $B$, we need to project into the subspace generated by the two states $\{|+\frac{3}{2}\rangle, |+d\rangle\}$. We then get:

$$\begin{aligned} H_{eff} = J_L & \left[ \begin{pmatrix} 0 & A \\ 0 & 0 \end{pmatrix} c^\dagger_{L\downarrow} c_{L\uparrow} + \begin{pmatrix} 0 & 0 \\ A & 0 \end{pmatrix} c^\dagger_{L\uparrow} c_{L\downarrow} + \begin{pmatrix} \frac{1}{2} & 0 \\ 0 & B \end{pmatrix} \tau^z_{\sigma\sigma'} c^\dagger_{L\sigma} c_{L\sigma'} \right] \\ & + \frac{W_L}{2} \begin{pmatrix} 1 & 0 \\ 0 & 1 \end{pmatrix} \tau^0_{\sigma\sigma'} c^\dagger_{L\sigma} c_{L\sigma'} \\ & + J_R \left[ \begin{pmatrix} 0 & C \\ 0 & 0 \end{pmatrix} c^\dagger_{R\downarrow} c_{R\uparrow} + \begin{pmatrix} 0 & 0 \\ C & 0 \end{pmatrix} c^\dagger_{R\uparrow} c_{R\downarrow} + \begin{pmatrix} \frac{1}{2} & 0 \\ 0 & D \end{pmatrix} \tau^z_{\sigma\sigma'} c^\dagger_{R\sigma} c_{R\sigma'} \right] \\ & + \frac{W_R}{2} \begin{pmatrix} 1 & 0 \\ 0 & 1 \end{pmatrix} \tau^0_{\sigma\sigma'} c^\dagger_{R\sigma} c_{R\sigma'} \\ & + \frac{J^{RL}_H}{2} \left[ \begin{pmatrix} 0 & E \\ 0 & 0 \end{pmatrix} c^\dagger_{R\downarrow} c_{L\uparrow} + \begin{pmatrix} 0 & 0 \\ F & 0 \end{pmatrix} c^\dagger_{R\uparrow} c_{L\downarrow} + \begin{pmatrix} 1 & 0 \\ 0 & G \end{pmatrix} \tau^z_{\sigma\sigma'} c^\dagger_{R\sigma} c_{L\sigma'} \right] \\ & + \frac{W^{RL}_H}{2} \left[ \begin{pmatrix} 1 & 0 \\ 0 & H \end{pmatrix} \sum_\sigma c^\dagger_{R\sigma} c_{L\sigma} \right] \\ & + \frac{J^{LR}_H}{2} \left[ \begin{pmatrix} 0 & F \\ 0 & 0 \end{pmatrix} c^\dagger_{L\downarrow} c_{R\uparrow} + \begin{pmatrix} 0 & 0 \\ E & 0 \end{pmatrix} c^\dagger_{L\uparrow} c_{R\downarrow} + \begin{pmatrix} 1 & 0 \\ 0 & G \end{pmatrix} \tau^z_{\sigma\sigma'} c^\dagger_{L\sigma} c_{R\sigma'} \right] \\ & + \frac{W^{LR}_H}{2} \left[ \begin{pmatrix} 1 & 0 \\ 0 & H \end{pmatrix} \sum_\sigma c^\dagger_{L\sigma} c_{R\sigma} \right] \end{aligned} \tag{4.4}$$

where the explicit dependence of $A, B, C, D, E, F, G, H$ on $J_{12}$, $J_{23}$ and $J_{31}$ can be found in Appendix C.1 and for the special case $J_{23} = J_{31}$ they become:

$$\begin{cases} A = \frac{1}{\sqrt{6}} \\ B = \frac{1}{3} \\ C = -\sqrt{\frac{2}{3}} \\ D = -\frac{1}{6} \\ E = -2\sqrt{\frac{2}{3}} \\ F = \sqrt{\frac{2}{3}} \\ G = \frac{1}{6} \\ H = -\frac{1}{2} \end{cases} \tag{4.5}$$

When, on the contrary, $J_{23} = J_{12}$, the couplings become:

$$\begin{cases} A = \frac{1}{\sqrt{6}} \\ B = \frac{1}{3} \\ C = \frac{1}{\sqrt{6}} \\ D = \frac{1}{3} \\ E = \sqrt{\frac{2}{3}} \\ G = \frac{2}{3} \\ H = 1 \end{cases} \tag{4.6}$$

### 4.1.3. General expression for the low energy Hamiltonian at $B = 0$ and $B > 0$

Notice that both in (4.1) and (4.4) we have obtained an effective anisotropic Kondo Model, which can in general be rewritten in the following way:

$$H = \sum_{\alpha,\alpha',k,k'} \Big[ J^{+}_{\alpha'\alpha} \tau^{+} c^{\dagger}_{\alpha' k' \downarrow} c_{\alpha k \uparrow} + J^{-}_{\alpha'\alpha} \tau^{-} c^{\dagger}_{\alpha' k' \uparrow} c_{\alpha k \downarrow} + J^{z\uparrow}_{\alpha'\alpha} \tau^{z} c^{\dagger}_{\alpha' k' \uparrow} c_{\alpha k \uparrow} + J^{z\downarrow}_{\alpha'\alpha} \tau^{z} c^{\dagger}_{\alpha' k' \downarrow} c_{\alpha k \downarrow} + J^{0\uparrow}_{\alpha'\alpha} \tau^{0} c^{\dagger}_{\alpha' k' \uparrow} c_{\alpha k \uparrow} + J^{0\downarrow}_{\alpha'\alpha} \tau^{0} c^{\dagger}_{\alpha' k' \downarrow} c_{\alpha k \downarrow} \Big] \tag{4.7}$$

by introducing the new coefficients $J^{+}_{\alpha'\alpha}, J^{-}_{\alpha'\alpha}, J^{z\uparrow}_{\alpha'\alpha}, J^{z\downarrow}_{\alpha'\alpha}, J^{0\uparrow}_{\alpha'\alpha}, J^{0\downarrow}_{\alpha'\alpha}$ (for more details see Appendix C.1).
In the part of the Hamiltonian involving transport just through one of the leads (i.e. terms like $c^{\dagger}_{\alpha k' \sigma} c_{\alpha k \sigma}$) the anisotropy is just between the coefficient parallel to the magnetic field and the coefficient orthogonal to the magnetic field. On the contrary in the part of the Hamiltonian involving transport from one lead to the other (i.e. in the terms involving creation and annihilation operators of both the right and the left lead) also the two in-plane coefficients are different, leading to a "total anisotropy"also in the plane perpendicular to the magnetic field.

We now want to apply a scaling procedure to these two low-energy Hamiltonians. Such study allows us to focus on progressively decreasing energy ranges within the bandwidth of the leads. We can therefore follow the behavior of the system at very low temperatures and study the possible crossing to a strong coupling regime.

In order to go on with our plan, we now need to introduce in some more details the ideas of this ″Poor man's scaling″approach. This is done in the next section. In 4.3 we then generalize the ″Poor man's scaling″to a more complicated model, which will then allow us to study our specific Hamiltonians (4.1) and (4.4).

## 4.2. Poor man's scaling equations for the anisotropic Kondo model

When doing perturbation theory with a standard 1/2 Kondo model, we know that already at third order divergences appear (see Section 2.2). The divergent terms in the perturbative expansion arise in the form of logarithmic divergences $\ln(K_BT/D)$ where $D$ is the conduction band of the leads. This dependence on the cut-off energy is very different from a dependence of the kind $1/D$ or $1/D^2$, in which case the limit of infinite band width, $D \to \infty$, can be taken without any divergence arising from that. Physically the last situation means that the high energy excitations don't contribute to the physical interesting quantities when considering the low energy levels. On the contrary, with a logarithmic dependence on the conductance band the limit of an infinitely large conductance band leads to a divergence, meaning that contributions from high energy excitations must be taken into account. This can be done through a renormalization of the coupling constants. That is the essence of the scaling approach. When considering different widths of the conduction band one must rescale the coupling constants of the model in the proper way. Let us see how this come about.
One can consider the states lying at the edge of the conductance band and see what happens at the model Hamiltonian when eliminating virtual transitions to them 4.2 (a). One can end up writing down differential equations relating the change of the coupling coefficients with respect to the reduction of the band width. To see exactly how this works let us consider a general perturbative Kondo Hamiltonian of the form:

$$H' = \sum_{k,k'} \left[ (J^+\tau^+ c^\dagger_{k\downarrow} c_{k'\uparrow} + J^-\tau^- c^\dagger_{k\uparrow} c_{k'\downarrow}) + J^z\tau^z (c^\dagger_{k\uparrow} c_{k'\uparrow} - c^\dagger_{k\downarrow} c_{k'\downarrow}) \right] \tag{4.8}$$

when considering all the possible scattering processes involving virtual transitions to the band edges and eliminating the correspondent terms from the scattering matrix one finds an Hamiltonian that looks exactly the same as the original one (look, for example, [2] for a detailed treatment) but with modified couplings $J^\pm \to J^\pm + \delta J^\pm$ and $J^z \to J^z + \delta J^z$, where

$$\begin{aligned} \delta J^\pm &= -2J^\pm J^z \rho_0 |\delta D| \left[ \frac{1}{E - D + \varepsilon_k} + \frac{1}{E - D - \varepsilon_{k'}} \right] \\ \delta J^z &= -2J^+ J^- \rho_0 |\delta D| \left[ \frac{1}{E - D + \varepsilon_k} + \frac{1}{E - D - \varepsilon_{k'}} \right]. \end{aligned} \tag{4.9}$$

For low energy excitations relative to $D$ the $E$ dependence can be neglected and, when considering scattering of conduction electrons near the Fermi energy, $\varepsilon_k$ and $\varepsilon_{k'}$ can also be neglected relative to $D$. Therefore one can rewrite the previous equations in the following form:

$$\begin{aligned} \frac{dJ^\pm}{d\ln D} &= -4\rho_0 J^z J^\pm \\ \frac{dJ^z}{d\ln D} &= -4\rho_0 J^+ J^-. \end{aligned} \tag{4.10}$$

From these two equations one finds the invariant trajectories

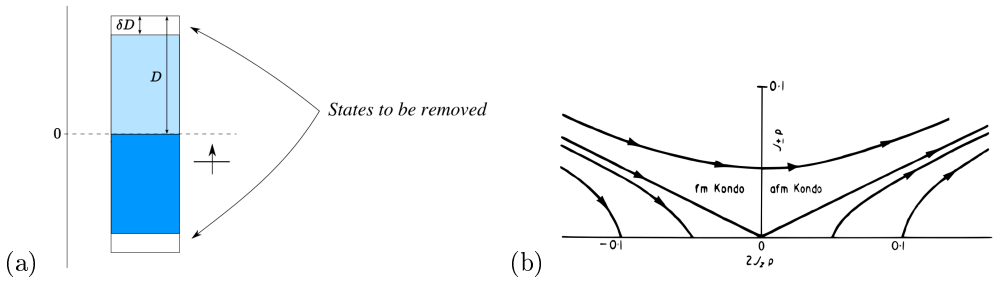


Figure 4.2.: (a)Sketch of the idea behind the scaling procedure (reproduced from [16]). The high energy states within the bandwidth are gradually eliminated and their contribution enters in a renormalization of the coupling constants of the model Hamiltonian. (b) Invariant trajectories of the scaling equations in the $J^z$-$J^\pm$ plane. The x-axis represents $J^z$, the y-axis $J^\pm$. For initial parameters in the region $J^z < 0, J^\pm < |J^z|$ the renormalization process leads to some finite limiting values of the coupling $J^z$ and $J^\pm \to 0$ so that the new renormalized model describes almost non-interacting particles.

$$(J^z)^2 - J^+J^- = \text{const} \tag{4.11}$$

which correspond to the trajectories of Figure 4.2 (b). Notice that some initial coefficients $J_0^z$ and $J_0^\pm$ lead to a situation with divergent couplings at a well specific energy scale. Others lead instead to a completely different scenario where the z-coupling $J^z$ increases up to a finite value while the orthogonal coupling goes to zero. These initial values are those that satisfy the following:

$$\begin{cases} J^z < 0 \\ J^\perp > 0 \\ |J^z| > J^\perp \end{cases} \quad \text{or} \quad \begin{cases} J^z < 0 \\ J^\perp < 0 \\ |J^z| > |J^\perp| \end{cases} \tag{4.12}$$

corresponding to the trajectories in the left-lowest part of Figure 4.2, i.e. the trajectories under the line $J_0^z = -J_0^\perp$ and the specular area in the half plane $J^\perp < 0$ (not shown in figure).
When $J^\perp = 0$ exchange coupling processes with different initial and final spin states in the dot are not possible. This means that for initial values satisfying (4.12) the scaling of the coupling constants can continue indefinitely, giving a limiting situation with an almost free spin system in the dot. In conclusion for initial values of the couplings satisfying (4.12) there is no Kondo effect.
When analyzing specific situations we will therefore have to check in what part of Figure 4.2 the initial conditions are situated.

## 4.3. Poor man's scaling equations for the completely anisotropic Kondo model

It is now time to deal with the complete low-energy models given by (4.1) and (4.4), respectively for the degeneracy at $B = 0$ and at $B > 0$. We should then find a way to write down scaling equations for all the coupling constants of our models. In order to do that, let us derive once again the scaling equations in more details.

As we have seen in (4.7) both our low energy Hamiltonians can be written in the following form:

$$H = \sum_{\alpha,\alpha',k,k'} \Big[ J^{+}_{\alpha'\alpha}\tau^{+}c^{\dagger}_{\alpha'k'\downarrow}c_{\alpha k\uparrow} + J^{-}_{\alpha'\alpha}\tau^{-}c^{\dagger}_{\alpha'k'\uparrow}c_{\alpha k\downarrow} + J^{z\uparrow}_{\alpha'\alpha}\tau^{z}c^{\dagger}_{\alpha'k'\uparrow}c_{\alpha k\uparrow} + J^{z\downarrow}_{\alpha'\alpha}\tau^{z}c^{\dagger}_{\alpha'k'\downarrow}c_{\alpha k\downarrow} + J^{0\uparrow}_{\alpha'\alpha}\tau^{0}c^{\dagger}_{\alpha'k'\uparrow}c_{\alpha k\uparrow} + J^{0\downarrow}_{\alpha'\alpha}\tau^{0}c^{\dagger}_{\alpha'k'\downarrow}c_{\alpha k\downarrow} \Big] \tag{4.13}$$

where $\alpha$ and $\alpha'$ label the leads and the $\tau$ operators represent the low energy projections of the full dot operators (i.e. the operators $\vec{S}_\alpha$ and $\vec{T}_{\alpha'\alpha}$).
In order to remove scattering to the band edges let us project the Hamiltonian into the Hilbert space where one excitation exists in the upper band:

$$H_{21} = \sum_{\beta,q,k} \Big[ J^{+}_{\beta\alpha}\tau^{+}c^{\dagger}_{\beta q\downarrow}c_{\alpha k\uparrow} + J^{-}_{\beta\alpha}\tau^{-}c^{\dagger}_{\beta q\uparrow}c_{\alpha k\downarrow} + J^{z\uparrow}_{\beta\alpha}\tau^{z}c^{\dagger}_{\beta q\uparrow}c_{\alpha k\uparrow} + J^{z\downarrow}_{\beta\alpha}\tau^{z}c^{\dagger}_{\beta q\downarrow}c_{\alpha k\downarrow} + J^{0\uparrow}_{\beta\alpha}\tau^{0}c^{\dagger}_{\beta q\uparrow}c_{\alpha k\uparrow} + J^{0\downarrow}_{\beta\alpha}\tau^{0}c^{\dagger}_{\beta q\downarrow}c_{\alpha k\downarrow} \Big] \tag{4.14}$$

where $q$ labels the high-energy excitation in the upper band. The Hamiltonian describing the presence of a hole in the lower band instead is given by:

$$H_{01} = \sum_{\beta,q,k'} \Big[ J^{+}_{\beta\alpha'}\tau^{+}c_{\beta q\uparrow}c^{\dagger}_{\alpha'k'\downarrow} + J^{-}_{\beta\alpha'}\tau^{-}c_{\beta q\downarrow}c^{\dagger}_{\alpha'k'\uparrow} + J^{z\uparrow}_{\beta\alpha'}\tau^{z}c_{\beta q\uparrow}c^{\dagger}_{\alpha'k'\uparrow} + J^{z\downarrow}_{\beta\alpha'}\tau^{z}c_{\beta q\downarrow}c^{\dagger}_{\alpha'k'\downarrow} + J^{0\uparrow}_{\beta\alpha'}\tau^{0}c_{\beta q\uparrow}c^{\dagger}_{\alpha'k'\uparrow} + J^{0\downarrow}_{\beta\alpha'}\tau^{0}c_{\beta q\downarrow}c^{\dagger}_{\alpha'k'\downarrow} \Big] \tag{4.15}$$

where $q$ this time labels the excitation in the lower band. Calling $\psi_1$ the wavefunction of the unexcited system, $\psi_2$ the state of the system with one excitation in the upper band and $\psi_0$ the state with one hole in the lowest band, we can write the following Schrödinger equation:

$$\begin{pmatrix} H_{00} & H_{01} & 0 \\ H_{10} & H_{11} & H_{12} \\ 0 & H_{21} & H_{22} \end{pmatrix} \begin{pmatrix} \psi_0 \\ \psi_1 \\ \psi_2 \end{pmatrix} = E \begin{pmatrix} \psi_0 \\ \psi_1 \\ \psi_2 \end{pmatrix} \tag{4.16}$$

which, once we have eliminated the excited states, gives:

$$\big[ H_{10}(E - H_{00})^{-1}H_{01} + H_{11} + H_{12}(E - H_{22})^{-1}H_{21} \big] = E\psi_1 \tag{4.17}$$

where $H_{10} = H^{\dagger}_{01}$ and $H_{12} = H^{\dagger}_{21}$.
Calculating the different terms in (4.17), we end up with a model formally similar to the one we started from, but with renormalized coefficients. We namely obtain a Hamiltonian of the same form as (4.13) but with new couplings $J \to J + \delta J$. The relation between these new coupling

coefficients and the initial ones is given by the following scaling equations:

$$\begin{aligned}
\frac{dJ^{z\uparrow}_{\alpha'\alpha}}{d\ln D} &= -4J^{+}_{\alpha'\beta}J^{-}_{\beta\alpha}\rho_0 \\
\frac{dJ^{0\uparrow}_{\alpha'\alpha}}{d\ln D} &= 0 \\
\frac{dJ^{+}_{\alpha'\alpha}}{d\ln D} &= 2\left(-J^{z\uparrow}_{\alpha'\beta}J^{+}_{\beta\alpha} + J^{+}_{\alpha'\beta}J^{z\downarrow}_{\beta\alpha}\right)\rho_0 \\
\frac{dJ^{-}_{\alpha'\alpha}}{d\ln D} &= 2\left(J^{z\downarrow}_{\alpha'\beta}J^{-}_{\beta\alpha} - J^{-}_{\alpha'\beta}J^{z\uparrow}_{\beta\alpha}\right)\rho_0 \\
\frac{dJ^{z\downarrow}_{\alpha'\alpha}}{d\ln D} &= 4J^{-}_{\alpha'\beta}J^{+}_{\beta\alpha}\rho_0 \\
\frac{dJ^{0\uparrow}_{\alpha'\alpha}}{d\ln D} &= 0.
\end{aligned} \tag{4.18}$$

The calulations leading to the previous equations are shown in detail in Appendix D.

Note that in the case $\alpha = \alpha'$ and $J^{z\downarrow}_{\alpha'\alpha} = -J^{z\uparrow}_{\alpha'\alpha}$ (D.4) become:

$$\begin{aligned}
\frac{dJ^{z\uparrow}}{d\ln D} &= -\frac{dJ^{z\downarrow}}{d\ln D} = -4J^{+}J^{-}\rho_0 \\
\frac{dJ^{+}}{d\ln D} &= -4J^{z\uparrow}J^{+}\rho_0 \\
\frac{dJ^{-}}{d\ln D} &= -4J^{-}J^{z\downarrow}\rho_0
\end{aligned} \tag{4.19}$$

which completely agree with (4.10).

Notice that the procedure applied in this section gives a renormalization of the coupling coefficients due to the elimination of virtual scattering events to the band edges of the leads. We have gradually adjusted the value of the couplings to the new band width until we have got to an energy scale where this procedure broke down, giving diverging couplings. We have therefore started from a very big band width and gone all the way down to the energies of the two degenerate ground states, so we have completly eliminated any influence that the higher energy states of the dot may have in setting the Kondo temperature. A more careful treatment would consider also these states by applying a similar renormalization procedure until the energy of the highest excited state. Then we would reiterate the same approach starting from this new energy scale (and the correspondent initial conditions on the coupling coefficients) and going all the way to the second highest energy state. This will have to be reiterated until we get to the lowest degenerate ground state and in this way we would have a more accurate estimate of the Kondo temperature. Nevertheless, let us try to see what our approach predicts.

We now solve the scaling equations (D.4) for the two degeneracies (at $B = 0$ and $B > 0$) of the TTD. Since the initial conditions for the coupling constants now depend on the internal inter-dot couplings ($J_{12}$, $J_{23}$ and $J_{31}$), their flux and the Kondo temperature will also depend on these quantities. Evaluating the crossover conditions from a weak coupling to a strong coupling regime in our system is therefore non-trivial.

We start by studying the ground state degeneracy at $B > 0$ first and then we turn to the degeneracy at $B = 0$.

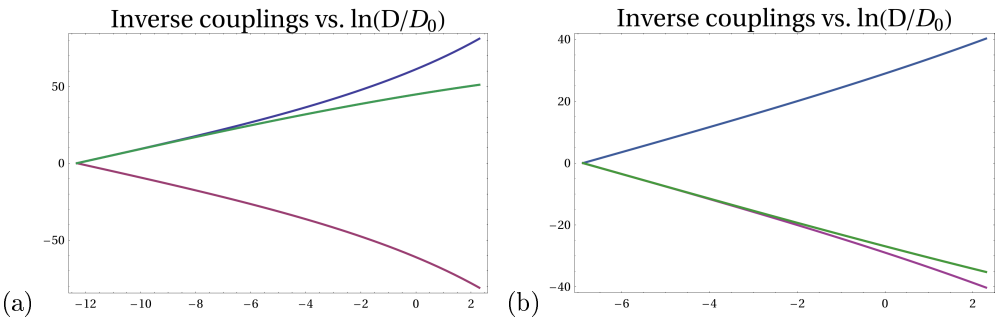


Figure 4.3.: Inverse couplings $J^{\pm}$ and $J^z$ against $\ln(D/D_0)$ plotted for a specific choice of the internal couplings $J_{12}$, $J_{23}$ and $J_{31}$. (a) is calculated in the limiting case of $t_R = 0$, (b) is calculated for $t_L = 0$. Note that in both cases there is a value of D, which we define as the Kondo temperature, at which both the couplings $J^{\pm}$ and $J^z$ diverge (i.e. their inverse go to zero).

## 4.4. Renormalized coupling constants for the low-energy model at $B > 0$

Solving numerically the scaling equations (D.4) with the initial conditions defined in (C.4) we can evaluate the Kondo temperature of the system, which we define in this context as the temperature (if such quantity exists) at which all the coupling constants diverge. This rough definition agrees with the general statement that the Kondo temperature should give the energy scale marking the transition to a strong coupling regime. If all the couplings diverge for a very specific energy scale, then it is reasonable to believe that this scale can be a good quantity to consider.
It is convenient to start by studying the Kondo temperature in the two simplifying cases $t_R = 0$ and $t_L = 0$. With such assumptions the scaling equations (D.4) reduce to the usual form (4.10).

In the case $t_R = 0$ the low-energy effective Hamiltonian for the TTD system becomes:

$$H_{eff} = J_L^{\perp}\left[\tau^+ c_{L\downarrow}^\dagger c_{L\uparrow} + \tau^- c_{L\uparrow}^\dagger c_{L\downarrow}\right] + J_L^z \tau^z (c_{L\uparrow}^\dagger c_{L\uparrow} - c_{L\downarrow}^\dagger c_{L\downarrow}) + J_L^0 \tau^0 (c_{L\uparrow}^\dagger c_{L\uparrow} - c_{L\downarrow}^\dagger c_{L\downarrow}). \quad (4.20)$$

We then need to solve (4.10) with the initial conditions for the couplings at $D = D_0$:

$$\begin{aligned} J_L^{\perp}(\ln D_0) &= \frac{J_L A}{2} \\ J_L^z(\ln D_0) &= \frac{J_L(1/2 - B)}{2} \\ J_L^0(\ln D_0) &= \frac{J_L(1/2 + B)}{2} + \frac{W_L}{2}. \end{aligned} \quad (4.21)$$

All the coupling constants are seen to diverge at some energy scale, which depends on the choice of the inter-dot couplings (Figure 4.3 (a)). We then want to study in more details how this energy scale depend on the internal couplings and find an explanation for such behavior.
Let us start our study of the Kondo temperature by considering the physical phenomena which can influence its magnitude. Roughly speaking, the Kondo temperature gives the energy scale at which virtual exchange processes start to dominate, when compared to the weak coupling cotunneling processes. We therefore need to look more closely at the matrix elements $|\langle +d \mid H_{eff} \mid +\frac{3}{2}\rangle|$.

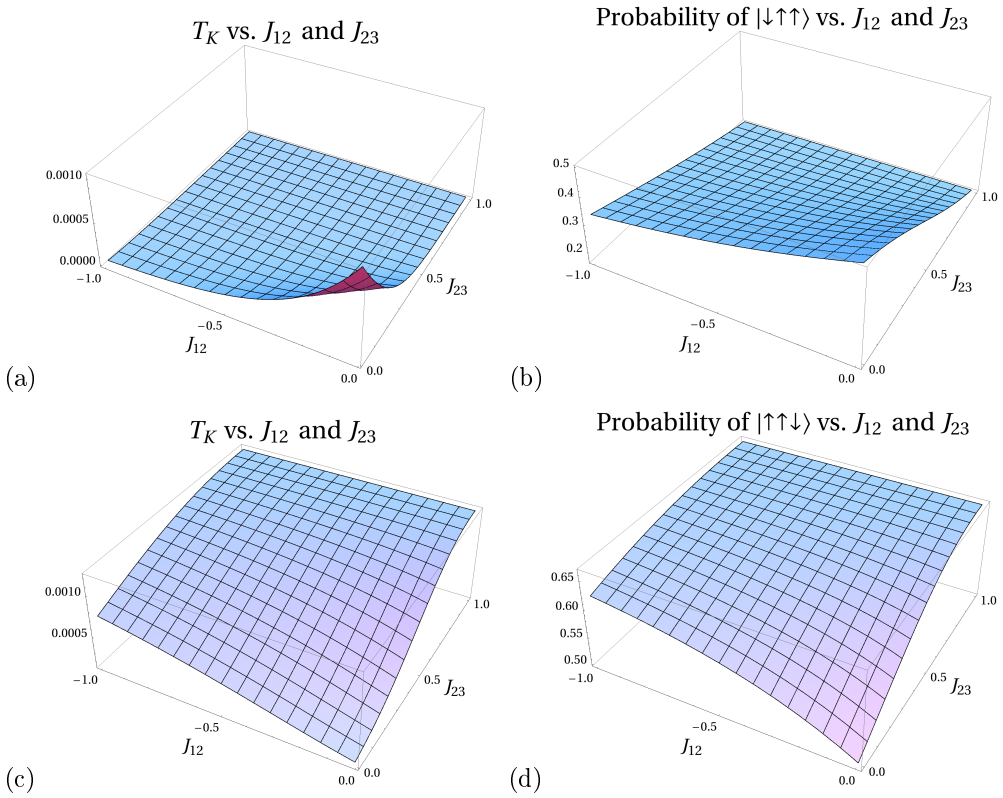


Figure 4.4.: Left column: plots of the dependence of the Kondo temperature against two of the internal coupling constants (the third is fixed) for the Kondo peak at $B > 0$ in the limit $t_R = 0$ (a) and $t_L = 0$ (c). Right column: probability of the single-spin states $|\downarrow\uparrow\uparrow\rangle$ (b) and $|\uparrow\uparrow\downarrow\rangle$ (d) vs. $J_{12}$ and $J_{23}$ ($J_{13}$ fixed).

If $J_{12}$ is ferromagnetic and $J_{23}$, $J_{23}$ are antiferromagnetic, the privileged spin configuration will have the spin in the left dot aligned to that in the central dot and antiparallel to the one in the right dot. Rewriting the competing ground states $|+d\rangle$ and $|+\frac{3}{2}\rangle$ in the single-spin basis (3.10), we obtain the following representation of the low-energy doublet: $|+\frac{3}{2}\rangle = |\uparrow\uparrow\uparrow\rangle$ and $|+d\rangle = \mathrm{a}\,|\uparrow\downarrow\uparrow\rangle + \mathrm{b}\,|\uparrow\uparrow\downarrow\rangle + \mathrm{c}\,|\downarrow\uparrow\uparrow\rangle$, where a, b, c are assumed to be normalized to 1. The only exchange scattering process that can couple the two competing ground states when $t_R = 0$ is the following:

$$|\downarrow\uparrow\uparrow\rangle \rightsquigarrow |\uparrow\uparrow\uparrow\rangle \quad \propto J_L. \tag{4.22}$$

Then the only contribution to the exchange term is given by the single-spin state $|\downarrow\uparrow\uparrow\rangle$, which enters in the low-energy state $|+d\rangle$ with amplitude c. The probability $|\mathrm{c}|^2$ of finding the state $|+d\rangle$ in the configuration $|\downarrow\uparrow\uparrow\rangle$ will then be small, since the spin in the left dot and the spin in the central dot are antiparallel. If the probability $|\mathrm{c}|^2$ increases with the internal couplings $J_{12}$, $J_{23}$ and $J_{31}$, then the probability of the exchange process (4.26) will also increase. Following the intuitive picture which links the Kondo temperature to the likeliness of exchange processes connecting the two low-energy states, we then expect the Kondo temperature to follow the same trend, e.g. increase with the internal couplings. The Kondo temperature then follows the same dependence on the internal couplings as the probability for the dots to be in the proper spin state allowing exchange processes between the two competing low-energy states. This conclusion is qualitatively depicted in Figure 4.6.

Let us now consider the other extreme case, $t_L = 0$, in which the effective Hamiltonian becomes:

$$H_{eff} = J_R^{\perp}\left[\tau^+ c_{R\downarrow}^\dagger c_{R\uparrow} + \tau^- c_{R\uparrow}^\dagger c_{R\downarrow}\right] + J_R^z \tau^z (c_{R\uparrow}^\dagger c_{R\uparrow} - c_{R\downarrow}^\dagger c_{R\downarrow}) + J_R^0 \tau^0 (c_{R\uparrow}^\dagger c_{R\uparrow} - c_{R\downarrow}^\dagger c_{R\downarrow}) \tag{4.23}$$

and the initial values are

$$\begin{aligned} J_R^{\perp}(\ln D_0) &= \frac{J_R C}{2} \\ J_R^z(\ln D_0) &= \frac{J_R(1/2 - D)}{2} \\ J_R^0(\ln D_0) &= \frac{J_R(1/2 + D)}{2} + \frac{W_R}{2}. \end{aligned} \tag{4.24}$$

In this case the process giving exchange coupling between the two low-energy states, through tunneling to the right lead, is the following:

$$|\uparrow\uparrow\downarrow\rangle \rightsquigarrow |\uparrow\uparrow\uparrow\rangle \quad \propto J_R \tag{4.25}$$

so one has to look at how the coefficient of the state $|\uparrow\uparrow\downarrow\rangle$, as entering in the state $|+d\rangle$, change with $J_{12}, J_{23}, J_{13}$ (Figure 4.6 (d) ). In the same way as before, one can then explain the behavior of the Kondo temperature when changing the internal couplings. When $J_{12}, J_{23}, J_{13}$ are well turned on, with $J_{12} < 0$ (ferromagnetic) and $J_{23}, J_{13} > 0$ (antiferromagnetic), the spin-configuration in $|\uparrow\uparrow\downarrow\rangle$ is also the most likely in $|+d\rangle$, having the two spin coupled by $J_{12}$ parallel to each other. We then expect exchange processes coupling the two ground state to be more likely now then in the previous case, where $t_R = 0$. In fact in that case the allowed processes required a spin configuration $|\downarrow\uparrow\uparrow\rangle$, which is clearly not likely when $J_{12}$ is ferromagnetic. When all the internal couplings are on, we then expect a much higher Kondo temperature for the very asymmetrical coupled situation with $t_L \ll t_R$ then in the opposite case ($t_R \ll t_L$). A comparison between Figure 4.6 (a) and (c) clearly confirms this statement.

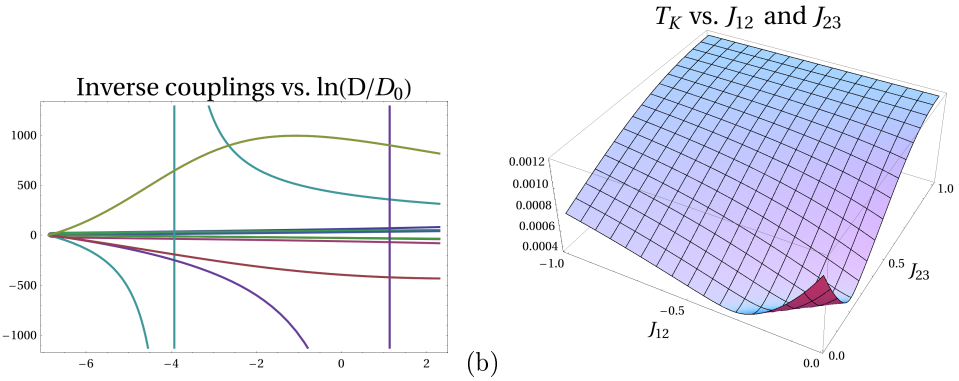


Figure 4.5.: (a) Inverse couplings (for a specific choice of the internal couplings $J_{12}$, $J_{23}$ and $J_{31}$) against $\ln(D/D_0)$ for the complete Hamiltonian (4.1) describing the degenerate ground state at finite $B$ field. All the inverse couplings flow to zero for a certain energy scale, i.e. the Kondo temperature. (b) Kondo temperature dependence on $J_{12}$, $J_{23}$ ($J_{31}$ fixed) for the full Hamiltonian (4.1) when both the couplings to the leads $t_L$ and $t_R$ are on. A qualitative explanation for this behaviour exploits the study of all the exchange processes coupling the two degenerate states $|+d\rangle$ and $|+\frac{3}{2}\rangle$.

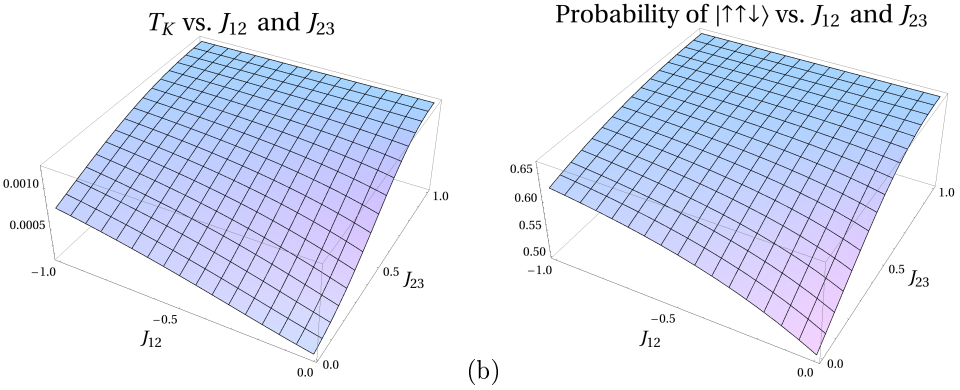


Figure 4.6.: (a)Plots of the dependence of the Kondo temperature against two of the internal coupling constants (expressed in units of the third one, $J_{31}$) for the Kondo peak at $B > 0$ in the limit $t_L = 0$. (b) Occupation probability of the single-spin states $|\uparrow\uparrow\rangle\downarrow$ against $J_{12}$ and $J_{23}$ (in units of $J_{13}$).

All the coupling constants are seen to diverge at some energy scale, which depends on the choice of the inter-dot couplings (Figure 4.3 (a)). We then want to study in more details how this energy scale depend on the internal couplings and find an explanation for such behavior.
Let us start our study of the Kondo temperature by considering the physical phenomena which can influence its magnitude. Roughly speaking, the Kondo temperature gives the energy scale at which virtual exchange processes start to dominate, when compared to the weak coupling cotunneling processes. We therefore need to look more closely at the matrix elements $|\langle +d \mid H_{eff} \mid +\frac{3}{2}\rangle|$.
If $J_{12}$ is ferromagnetic and $J_{23}$, $J_{23}$ are antiferromagnetic, the privileged spin configuration will have the spin in the left dot aligned to that in the central dot and antiparallel to the one in the right dot. Rewriting the competing ground states $\mid +d\rangle$ and $\mid +\frac{3}{2}\rangle$ in the single-spin basis (3.10), we obtain the following representation of the low-energy doublet: $\mid +\frac{3}{2}\rangle = |\uparrow\uparrow\uparrow\rangle$ and $\mid +d\rangle = \mathrm{a}\,|\uparrow\downarrow\uparrow\rangle + \mathrm{b}\,|\uparrow\uparrow\downarrow\rangle + \mathrm{c}\,|\downarrow\uparrow\uparrow\rangle$, where a, b, c are assumed to be normalized to 1. The only exchange scattering process that can couple the two competing ground states when $t_L = 0$ is the following:

$$|\uparrow\uparrow\downarrow\rangle \rightsquigarrow |\uparrow\uparrow\uparrow\rangle \quad \propto J_R \tag{4.26}$$

Then the only contribution to the exchange term is given by the single-spin state $|\uparrow\uparrow\downarrow\rangle$, which enters in the low-energy state $\mid +d\rangle$ with amplitude b. The probability $|\mathrm{b}|^2$ of finding the state $\mid +d\rangle$ in the configuration $|\uparrow\uparrow\downarrow\rangle$ will then be small, since the spin in the left dot and the spin in the central dot are antiparallel. If the probability $|\mathrm{b}|^2$ increases with the internal couplings $J_{12}$, $J_{23}$ and $J_{31}$, then the probability of the exchange process (4.26) will also increase. Following the intuitive picture which links the Kondo temperature to the likeliness of exchange processes connecting the two low-energy states, we then expect the Kondo temperature to follow the same trend, e.g. increase with the internal couplings. The Kondo temperature then follows the same dependence on the internal couplings as the probability for the dots to be in the proper spin state allowing exchange processes between the two competing low-energy states. This conclusion is qualitatively depicted in Figure 4.6.

Let us now consider the other extreme case, $t_L = 0$, in which the effective Hamiltonian becomes:

$$H_{eff} = J_L^{\perp}\left[\tau^+ c_{L\downarrow}^\dagger c_{L\uparrow} + \tau^- c_{L\uparrow}^\dagger c_{L\downarrow}\right] + J_L^z \tau^z (c_{L\uparrow}^\dagger c_{L\uparrow} - c_{L\downarrow}^\dagger c_{L\downarrow}) + J_L^0 \tau^0 (c_{L\uparrow}^\dagger c_{L\uparrow} - c_{L\downarrow}^\dagger c_{L\downarrow}). \tag{4.27}$$

and the initial values are

$$\begin{aligned} J_L^{\perp}(\ln D_0) &= \frac{J_L A}{2} \\ J_L^z(\ln D_0) &= \frac{J_L(1/2 - B)}{2} \\ J_L^0(\ln D_0) &= \frac{J_L(1/2 + B)}{2} + \frac{W_L}{2}. \end{aligned} \tag{4.28}$$

In this case the process giving exchange coupling between the two low-energy states, through tunneling to the right lead, is the following:

$$|\downarrow\uparrow\uparrow\rangle \rightsquigarrow |\uparrow\uparrow\uparrow\rangle \quad \propto J_L. \tag{4.29}$$

so one has to look at how the coefficient of the state $|\uparrow\uparrow\downarrow\rangle$, as entering in the state $\mid +d\rangle$, change with $J_{12}, J_{23}, J_{13}$ (Figure 4.6 (d) ). In the same way as before, one can then explain the behavior of the Kondo temperature when changing the internal couplings. When $J_{12}, J_{23}, J_{13}$ are well turned on, with $J_{12} < 0$ (ferromagnetic) and $J_{23}, J_{13} > 0$ (antiferromagnetic), the spin-configuration in $|\uparrow\uparrow\downarrow\rangle$ is also the most likely in $\mid +d\rangle$, having the two spin coupled by $J_{12}$ parallel

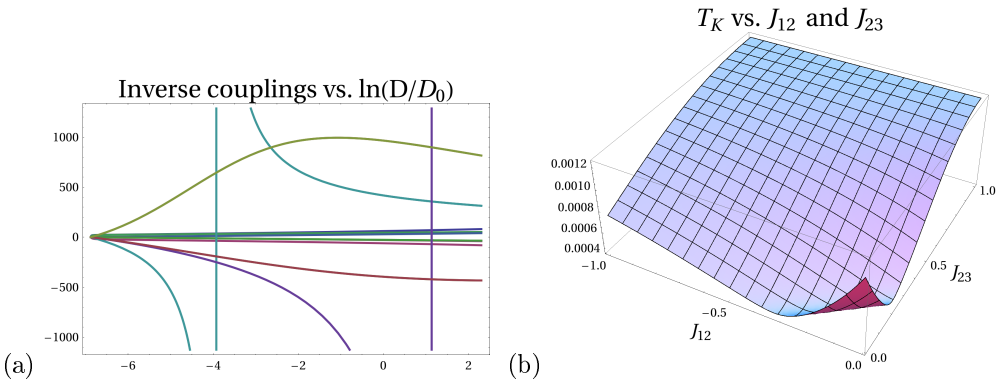


Figure 4.7.: (a) Inverse couplings (for a specific choice of the internal couplings $J_{12}$, $J_{23}$ and $J_{31}$) against $\ln(D/D_0)$ for the complete Hamiltonian (4.1) describing the degenerate ground state at finite $B$ field. All the inverse couplings flow to zero for a certain energy scale, i.e. the Kondo temperature. (b) Kondo temperature dependence on $J_{12}$, $J_{23}$ ($J_{31}$ fixed) for the full Hamiltonian (4.1) when both the couplings to the leads $t_L$ and $t_R$ are on. A qualitative explanation for this behaviour exploits the study of all the exchange processes coupling the two degenerate states $|+d\rangle$ and $|+\frac{3}{2}\rangle$.

to each other. We then expect exchange processes coupling the two ground state to be more likely now then in the previous case, where $t_R = 0$. In fact in that case the allowed processes required a spin configuration $|\downarrow\uparrow\uparrow\rangle$, which is clearly not likely when $J_{12}$ is ferromagnetic. When all the internal couplings are on, we then expect a much higher Kondo temperature for the very asymmetrical coupled situation with $t_L \ll t_R$ then in the opposite case ($t_R \ll t_L$). A comparison between Figure 4.6 (a) and (c) clearly confirms this statement.

The general situation with $t_R \sim t_L$ will be more involved and it requires to solve the full set of differential equations D.4 with initial conditions (C.4). The behavior of the Kondo temperature as a function of the internal couplings is shown in Figure 4.7.

## 4.5. Renormalized coupling constants for the low-energy model at $B = 0$

Now that we have learned how to deal with the scaling equations for the low-energy Hamiltonian obtained in the neighborhood of the degeneracy at $B > 0$, let us deal with the degeneracy at $B = 0$ where the relevant energy states are $|+d\rangle$ and $|-d\rangle$. Keeping in mind what we have learned so far, it is convenient to look directly at the plot of the inverse coupling constants against $\ln(D/D_0)$ (Figure 4.8). Figure 4.8 shows that in the limiting case of $t_R = 0$ there exists an energy scale (the Kondo temperature) at which the coupling coefficients in the effective Hamiltonian diverge. On the contrary in the case $t_L = 0$ the coupling coefficients of the low-energy Hamiltonian flow to zero. In this last case, we are then in a situation similar to that set by 4.12 and depicted in the left-lowest part Figure 4.2 (b). The coupling constants renormalize to smaller values, leading to a situation of almost-uncorrelated electrons. The physical picture justifying this behavior is the following. Assume the dot is initially in state $|+d\rangle$. Being $J_{12}$

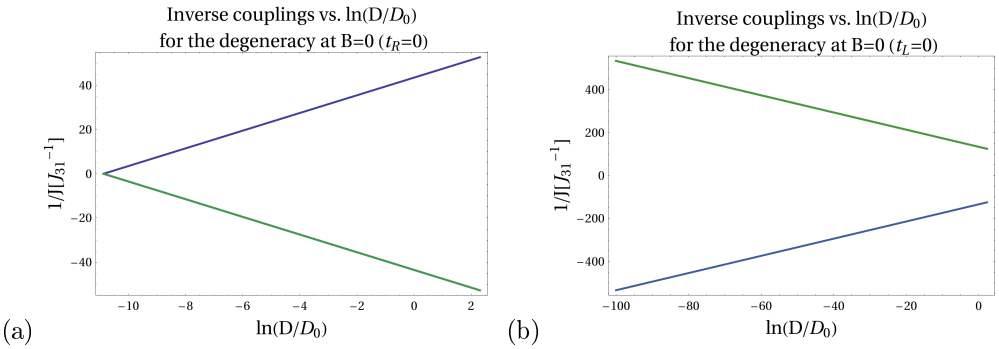


Figure 4.8.: Inverse couplings $J^{\pm}$ and $J^z$ against $\ln(D/D_0)$ (plotted for a specific choice of the internal couplings $J_{12}$, $J_{23}$ and $J_{31}$) for the model (4.4) describing the spin degeneracy at zero magnetic field. (a) is calculated in the limiting case of $t_R = 0$, (b) is calculated for $t_L = 0$. Note that in the last case the coupling constants don't diverge, but tend to a finite value instead. In this case the system then tend to a regime where dot and lead electrons are almost uncorrelated. In this situation it does not make sense to speak about Kondo temperature.

ferromagnetic the left and central spins tend to be bound in a parallel configuration, so that the most probable configuration of the three-spin system is $|\uparrow\uparrow\downarrow\rangle$. If only tunneling to the right lead is allowed, the spin system cannot flip to any configuration setting the three spins in the $|-d\rangle$ state. Therefore no Kondo resonance is allowed in this situation.
Let us now study in more detail the Kondo temperature for the limit $t_R = 0$. At $B = 0$ the low-energy doublet is given by:

$$\begin{aligned} |+d\rangle &= a\,|\uparrow\downarrow\uparrow\rangle + b\,|\uparrow\uparrow\downarrow\rangle + c\,|\downarrow\uparrow\uparrow\rangle \\ |-d\rangle &= l\,|\uparrow\downarrow\downarrow\rangle + m\,|\downarrow\downarrow\uparrow\rangle + n\,|\downarrow\uparrow\downarrow\rangle \end{aligned} \tag{4.30}$$

and therefore there exists more then one single-spin state in $|+d\rangle$ and $|-d\rangle$ that contribute to the exchange processes involving the left lead, giving a non-zero contribution to $\langle +d \mid H_{eff} \mid -d\rangle$.

The following processes contribute:

$$\begin{aligned} |\downarrow\downarrow\uparrow\rangle \rightsquigarrow |\uparrow\downarrow\uparrow\rangle \quad &\propto maJ_L \\ |\downarrow\uparrow\downarrow\rangle \rightsquigarrow |\uparrow\uparrow\downarrow\rangle \quad &\propto nbJ_L. \end{aligned} \tag{4.31}$$

From Figure 4.9 one sees that the interesting coefficients (the ones multiplying the states entering in (4.31)) have different behaviors when plotted against the same coupling constants ($J_{12}$, $J_{23}$ or $J_{13}$). Nevertheless what we are really interested in, is the product of these coefficients as they appear in (4.31). When looking at Figure 4.9 more carefully, one realizes that the two processes in (4.31) give a contribution that has the same overall behavior against the internal couplings $J_{13}$, $J_{12}$ and $J_{23}$. In some sense the two processes cooperate to give a certain behavior of the Kondo temperature. For example if we look at the evolution of the Kondo temperature with $J_{23}$, we see that it increases when $J_{23}$ increases. This is consistent with the fact that the probability of the processes in 4.31, i.e. the square of their amplitudes, also increases with $J_{23}$.

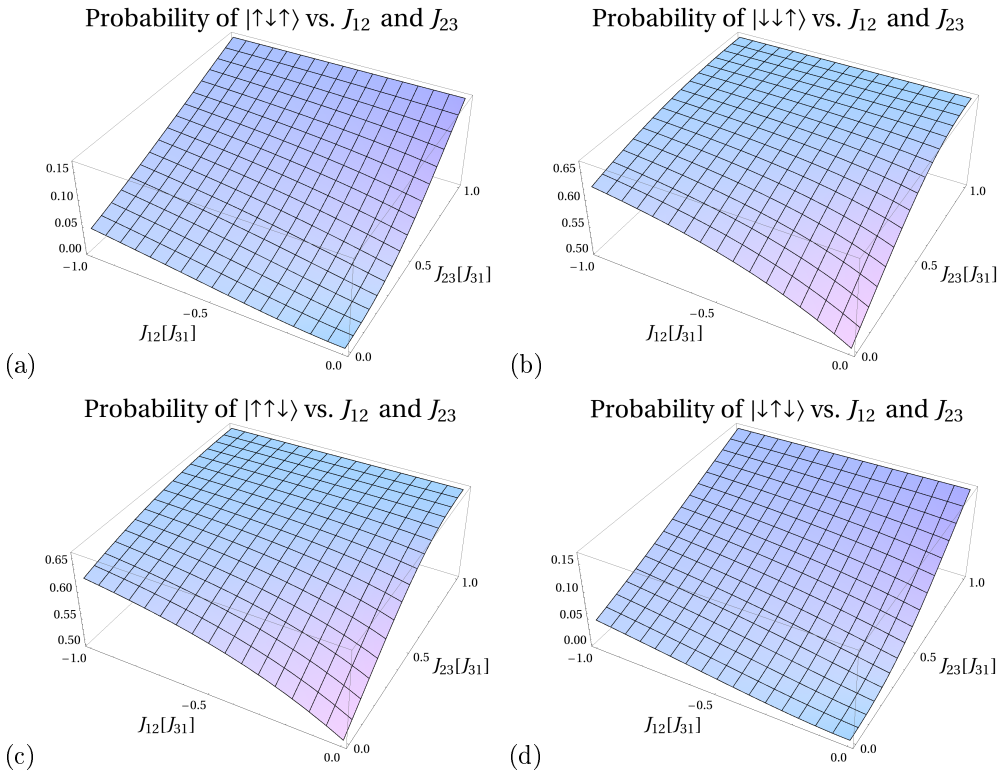


Figure 4.9.: Probability of the spin-configurations $|\uparrow\downarrow\uparrow\rangle$ (a) and $|\uparrow\uparrow\downarrow\rangle$ (c) in $|+d\rangle$ and the configurations $|\downarrow\downarrow\uparrow\rangle$ (b) and $|\downarrow\uparrow\downarrow\rangle$ (d) in $|-d\rangle$.

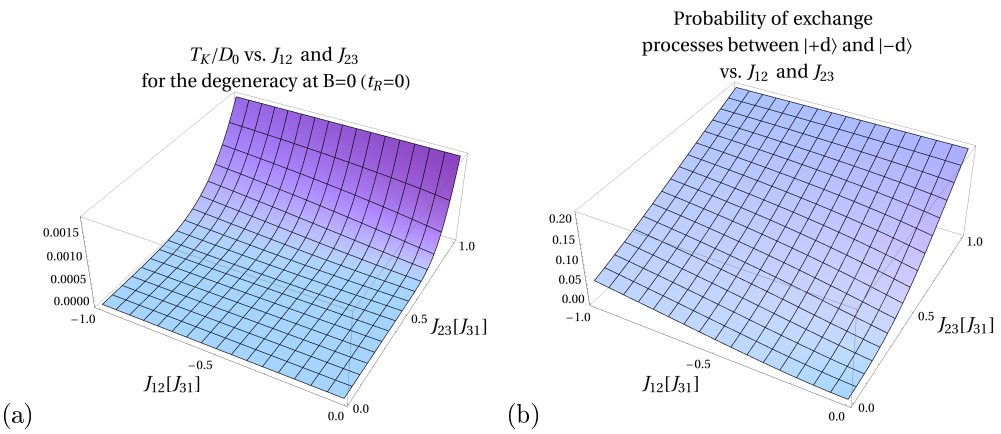


Figure 4.10.: Study of the Kondo temperature $T_K$ of the degeneracy at $B = 0$ in the limit $t_R = 0$. (a) Kondo temperature (in units of the initial bandwidth $D_0$) dependence on the internal coupling constants $J_{12}$ and $J_{23}$. The internal couplings are in units of $J_{31}$. The other coefficients are chosen to be $t_L = 0.83J_{31}$, $t_H = 0.93J_{31}$ and $U = 10J_{31}$. (b) Combined probability of the spin configurations allowing the exchange processes (4.31) against the internal couplings. Notice that the Kondo temperature dependence on the internal couplings is qualitatively the same as the occupation probabilities of the states that allow exchange processes between the two degenerate states of the system. The similar behavior of the two quantities is in agreement with the qualitative picture linking the value of the Kondo temperature with the probability of exchange processes between the degenerate states.

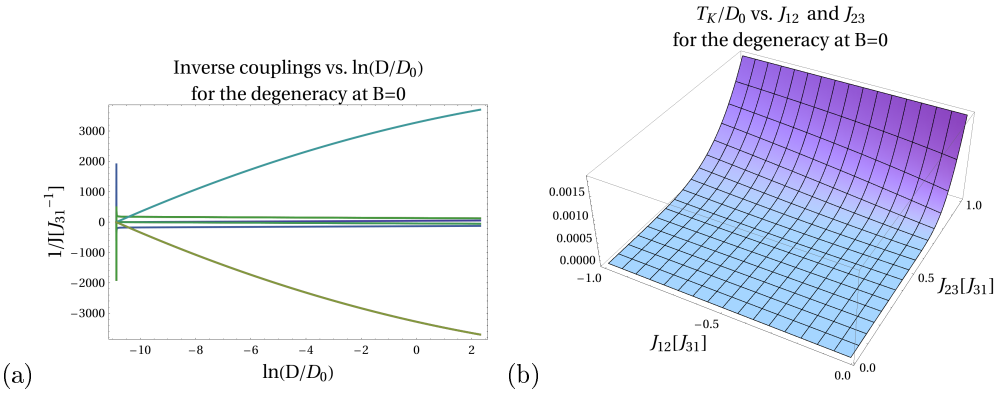


Figure 4.11.: (a) Inverse couplings $1/J$ (in units of $1/J_{31}$) for the complete Hamiltonian (4.4) against $\ln(D/D_0)$, where $D_0$ is the initial bandwidth. The internal couplings $J_{12}$, $J_{23}$ are chosen to be $J_{12} = -1.5J_{31}$, $J_{23} = 0.2J_{31}$ and $t_R = 0.76J_{31}$, $t_L = 0.83J_{31}$, $t_H = 0.93J_{31}$ and $U = 10J_{31}$. (b) Kondo temperature (in unit of the initial bandwidth $D_0$) dependence on $J_{12}$, $J_{23}$. $J_{12}$, $J_{23}$ are expressed in units of $J_{31}$.

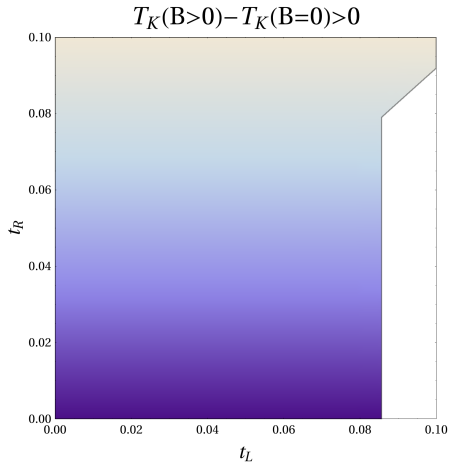


Figure 4.12.: The plot shows the region of the $t_L$-$t_R$ plane where $T_K(B > 0) \gtrsim T_K(B > 0)$. $t_L$ and $t_R$ are in units of the charging energy $U$. The darker color represent a smaller difference between the two Kondo temperatures, the lighter one a bigger Kondo temperature of the degeneracy at $B > 0$ when compared to the one at $B = 0$. Notice that at $t_L = 0$ the Kondo temperature of the system at $B > 0$ always prevails. This is in agreement with the calculation above, showing that in this limit, the system does not show Kondo behavior at zero field.

We have seen that the tunneling coupling to the right lead allows a renormalization process where the values of the coupling coefficients decrease. This leads to a situation where the lead and dot electrons behave as uncorrelated particles, in opposition to the strong coupling regime driven by tunneling to the left lead. In the intermediate situation, where both the tunneling couplings are on, we then expect the two regimes to compete. If the system is driven toward a strong coupling regime, then the Kondo temperature is likely to have a behavior similar to that found in the extreme case $t_R = 0$. This is seen in Figure 4.11.

## 4.6. Comparaison between the Kondo temperature of the two degeneracies for the case $J_{31} = J_{23}$

We have seen that in the simplified case where the two antiferromagnetic couplings $J_{31}$ and $J_{23}$ are equal, the eigenstates of the three-spin system uncoupled to the electrodes are independent of $J_{12}$, $J_{23}$ and $J_{31}$ (see Section 3.2.2). In this case also the coefficients of the low-energy Kondo Hamiltonian (4.7) are independent of $J_{12}$, $J_{23}$ and $J_{31}$ and the system is characterized by a well specific Kondo temperature, independent of the specific values assumed by the internal couplings. The only variables left are the tunneling couplings to the electrodes. We can thus compare the Kondo temperatures of the two degeneracies for different choices of the tunneling coefficients $t_L$ and $t_R$. Figure 4.12 shows that the Kondo temperature of the system at $B > 0$ is often bigger then the Kondo temperature at $B = 0$. Looking at the case $t_L = 0$, we see that the Kondo temperature at $B > 0$ is always bigger then the Kondo temperature at $B = 0$. This is in agreement with what discussed in the previous sections, where we observed that the renormalization process of the coupling coefficients for the system at $B = 0$ doesn't lead to a strong coupling regime, i.e. no Kondo effect is present in the system. This means that the

differential conductance spectrum of the system at very low temperatures (i.e. $T < T_K(B > 0)$) is likely to show a zero-bias Kondo peak at $B > 0$ and no Kondo effect at $B = 0$. In the limit $t_L = 0$, the system shows a transition to a strong coupling regime both at $B = 0$ and at $B > 0$. As a consequence the two Kondo temperatures compete and one or the other are dominant, depending on the value of $t_R$.

## 4.7. Conclusions on Kondo physics in a TTD

We have studied the Kondo temperature for the effective doublets at $B > 0$ and $B = 0$ and we have found that for internal couplings $J_{12} < 0$, $J_{23} > 0$ and $J_{31} > 0$ a certain general behavior of the Kondo temperature can be found.
At a certain finite magnetic field $B > 0$ the two states $|+\frac{3}{2}\rangle$ and $|+d\rangle$ become degenerate. Since the coupling $J_{12}$ is ferromagnetic, when the central region is in state $|+d\rangle$, the privileged configuration of the three spins will have the first and the second spin aligned, i.e. $|\uparrow\uparrow\downarrow\rangle$. This is reflected in the normalized amplitude of this configuration in $|+d\rangle$, which is in fact bigger in absolute value then the amplitude of states $|\uparrow\downarrow\uparrow\rangle$ and $|\downarrow\uparrow\uparrow\rangle$. This means that the prevalent exchange process between the two states of the doublet will be given by

$$|\uparrow\uparrow\downarrow\rangle \rightsquigarrow |\uparrow\uparrow\uparrow\rangle \quad \propto J_R \tag{4.32}$$

thus privileging exchange processes involving the right lead. Generally speaking we therefore expect the Kondo temperature given by exchange to the right lead to be bigger then the Kondo temperature arising by processes involving the left lead. This statement is confirmed by the data.
At $B = 0$ the degenerate states are $|+d\rangle$ and $|-d\rangle$. We have seen that exchange processes involving the right lead tend to give a renormalized model with almost independent electrons in the dot. On the contrary, exchange involving the left lead renormalizes the model coupling coefficients to always bigger values. The divergence of these coefficients marks the transition to a strong coupling regime, where perturbation theory stops to be valid. The energy scale giving this crossover is thus determined by the processes involving scattering to the left lead. Given that the states of the low-energy doublet are $|+d\rangle$ and $|-d\rangle$, it is complicated to find just one prevalent process giving exchange scattering between the two states. We can nevertheless say that the two predominant processes will be the ones involving the most probable state in $|+d\rangle$ and $|-d\rangle$, namely $|\uparrow\uparrow\downarrow\rangle$ and $|\downarrow\downarrow\uparrow\rangle$, respectively, i.e.:

$$\begin{aligned} |\downarrow\downarrow\uparrow\rangle &\rightsquigarrow |\uparrow\downarrow\uparrow\rangle \quad \propto J_L \\ |\uparrow\uparrow\downarrow\rangle &\rightsquigarrow |\downarrow\uparrow\downarrow\rangle \quad \propto J_L. \end{aligned} \tag{4.33}$$

Considering the two degeneracy points together one comes to the conclusion that Kondo peaks should in general be present. The visibility of such peaks in a real conductance spectrum really depends on the value of the Kondo temperature when compared with the characteristic energy scales of the cotunneling processes. A qualitative prediction can nevertheless be made, by considering the following observations:

- in the limit $t_R = 0$ both the degenerate doublet at $B > 0$ and that at $B = 0$ show a Kondo peak, at temperatures lower than the respective Kondo temperatures.
- in the limit $t_L = 0$ the situation is very different for the low-energy doublet at $B > 0$ and the one at $B = 0$. For the doublet at $B > 0$ the coupling coefficients flow to bigger values, giving a Kondo peak. On the contrary for the doublet at $B = 0$ there is no Kondo effect,

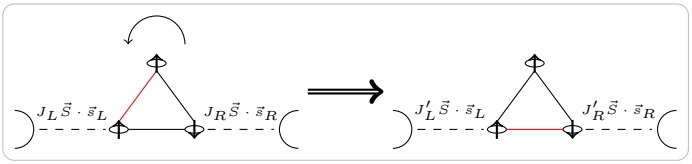


Figure 4.13.: Sketch of the suggested device allowing the study of the two-channel Kondo effect. Rotating the central region we can manipulate the coupling coefficients of the two Kondo channel.

because the coefficients flow to a limiting situation with lead electrons uncoupled to the dot electrons. The conductance spectrum of the system should therefore show a Kondo peak at $B > 0$ and no Kondo effect at $B = 0$.

In the case of very asymmetric coupling with $t_R >> t_L$, we then expect a Kondo peak to be visible when an external magnetic field of the proper strength is applied and no Kondo peak at $B = 0$.

## 4.8. Outlook

All together we have seen that a competition between two different channels (the coupling to the right lead and the coupling to the left lead) contributes to screening the dot region and therefore to set the Kondo temperature of the system. Turning off the tunneling coupling to one of the leads or the other we obtain a Kondo model that (roughly speaking) looks like $H \approx J_\alpha S \cdot s_\alpha$. When the couplings to the two independent leads are considered together the model Hamiltonian will have a contribution from each of the channels: $H \approx J_L S \cdot s_L + J_R S \cdot s_R$. This Hamiltonian has attracted substantial theoretical interest in the last twenty years because of the non-Fermi liquid low-energy behavior. Nevertheless a clear experimental evidence for such behavior hasn't been found yet, despite the interesting attempts of the last years [18].
The main difference between the two-channel model Hamiltonian and the Shrieffer Wolff Hamiltonian of a dot coupled to two different leads is the intrinsic independence of the two leads. In a standard Shrieffer-Wolff Hamiltonian the coupling coefficient $J$ is built up as the product of the tunneling coupling to the two leads: $J \approx \frac{t_L t_R}{U}$ (see 2.2). The two leads in this case only appear to be independent, while in fact they are not. A simple unitary transformation on the left-right lead space is in fact enough to notice that the dot electrons interact just with a specific combination of the lead electrons. Let us see how this come about.
The tunneling Hamiltonian of a single dot coupled to two leads has a tunneling term that looks like this:

$$H_T = \sum_{k,\sigma} \left( t_{Lk} d^\dagger_\sigma c_{Lk\sigma} + t^*_{Lk} c^\dagger_{Lk\sigma} d_\sigma \right) + \sum_{k,\sigma} \left( t_{Rk} d^\dagger_\sigma c_{Rk\sigma} + t^*_{Rk} c^\dagger_{Rk\sigma} d_\sigma \right). \tag{4.34}$$

This includes tunneling processes between the dot and both the leads. (4.34) can be rewritten in the following way:

$$H_T = \sum_{k,\sigma} \sqrt{|t_L|^2 + |t_R|^2} \left( d^\dagger_\sigma c_{ek\sigma} + c^\dagger_{ek\sigma} d_\sigma \right) \tag{4.35}$$

when the following rotation in the left-right space is performed:

$$\begin{pmatrix} c_{ek\sigma} \\ c_{ok\sigma} \end{pmatrix} = \frac{1}{\sqrt{|t_L|^2 + |t_R|^2}} \begin{pmatrix} t^*_L & t^*_R \\ -t_R & t_L \end{pmatrix} \begin{pmatrix} c_{Lk\sigma} \\ c_{Rk\sigma} \end{pmatrix}. \tag{4.36}$$

The Hamiltonian (4.35) shows that the dot coupled to two leads can really be described by a one-channel model because only the even combination $c_e$ of left and right lead electrons is tunnel coupled to the dot.
In our situation a similar approach cannot be performed because, even though we derived our model Hamiltonian (4.7) from an Anderson Hamiltonian, we have later on assumed that the internal coupling coefficients $J_{12}$, $J_{23}$ and $J_{31}$ can be both positive and negative, their real origine in a molecular system being a competition of the internal electron-electron interactions (see the discussion at the end of Section 3.1.5). In our system the lead electrons of the two leads are therefore fully independent and this allows us in principle to access the two-channel Kondo physics. We can infact think about a device where our three-spin system is allowed to rotate with respect to the position of the lead electrodes. We can then switch between a position where the ferromagnetic coupling breaks the symmetry of the system (Figure 4.13 left) and a position where the dots tunnel coupled to the leads are ferromagnetically coupled (Figure 4.13 right). Such a device would allow control over the two-channel Kondo coupling coefficients and might therefore be used to investigate experimentally the non-fermi liquid behavior of the system.

# 5. Singlet-triplet ground state transition in a double quantum dot

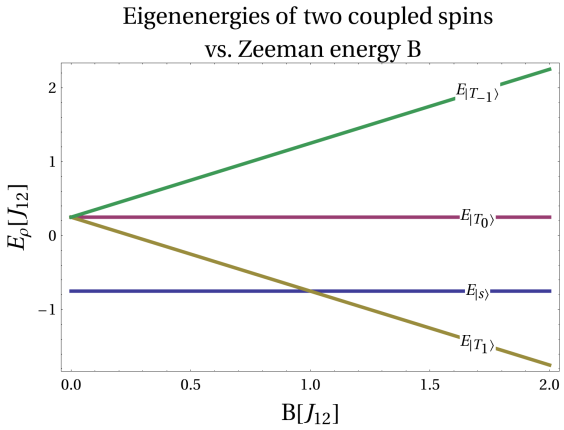


Figure 5.1.: Eigenvalues of the bare Hamiltonian of a double dot (with antiferromagnetic coupling $J_{12}$) plotted against the magnetic field. At $\frac{B}{J_{12}} \approx 1$ a crossing from a singlet to a triplet ground state can be observed.

In this chapter we turn to the study of the degeneracy features of a double dot (DD). From Figure 5.1 we see that tuning an external magnetic field the energy spectrum of a two-spin system presents a crossing from a singlet (at $B < J_{12}$ in Figure 5.1) to a triplet ground state (at $B > J_{12}$). Our main goal is to study the differential conductance in the neighborhood of the transition. We assume that the energy levels are gate-dependent and moreover the two competing ground states are mixed by a weak interaction (possibly a weak spin-orbit-like term). In this case an interesting feature arises in the differential conductance map at the singlet-triplet degeneracy point. We will discuss the main characteristics of this new feature and compare them with the experimental data from [5], which show similar characteristics.

## 5.1. Differential conductance near the degeneracy of weak-coupled singlet-triplet ground states

In this section our major goal is the study of the differential conductance in the proximity of a singlet-triplet ground state transition in a double dot (DD). Our system is once again the same discussed in 3.1.4, where the ground state is an effective two-electron dot, allowing only virtual (classical forbidden) fluctuations to the zero- and three-electron states.
As seen in 3.2.1, the uncoupled dot Hamiltonian is diagonalized by the singlet-triplet basis (3.23), and the eigenenergies of the singlet state $|\, s\rangle$ and the triplet state $|\, T_{+1}\rangle$ become degenerate at finite field $B > 0$ (Figure 3.9).

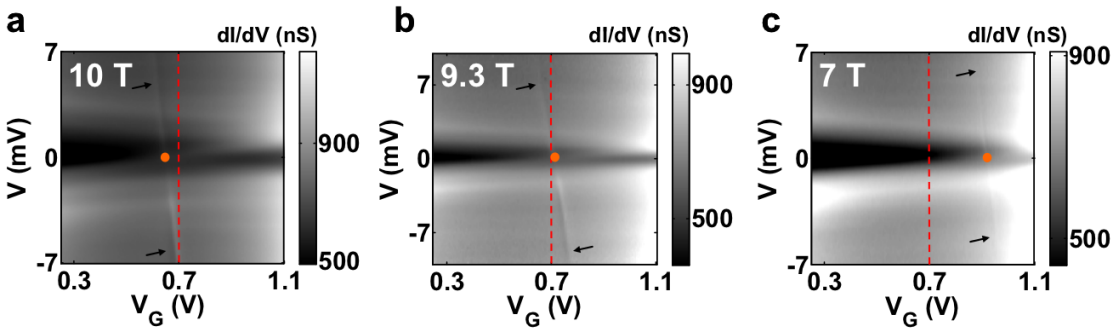


Figure 5.2.: Reproduced from [5] (supplementary information). Experimental measurements (for different values of the external magnetic field) of the differential conductance against bias and gate voltage. The measurments point out the presence of an almost vertical line (marked by black arrows in figure) at the singlet-triplet transition point. The red dot corresponds to the singlet-triplet crossing at zero bias, the red line is used as a guide to the eye.

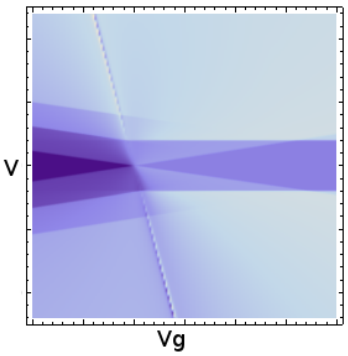


Figure 5.3.: Density plot of the differential conductance against gate (x axis) and bias (y axis) voltage (all in a.u.), in the neighborhood of the singlet-triplet ground state transition as obtained from the model described in the text.

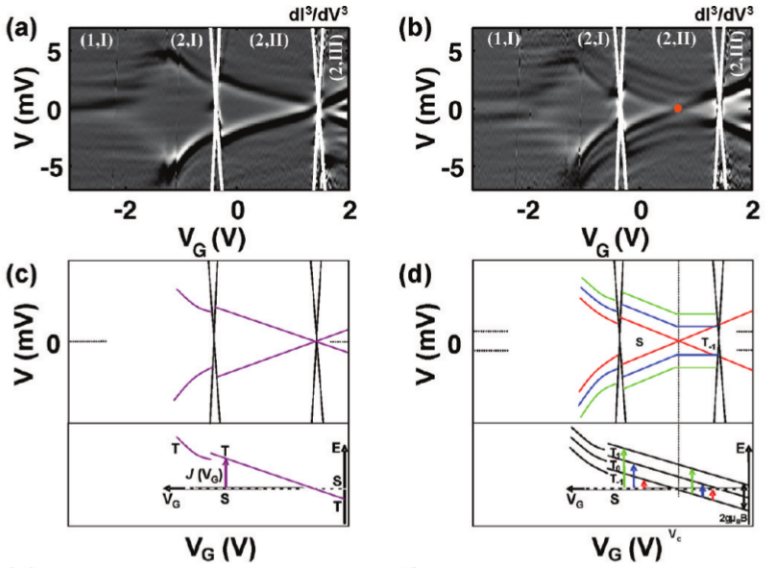


Figure 5.4.: Reproduced from [5]. Density plot of $dI^3/dV^3$ against bias ($V$) and gate ($V_g$) voltage at zero (a) and finite (b) magnetic field ($B = 10T$). In (c) and (d) the essential features of (a) and (b) are schematically drawn and an energy level diagram is sketched. A singlet to triplet ground state transition is seen to occur at $V_g \approx 1V$ (point marked by a red circle).

If we now assume the singlet and triplet competing ground states to be weakly coupled (e.g. by a spin-orbit term), and moreover we add a weak gate and bias dependence of the internal coupling $J_{12}(V, V_g) = J_{12}(1 - V\alpha - \mathrm{Vg}\beta)$, the dot Hamiltonian in the singlet triplet basis $\{|\, T_{+1}\rangle, |\, T_0\rangle, |\, T_{-1}\rangle, |\, s\rangle\}$ becomes:

$$\begin{pmatrix} -B + \frac{1}{4}J_{12}(V,V_g) & 0 & 0 & -\lambda \\ 0 & \frac{1}{4}J_{12}(V,V_g) & 0 & 0 \\ 0 & 0 & B + \frac{1}{4}J_{12}(V,V_g) & 0 \\ -\lambda & 0 & 0 & -\frac{3}{4}J_{12}(V,V_g) \end{pmatrix} \tag{5.1}$$

where the off-diagonal spin-orbit term is here assumed to be a constant ($\lambda$).

The addition of a somehow artificial gate and bias dependence is justified when considering the real system we have in mind. In fact, in this section we mostly refer to a three-terminal molecular junction containing a Mn-transition metal complex [5]. This system presents a singlet to triplet ground state transition inside the charge state 2 Coulomb diamond, as confirmed by measurements of the magnetic field dependence of the inelastic cotunneling lines (Figure 5.4). The energy levels of the different spin states are seen to be gate dependent, so that we can model the inter-dot interaction through a gate-dependent exchange coupling $J_{12}(V_g)$. Figure 5.4 ((c) and (d)) shows a schematic view of the gate-dependent singlet and triplet energy levels. On the left hand side the ground state is a singlet. Inelastic cotunneling to the triplet states then gives gate dependent high-conductance lines in the density plot (a) and (b). When an external magnetic field is turned on these cotunneling lines are seen to be equally spaced, as predicted by a Zeeman spitting $\approx g\mu_B B$. On the right hand side $|\, T_{+1}\rangle$ is the ground state, and the inelastic cotunneling transitions $|\, T_{+1}\rangle \rightarrow |\, T_0\rangle$, $|\, T_{+1}\rangle \rightarrow |\, T_{-1}\rangle$ become gate-independent, being the Zeeman splitting $\approx g\mu_B B$ a constant, while the transition to the singlet state depends on

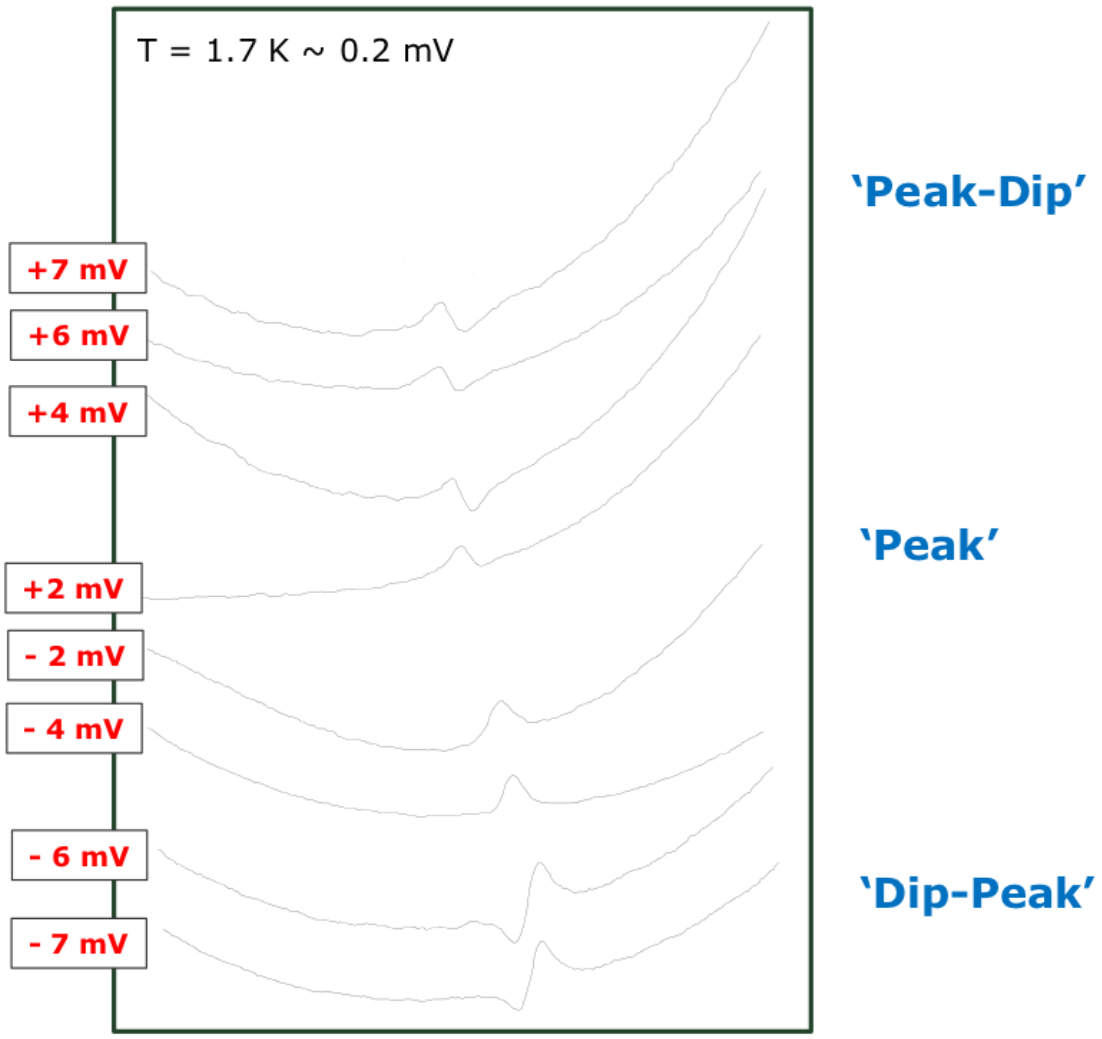


Figure 5.5.: Differential conductance vs. gate voltage in the neighborhood of the singlet-triplet ground state transition for different fixed values of the bias voltage. The plots are offset: from bottom to top higher (from high negative to high positive) values of the bias have been chosen.

(a) 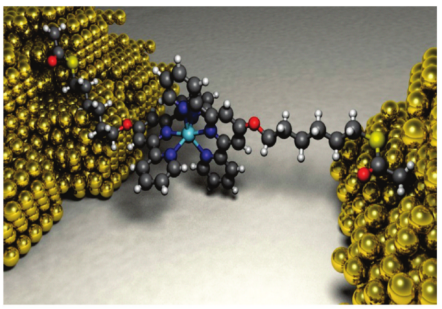

(b) 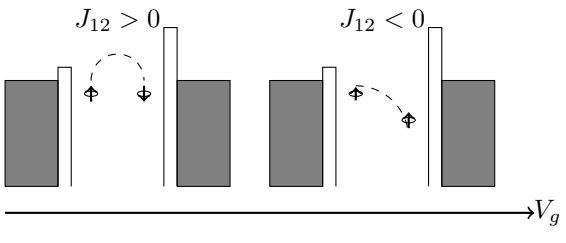


Figure 5.6.: (a) Artistic impression of the molecular junction used in [5]. The specific geometric configuration suggested in Figure would justify an asymmetric coupling to the electrodes. (b) Schematic representation of the gate dependent inter-spin coupling $J_{12}$.

gate.
Having studied how a gate-dependent $J_{12}$ coupling can account for the main featured experimentally observed, let us try to give a physical argument for it. An asymmetry in the coupling of the two edges of the molecular complex to the leads could in fact account for the $V_g$ energy level dependence. If one edge of the molecule happens to be more strongly coupled to the nearby electrode then the other edge to the second electrode, then its electrons will be screened by the electrode's potential and consequently its gate dependence will be weaker. This also accounts for a very weak bias dependence, given by the consequent change of capacitive coupling to the gate.

The overall picture is revisited in Figure 5.6, where the right spin is assumed to be more strongly coupled to the left lead then the right spin to the right lead. Increasing the gate coupling then affects almost uniquely the right spin, whose energy lowers. The antiferromagnetic inter-spin coupling $J_{12}$ becomes ferromagnetic, thus suggesting an interplay between an antiferromagnetic spin coupling and the ferromagnetic Hund's rule, favoring the latter.

The projection of (5.1) into the low energy subspace $\{|\, T_{+1}\rangle, |\, s\rangle\}$ is:

$$\begin{pmatrix} -B + \frac{1}{4}J_{12}(V, V_g) & -\lambda \\ -\lambda & -\frac{3}{4}J_{12}(V, V_g) \end{pmatrix} \tag{5.2}$$

which, defining $x := \frac{1}{2}\left[B - J_{12}(1 - V\alpha - \mathrm{Vg}\beta)\right]$, has eigenvalues

$$E_{\pm} = -\frac{5}{4}B + \frac{x}{2} \pm \sqrt{x^2 + \lambda^2} \tag{5.3}$$

and corresponding (normalized) eigenstates

$$\begin{aligned} |\pm\rangle &= \alpha_{\pm}\,|\, s\rangle + \beta_{\pm}\,|\, T_{+1}\rangle \\ &= \frac{\lambda}{\sqrt{\lambda^2 + \left[x \mp \sqrt{x^2+\lambda^2}\right]^2}}\,|\, s\rangle + \frac{x \mp \sqrt{x^2+\lambda^2}}{\sqrt{\lambda^2 + \left[x \mp \sqrt{x^2+\lambda^2}\right]^2}}\,|\, T_{+1}\rangle. \end{aligned} \tag{5.4}$$

Notice that $\alpha_{\pm}^2 = 1 - \beta_{\pm}^2$. We can then calculate the current and the differential conductance as in (3.32), representing all the operators in the basis (5.4). Fixing the bias voltage and plotting the differential conductance as a function of the gate voltage in the neighborhood of the

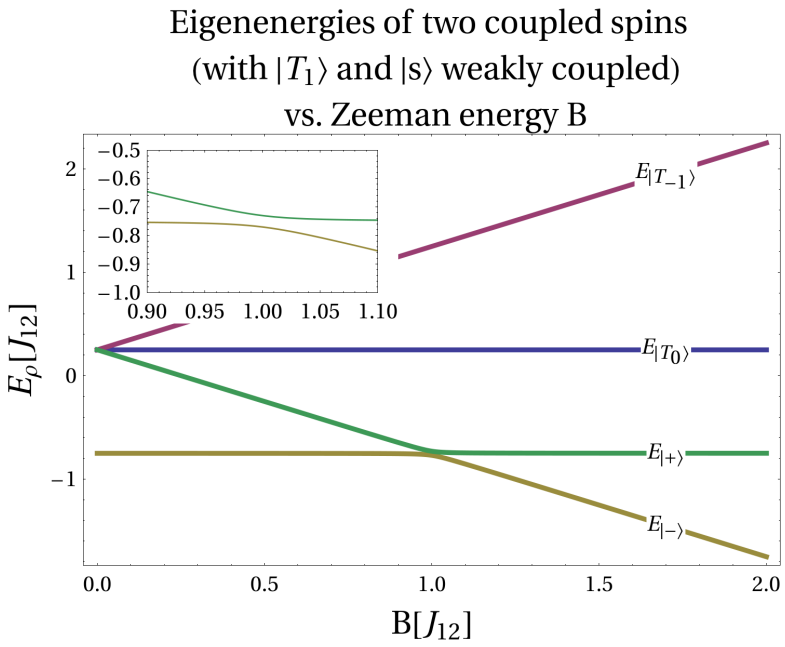


Figure 5.7.: Eigenvalues of the bare Hamiltonian of a double dot with spin-orbit coupled $|\, s\rangle$ and $|\, T_{+1}\rangle$ states, plotted against the magnetic field $B$. The values are in units of $J_{12}$. Notice the avoided crossing (zoom in the inset) of the low energy states of the system.

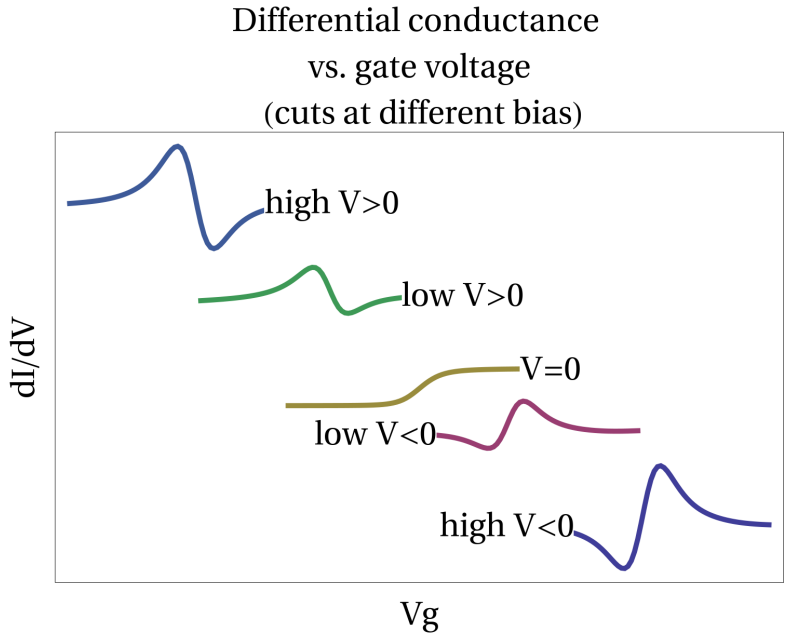


Figure 5.8.: Differential conductance vs. gate voltage in the neighborhood of the singlet-triplet ground state transition for different fixed values of the bias voltage. The plots are offset: from bottom to top higher (from high negative to high positive) values of the bias have been chosen.

singlet-triplet ground state transition, a very peculiar feature can be observed (Figure 5.8). At high negative bias we can observe a dip-peak line, which gets less sharp at smaller negative bias and reduce to a step at $V \approx 0$. Going to positive bias a reversed, but otherwise similar, feature can be observed: a peak-dip line which gets deeper and deeper when going to higher bias. This situation is seen to be preserved also for a simplified model where $t_H = 0$. In the following we will therefore deal with this simplified version of the system, in order to get easier calculation, in any case still preserving the main physics.
Figure 5.8 has many characteristics, which need to be discussed. We start by giving an explanation of the step, that can be observed at zero bias. At zero bias voltage the dominant contribution to the differential conductance is given by elastic cotunneling. A step at the singlet-triplet ground state transition then means that one of the two competing ground states gives a bigger elastic contribution then the other. We can try to estimate this contribution by calculating the equilibrium elastic current. Let us assume that the ground state is either $\mid s\rangle$ or $\mid T_{+1}\rangle$. We are then well inside the $\{Vg, V\}$ area where either the singlet or $\mid T_{+1}\rangle$ are the undiscussed ground state. We can then safely assume that in such a region either $n_{|s\rangle} = 1$ or $n_{|T_{+1}\rangle} = 1$. Let us deal with both the possibilities at once and assume that a certain state $\rho$ is occupied with unitary probability ($n_\rho = 1$), while all the other states are empty. Under such assumptions the current (3.32) becomes:

$$\begin{aligned} I = e2\pi\nu_L\nu_R \Bigg[ & eV \left\{ 2\sum_i \left(\mathbf{T}^{RL*}_{\rho\rho}\right)^i \left(\mathbf{T}^{RL}_{\rho\rho}\right)^i + 2\left|\mathbf{P}^{RL}_{\rho\rho}\right|^2 \right\} \\ & + \sum_{\rho'\neq\rho} \left[(\Delta_{\rho'\rho} - eV)n_B(\Delta_{\rho'\rho} - eV) - (\Delta_{\rho'\rho} + eV)n_B(\Delta_{\rho'\rho} + eV)\right] \\ & \left\{ 2\sum_i \left(\mathbf{T}^{RL*}_{\rho'\rho}\right)^i \left(\mathbf{T}^{RL}_{\rho'\rho}\right)^i + 2\left|\mathbf{P}^{RL}_{\rho'\rho}\right|^2 \right\} \Bigg] \end{aligned} \tag{5.5}$$

so that the elastic cotunneling contribution is given by:

$$I_{elas} = e2\pi\nu_L\nu_R \left[ eV \left\{ 2\sum_i \left(\mathbf{T}^{RL*}_{\rho\rho}\right)^i \left(\mathbf{T}^{RL}_{\rho\rho}\right)^i + 2\left|\mathbf{P}^{RL}_{\rho\rho}\right|^2 \right\} \right]. \tag{5.6}$$

We then find for the singlet ground state $\rho = \mid s\rangle$:

$$I_{elas} \approx e^2 2\pi\nu_L\nu_R V \left\{0 + 2W^2\right\} \tag{5.7}$$

and for the triplet ground state $\rho = \mid T_{+1}\rangle$:

$$I_{elas} \approx e^2 2\pi\nu_L\nu_R V \left\{2|J|^2 + 2|W|^2\right\}. \tag{5.8}$$

We can then observe that a triplet ground state gives a contribution to the elastic cotunneling current which is bigger then the one given by a singlet ground state. This accounts for the step in Figure 5.8 at zero bias. We then conclude that looking at the differential conductance deep inside the singlet (triplet) ground state region, a lower (higher) value is observed, when compared to the triplet (singlet) region. This can be seen in the density plot 5.3, where different colors (i.e. different values of the elastic differential conductance) characterize the two regions where either $\mid s\rangle$ or $\mid T_{+1}\rangle$ is the undiscussed ground state.

We now turn to the dip-peak feature running along the singlet-triplet line. Let us start by observing that the characterizing dip-peak structure changes into a simple dip (at negative bias)

or a simple peak (at positive bias) for very asymmetric couplings to the leads (Figure 5.9). The presence of a peculiar peak (or dip) at the singlet-triplet transition appears then to be an equilibrium effect, while the peak-plus-dip (dip-plus-peak) effect seems to be due to non-equilibrium effects.

Let us now study how the dip-peak structure changes with the strength of the off-diagonal mixing term $\lambda$. In the case of very asymmetric couplings to the leads temperature is the energy scale setting the shape and width of the feature at the singlet-triplet transition. This can be seen in Figure 5.10 (b) where a very clear dip at high negative bias is seen to set at $\lambda = 0$ and to survive until $\lambda \approx t$. When $\lambda > t$, $\lambda$ becomes the predominant energy scale, which smears the dip structure. The bigger $\lambda$ when compared to $t$, the wider and less sharp the dip in the conductance. When non-equilibrium effects play a strong role, a dip-peak can be seen (Figure 5.10 (a)). When $\lambda = 0$, the singlet and triplet competing ground states are not mixed and the current presents a step at the singlet-triplet degeneracy, which translates into a peak in the differential conductance (not really visible in Figure 5.10 because of the scale used). But when $\lambda$ is turned on the current presents a dip (peak) at the degeneracy point for high negative (positive) bias. The width of the dip (peak) is set by the strength of $\lambda$, which is then the crucial energy scale. The $\lambda$-dependent dip (peak) in the current translates into the dip-plus-peak (peak-plus-dip) seen in the differential conductance. Figure 5.10 shows that smaller values of the off-diagonal coupling $\lambda$ lead to a sharper dip-peak in the differential conductance. A gradual decreasing of the value of $\lambda$ then leads to an abrupt transition from a dip-peak (peak-dip) at positive $\lambda$ to a dip (peak) at $\lambda = 0$. Such a transition is highly unphysical, as it is our model when very low-energies are considered. In fact, in our treatment we have never taken into account the broadening of the energy levels due to tunneling. A calculation taking care of such broadening would set a limit at the height and sharpness of our feature.
To sum up, we have observed the following crucial features:

- when the gate and bias voltage are tuned well inside the region where $\mid T_{+1}\rangle$ is the ground state, the elastic cotunneling contribution is bigger then the correspondent contribution inside the $\mid s\rangle$-ground state region.

- when approaching the singlet-triplet degeneracy, $\mid T_{+1}\rangle$ and $\mid s\rangle$ are mixed into a bonding- and an anti-bonding-like states; cotunneling processes result in an interesting behavior of the differential conductance:

- for very asymmetric couplings to the two leads, a step is observed in the current as a function of the gate voltage, which translates into a peak (at positive bias) or a dip (at negative bias) in the differential conductance;

- for situations where non-equilibrium effects play an important role ($t_R \approx t_L$) the peak (dip) feature becomes a peak-dip (dip-peak); this line shape is seen to be related to the values of the occupation probabilities and it is seen to be highly enhanced by a population inversion in the occupation probabilities of the two low-energy-states.

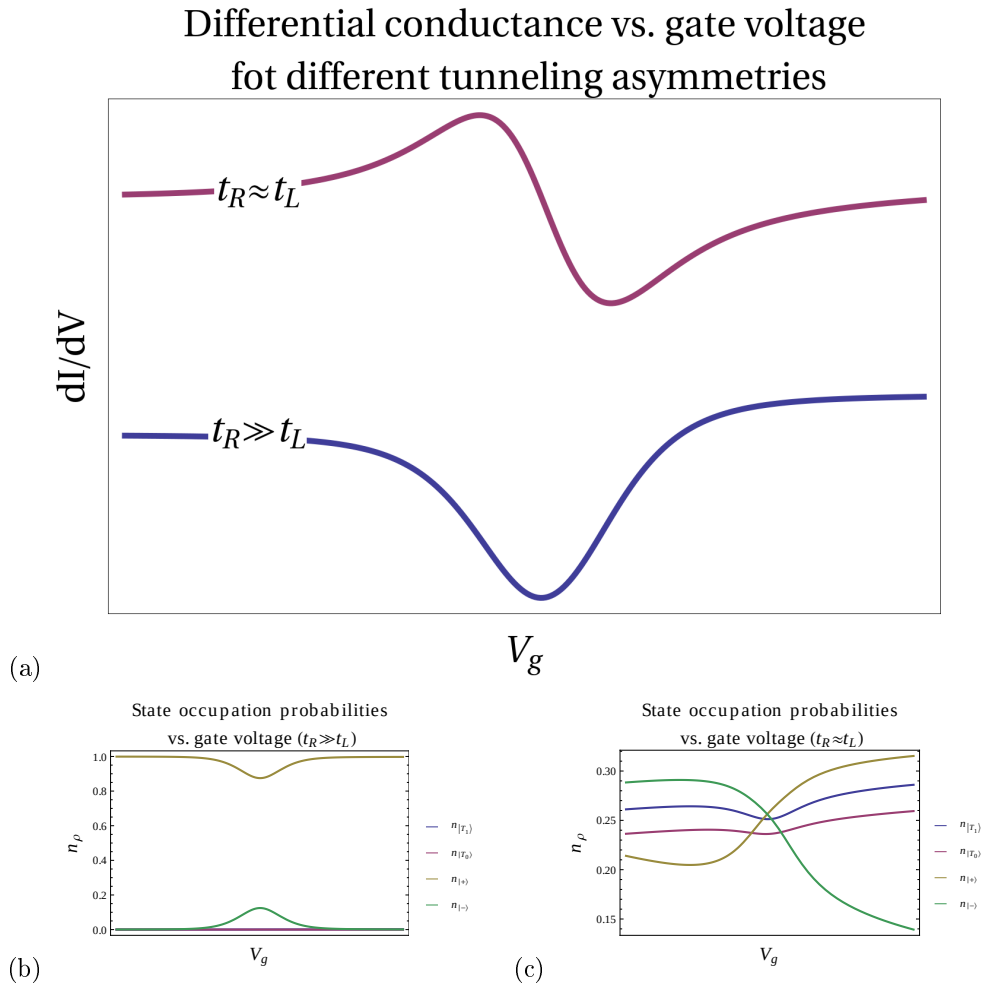


Figure 5.9.: (a) Differential conductance against gate voltage (in the very neighborhood of the singlet to triplet ground state transition) at fixed high (negative) bias for different asymmetries in the tunneling couplings to the leads (different plots are offset and scaled). The top line correspond to symmetric choice of the tunneling coefficients to the left and the right lead, the bottom one corresponds to $t_R \approx 100 t_L$(b) Occupation probability of the different states against gate voltage. (a) corresponds to the very asymmetric limit (yellow line in the $dI/dV$ plot), (b) has a weaker asymmetry (blue line in the $dI/dV$ plot), (c) is symmetrically coupled to right and left leads (red line in the $dI/dV$ plot).

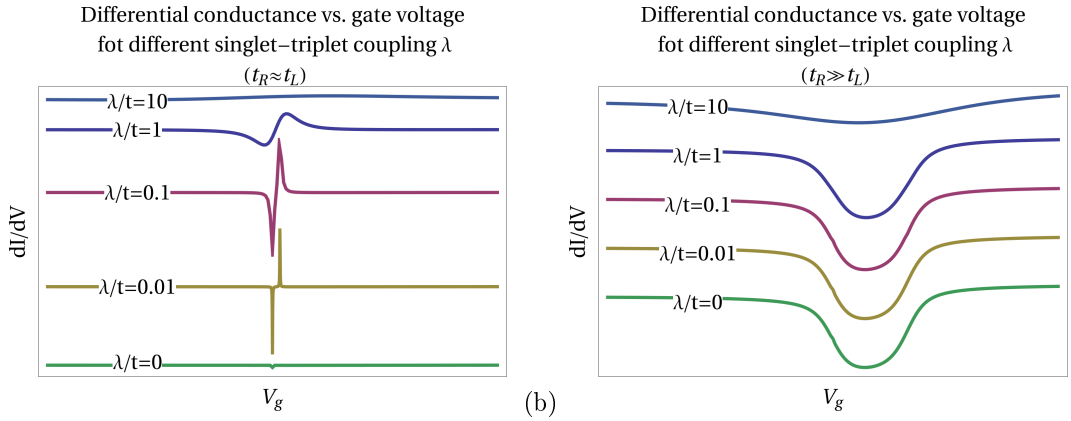


Figure 5.10.: Differential conductance vs. gate voltage (at high negative bias) in the neighborhood of the singlet-triplet ground state transition for different values of the spin-orbit coupling $\lambda$ (different ratio $\lambda/t$ where $t$ is the temperature). In (a) the tunneling coefficients to the leads are of the same order $t_L \approx t_R$, in (b) $t_L \ll t_R$. The plots are offset: from bottom to top higher values of the ratio $\lambda/t$. Notice that the blue line in (a) and (b) corresponds to the choice $\lambda \approx t$, while the purple line corresponds to $\lambda = 0$.

# 6. Conclusions

In this thesis we have built up a general theoretical framework for modelling low-spin molecular junctions inside the Coulomb blockade regime, where classical electronic transport is blocked. We have considered a number of two and three-dot configurations coupled to two electrods. We have further assumed that double- and zero-occupation of each dot are energetically expensive and therefore each dot is effectively singly occupied, leading to a model where single-spins play the role of the dots. We are therefore dealing with two and three localized spins, interacting both within each other (through what we call inter-dot coupling) and with the electrods.

We have studied the differential conductance as a function of the applied bias voltage. For the two-spin systems a plot of the differential conductance vs. bias voltage shows the usual symmetric structure with sharp increased values corresponding to the energy excitations coupling different dot-states (inelastic cotunneling peaks). For the three-spin case a richer structure can be observed. Depending on the values of the inter-dot couplings, the differential conductance can be symmetric (for equal couplings of the two edge-spins to the third central one) or asymmetric (for different values of those couplings). The origin of such an asymmetry is due to the peculiar second-order terms in the Shrieffer-Wolff Hamiltonian, which turn out to be non symmetric in the three-spin basis.

We have then focused on the low-energy states of the two- and three-spin systems. We have seen that at specific values of the external applied field the two low-energy states might become degenerate. A degenerate ground state can give rise to a Kondo peak in the zero-bias differential conductance. Such peak is a strong coupling effect which can be catched with non-perturbative methods. We have mostly been interested in finding the energy scale giving the crossover to the strong coupling regime (Kondo temperature), which can be captured by studing the renormalization of the coupling constants due to a finite band width in the leads. When a break-down of perturbation theory occurs, the renormalization procedure outlines a monotonous increase of the couplings. In such cases the Kondo temperature can be identifed with the energy scale at which the inverse couplings go to zero. In our three-dot case the Kondo temperature shows a complicated dependence on the inter-dot couplings, which makes it difficult to compare to the other energy scale of the system. Nevertheless, we have been able to conclude that in systems very asymmetrically coupled to the leads, we can predict the appearence or not of a Kondo peak at zero bias.
We then turned to the double-spin system at the singlet-triplet degenerate point and we have built up a model where a small perturbative term couples the two competing ground states. Such a model accounts for a very peculiar dip-peak line-shape observed in the differential conductance vs. the gate voltage at the singlet-triplet transition in experiments on a Mn-complex three-terminal junction [5]. Further work has still to be done in order to get a full understanding of the origin of this feature. Our results have nevertheless given a first insight on the non-equilibrium origin of the dip-peak structure.

# A. Shrieffer-Wolff tranformation for a two-dot lateral system

We here want to show the detailed procedure used in order to project out the zero- and doubly-occupied states of each dot in the two-dot system of Section 3.1.3. The following detailed study allows us to take the usual Shrieffer-Wolff [13] transformation one step further, in order to describe "two-stage" virtual processes in the central region. We end up finding the form of the operator describing virtual high-energy transitions (to doubly- and zero-occupied states) in the left dot first and in the right dot afterwards (or viceversa). Since we work on the basis of two combined spins (singlet-triplet basis), the final operator will be given in form of matrix elements on this basis states.
Let us then start by studying all the processes giving transport from the left to the right lead (the ones from the right to the left lead being the hermitian conjugate of these) through virtual transitions in the dots. For each process we calculate the matrix elements between the initial and final state written in the singlet-triplet basis, so that the operator describing all such processes will then be given as a sum of projector operators in this basis.

### Processes proportional to $c^\dagger_{R\downarrow}c_{L\uparrow}$

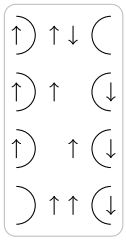

$$\propto J_{RL} d^\dagger_{L\uparrow} c_{L\uparrow} d^\dagger_{R\uparrow} d_{L\uparrow} c^\dagger_{R\downarrow} d_{R\downarrow} := \hat{O}$$

$$\text{and after reordering: } \hat{O} = J_{RL} d^\dagger_{L\uparrow} d_{L\uparrow} d^\dagger_{R\uparrow} d_{R\downarrow} c^\dagger_{R\downarrow} c_{L\uparrow}$$

$$\begin{cases} \langle T_{+1} \mid \hat{O} \mid s \rangle = \frac{1}{\sqrt{2}} \langle 0 \mid d_{R\uparrow} d_{L\uparrow} d^\dagger_{L\uparrow} d_{L\uparrow} d^\dagger_{R\uparrow} d_{R\downarrow} d^\dagger_{L\uparrow} d^\dagger_{R\downarrow} \mid 0 \rangle c^\dagger_{R\downarrow} c_{L\uparrow} \\ \qquad\qquad - \frac{1}{\sqrt{2}} \langle 0 \mid d_{R\uparrow} d_{L\uparrow} d^\dagger_{L\uparrow} d_{L\uparrow} d^\dagger_{R\uparrow} d_{R\downarrow} d^\dagger_{L\downarrow} d^\dagger_{R\uparrow} \mid 0 \rangle c^\dagger_{R\downarrow} c_{L\uparrow} \\ \qquad\qquad = \frac{1}{\sqrt{2}} c^\dagger_{R\downarrow} c_{L\uparrow} + 0 \\ \langle T_{+1} \mid \hat{O} \mid T_0 \rangle = \frac{1}{\sqrt{2}} c^\dagger_{R\downarrow} c_{L\uparrow} \end{cases}$$

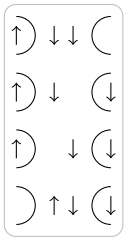

$$\propto J_{RL} d^\dagger_{L\uparrow} d_{L\downarrow} d^\dagger_{R\downarrow} d_{R\downarrow} c^\dagger_{R\downarrow} c_{L\uparrow} := \hat{O}$$

$$\begin{cases} \langle T_0 \mid \hat{O} \mid T_{-1} \rangle = \frac{1}{\sqrt{2}} \langle 0 \mid d_{R\downarrow} d_{L\uparrow} d^\dagger_{L\uparrow} d^\dagger_{R\downarrow} d_{L\downarrow} d_{R\downarrow} d^\dagger_{L\downarrow} d^\dagger_{R\downarrow} \mid 0 \rangle c^\dagger_{R\downarrow} c_{L\uparrow} \\ \qquad\qquad = \frac{1}{\sqrt{2}} c^\dagger_{R\downarrow} c_{L\uparrow} + 0 \\ \langle s \mid \hat{O} \mid T_{-1} \rangle = \frac{1}{\sqrt{2}} c^\dagger_{R\downarrow} c_{L\uparrow} \end{cases}$$

## Processes proportional to $c^\dagger_{R\uparrow}c_{L\downarrow}$

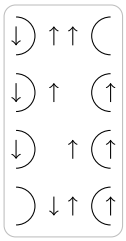

$$\propto J_{RL} d^\dagger_{L\downarrow} d_{L\uparrow} d^\dagger_{R\uparrow} d_{R\uparrow} c^\dagger_{R\uparrow} c_{L\downarrow} := \hat{O}$$

$$\begin{cases} \langle T_0 \mid \hat{O} \mid T_{+1} \rangle = \dfrac{1}{\sqrt{2}} \langle 0 \mid d_{R\uparrow} d_{L\downarrow} d^\dagger_{L\downarrow} d^\dagger_{R\uparrow} d_{L\uparrow} d_{R\uparrow} d^\dagger_{L\uparrow} d^\dagger_{R\uparrow} \mid 0 \rangle c^\dagger_{R\downarrow} c_{L\uparrow} \\ \qquad\qquad = \dfrac{1}{\sqrt{2}} c^\dagger_{R\uparrow} c_{L\downarrow} \\ \langle s \mid \hat{O} \mid T_{+1} \rangle = -\frac{1}{\sqrt{2}} c^\dagger_{R\uparrow} c_{L\downarrow} \end{cases}$$

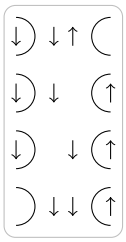

$$\propto J_{RL} d^\dagger_{L\downarrow} d_{L\downarrow} d^\dagger_{R\downarrow} d_{R\uparrow} c^\dagger_{R\uparrow} c_{L\downarrow} := \hat{O}$$

$$\begin{cases} \langle T_{-1} \mid \hat{O} \mid T_0 \rangle = \dfrac{1}{\sqrt{2}} \langle 0 \mid d_{R\downarrow} d_{L\downarrow} d^\dagger_{L\downarrow} d^\dagger_{R\downarrow} d_{L\downarrow} d_{R\uparrow} d^\dagger_{L\downarrow} d^\dagger_{R\uparrow} \mid 0 \rangle c^\dagger_{R\uparrow} c_{L\downarrow} \\ \qquad\qquad = \dfrac{1}{\sqrt{2}} c^\dagger_{R\uparrow} c_{L\downarrow} \\ \langle T_{-1} \mid \hat{O} \mid s \rangle = -\frac{1}{\sqrt{2}} c^\dagger_{R\uparrow} c_{L\downarrow} \end{cases}$$

## Processes proportional to $c^\dagger_{R\uparrow}c_{L\uparrow}$

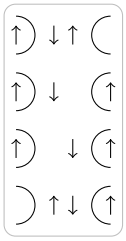

$$\propto J_H d^\dagger_{L\uparrow} d_{L\downarrow} d^\dagger_{R\downarrow} d_{R\uparrow} c^\dagger_{R\uparrow} c_{L\uparrow} := \hat{O}$$

$$\begin{cases} \langle T_0 \mid \hat{O} \mid T_0 \rangle = \dfrac{1}{\sqrt{2}\sqrt{2}} \langle 0 \mid d_{R\downarrow} d_{L\uparrow} d^\dagger_{L\uparrow} d^\dagger_{R\downarrow} d_{L\downarrow} d_{R\uparrow} d^\dagger_{L\downarrow} d^\dagger_{R\uparrow} \mid 0 \rangle c^\dagger_{R\uparrow} c_{L\uparrow} \\ \qquad\qquad = \dfrac{1}{2} c^\dagger_{R\uparrow} c_{L\uparrow} \\ \langle T_0 \mid \hat{O} \mid s \rangle = -\frac{1}{2} c^\dagger_{R\uparrow} c_{L\uparrow} \\ \langle s \mid \hat{O} \mid T_0 \rangle = \frac{1}{2} c^\dagger_{R\uparrow} c_{L\uparrow} \\ \langle s \mid \hat{O} \mid s \rangle = \frac{1}{2} c^\dagger_{R\uparrow} c_{L\uparrow} \end{cases}$$

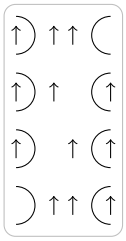

$$\propto J_{RL} d^\dagger_{L\uparrow} d_{L\uparrow} d^\dagger_{R\uparrow} d_{R\uparrow} c^\dagger_{R\uparrow} c_{L\uparrow} := \hat{O}$$

$$\begin{cases} \langle T_{+1} \mid \hat{O} \mid T_{+1} \rangle = \langle 0 \mid d_{R\uparrow} d_{L\uparrow} d^\dagger_{L\uparrow} d^\dagger_{R\uparrow} d_{L\uparrow} d_{R\uparrow} d^\dagger_{L\uparrow} d^\dagger_{R\uparrow} \mid 0 \rangle c^\dagger_{R\uparrow} c_{L\uparrow} \\ \qquad\qquad = c^\dagger_{R\uparrow} c_{L\uparrow} \end{cases}$$

## Processes proportional to $c^{\dagger}_{R\downarrow}c_{L\downarrow}$

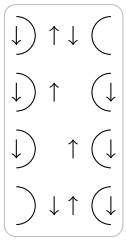

$$\propto J_{RL}d^{\dagger}_{L\downarrow}d_{L\uparrow}d^{\dagger}_{R\uparrow}d_{R\downarrow}c^{\dagger}_{R\downarrow}c_{L\downarrow} := \hat{O}$$

$$\begin{cases} \langle T_0 \mid \hat{O} \mid T_0\rangle = \dfrac{1}{\sqrt{2}\sqrt{2}}\langle 0 \mid d_{R\uparrow}d_{L\downarrow}d^{\dagger}_{L\downarrow}d^{\dagger}_{R\uparrow}d_{L\uparrow}d_{R\downarrow}d^{\dagger}_{L\uparrow}d^{\dagger}_{R\downarrow} \mid 0\rangle c^{\dagger}_{R\downarrow}c_{L\downarrow} \\ \qquad\qquad = \dfrac{1}{2}c^{\dagger}_{R\downarrow}c_{L\downarrow} \\ \langle s \mid \hat{O} \mid T_0\rangle = -\frac{1}{2}c^{\dagger}_{R\downarrow}c_{L\downarrow} \\ \langle T_0 \mid \hat{O} \mid s\rangle = \frac{1}{2}c^{\dagger}_{R\downarrow}c_{L\downarrow} \\ \langle s \mid \hat{O} \mid s\rangle = -\frac{1}{2}c^{\dagger}_{R\downarrow}c_{L\downarrow} \end{cases}$$

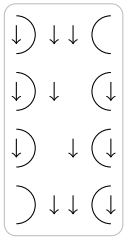

$$\propto J_{RL}d^{\dagger}_{L\downarrow}d_{L\downarrow}d^{\dagger}_{R\downarrow}d_{R\downarrow}c^{\dagger}_{R\downarrow}c_{L\downarrow} := \hat{O}$$

$$\begin{cases} \langle T_{-1} \mid \hat{O} \mid T_{-1}\rangle = \langle 0 \mid d_{R\downarrow}d_{L\downarrow}d^{\dagger}_{L\downarrow}d^{\dagger}_{R\downarrow}d_{L\downarrow}d_{R\downarrow}d^{\dagger}_{L\downarrow}d^{\dagger}_{R\downarrow} \mid 0\rangle c^{\dagger}_{R\downarrow}c_{L\downarrow} \\ \qquad\qquad = c^{\dagger}_{R\downarrow}c_{L\downarrow} \end{cases}$$

## Total operator describing two-stage transport processes from the left to the right lead

The resulting coupling Hamiltonian describing the processes proportional to $J_{RL} \approx \frac{t_L t_H t_R}{U*U}$ can therefore be written in the following way:

$$\begin{aligned} H'_{RL} = J_{RL}\Bigg[ & \frac{1}{\sqrt{2}}\left(\mid T_{+1}\rangle\langle s \mid + \mid T_{+1}\rangle\langle T_0 \mid + \mid T_0\rangle\langle T_{-1} \mid + \mid s\rangle\langle T_{-1} \mid\right) c^{\dagger}_{R\downarrow}c_{L\uparrow} \\ & + \frac{1}{\sqrt{2}}\left(\mid T_0\rangle\langle T_{+1} \mid - \mid s\rangle\langle T_{+1} \mid + \mid T_{-1}\rangle\langle T_0 \mid - \mid T_{-1}\rangle\langle s \mid\right) c^{\dagger}_{R\uparrow}c_{L\downarrow} \\ & + \frac{1}{2}\left(\mid T_0\rangle\langle T_0 \mid - \mid T_0\rangle\langle s \mid + \mid s\rangle\langle T_0 \mid - \mid s\rangle\langle s \mid +2 \mid T_{+1}\rangle\langle T_{+1} \mid\right) c^{\dagger}_{R\uparrow}c_{L\uparrow} \\ & + \frac{1}{2}\left(2 \mid T_{-1}\rangle\langle T_{-1} \mid + \mid T_0\rangle\langle T_0 \mid - \mid s\rangle\langle T_0 \mid + \mid T_0\rangle\langle s \mid - \mid s\rangle\langle s \mid\right) c^{\dagger}_{R\downarrow}c_{L\downarrow}\Bigg]. \end{aligned}$$

Proceeding as above one can calculate $H'_{LR}$ and therefore verify that the ralation $H'^{\dagger}_{LR} = H'_{RL}$ holds.
Our next goal is to put this Hamiltonian in a form involving the spin operators $\vec{S}_L$ and $\vec{S}_R$ of the two dots. Therefore one needs to find relations between these operators and the projectors $\mid \psi\rangle\langle\varphi \mid$ appearing in the Hamiltonian.
Let us define:

$$(\vec{S}_L + \vec{S}_R)^{\pm} = (\vec{S}_L + \vec{S}_R)^x \pm i(\vec{S}_L + \vec{S}_R)^y = \vec{S}^{\pm}_L + \vec{S}^{\pm}_R \tag{A.1}$$

and see how it acts on the triplet and singlet states:

$$
\begin{aligned}
&(\vec{S}_L+\vec{S}_R)^+ \mid T_{+1}\rangle = 0\\
&(\vec{S}_L+\vec{S}_R)^+ \mid T_{-1}\rangle = |\uparrow\downarrow\rangle + |\downarrow\uparrow\rangle = \sqrt{2}\\
&(\vec{S}_L+\vec{S}_R)^+ \mid T_0\rangle = (\vec{S}_L+\vec{S}_R)^+ \left(\frac{|\uparrow\downarrow\rangle + |\downarrow\uparrow\rangle}{\sqrt{2}}\right) = \frac{1}{\sqrt{2}}(|\uparrow\uparrow\rangle + |\uparrow\uparrow\rangle) = \sqrt{2} \mid T_{+1}\rangle\\
&(\vec{S}_L+\vec{S}_R)^+ \mid s\rangle = (\vec{S}_L+\vec{S}_R)^+ \left(\frac{|\uparrow\downarrow\rangle - |\downarrow\uparrow\rangle}{\sqrt{2}}\right) = \frac{1}{\sqrt{2}}(|\uparrow\uparrow\rangle - |\uparrow\uparrow\rangle) = 0\\
&(\vec{S}_L+\vec{S}_R)^- \mid T_{+1}\rangle = |\downarrow\uparrow\rangle + |\uparrow\downarrow\rangle = \sqrt{2} \mid T_0\rangle\\
&(\vec{S}_L+\vec{S}_R)^- \mid T_{-1}\rangle = 0\\
&(\vec{S}_L+\vec{S}_R)^- \mid T_0\rangle = (\vec{S}_L+\vec{S}_R)^- \left(\frac{|\uparrow\downarrow\rangle + |\downarrow\uparrow\rangle}{\sqrt{2}}\right) = \frac{1}{\sqrt{2}}(|\downarrow\downarrow\rangle + |\downarrow\downarrow\rangle) = \sqrt{2} \mid T_{-1}\rangle\\
&(\vec{S}_L+\vec{S}_R)^- \mid s\rangle = (\vec{S}_L+\vec{S}_R)^- \left(\frac{|\uparrow\downarrow\rangle - |\downarrow\uparrow\rangle}{\sqrt{2}}\right) = \frac{1}{\sqrt{2}}(|\downarrow\downarrow\rangle - |\downarrow\downarrow\rangle) = 0.
\end{aligned}
$$

From this we see that the two operators $S^{\pm} = (\vec{S}_L+\vec{S}_R)^{\pm}$ can be rewritten as:

$$S^+ = (\vec{S}_L+\vec{S}_R)^+ = \sqrt{2} \mid T_{+1}\rangle\langle T_0 \mid + \sqrt{2} \mid T_0\rangle\langle T_{-1} \mid \tag{A.2}$$

$$S^- = (\vec{S}_L+\vec{S}_R)^- = \sqrt{2} \mid T_{-1}\rangle\langle T_0 \mid + \sqrt{2} \mid T_0\rangle\langle T_{+1} \mid . \tag{A.3}$$

One can then calculate the commutator between $S^+$ and $S^-$:

$$[S^+, S^-] = S^+S^- - S^-S^+ = 2(\mid T_{+1}\rangle\langle T_{+1} \mid - \mid T_{-1}\rangle\langle T_{-1} \mid) := S^z \tag{A.4}$$

where we defined $S^z$ in such a way that the commutation relations for spin operators are satisfied. In fact with the definition:

$$S^z = \mid T_{+1}\rangle\langle T_{+1} \mid - \mid T_{-1}\rangle\langle T_{-1} \mid \tag{A.5}$$

we get the following standard relations:

$$
\begin{aligned}
[S^+, S^-] &= 2S^z\\
[S^+, S^z] &= -S^+\\
[S^-, S^z] &= S^-.
\end{aligned}
$$

Let us now see how the operator $\vec{S}_L \cdot \vec{S}_R$ defined as:

$$
\begin{aligned}
\vec{S}_L \cdot \vec{S}_R &= S_L^x S_R^x + S_L^y S_R^y + S_L^z S_R^z\\
&= \frac{S_L^+ + S_L^-}{2}\frac{S_R^+ + S_R^-}{2} + \frac{S_L^+ - S_L^-}{2i}\frac{S_R^+ - S_R^-}{2i} + S_L^z S_R^z\\
&= \frac{1}{4}\left[S_L^+S_R^+ + S_L^+S_R^- + S_L^-S_R^+ + S_L^-S_R^-\right] - \frac{1}{4}\left[S_L^+S_R^+ - S_L^+S_R^- - S_L^-S_R^+ + S_L^-S_R^-\right] + S_L^zS_R^z\\
&= \frac{1}{2}\left[S_L^+S_R^- + S_L^-S_R^+\right] + S_L^zS_R^z
\end{aligned}
$$

acts:

$$\vec{S}_L \cdot \vec{S}_R \mid T_{+1}\rangle = \frac{1}{4} \mid T_{+1}\rangle$$
$$\vec{S}_L \cdot \vec{S}_R \mid T_{-1}\rangle = \frac{1}{4} \mid T_{-1}\rangle$$
$$\vec{S}_L \cdot \vec{S}_R \mid T_{0}\rangle = \frac{1}{4} \mid T_{0}\rangle$$
$$\vec{S}_L \cdot \vec{S}_R \mid s\rangle = -\frac{3}{4} \mid s\rangle.$$

So the operator $\vec{S}_L \cdot \vec{S}_R$ can be rewrtitten like:

$$\vec{S}_L \cdot \vec{S}_R = \frac{1}{4}\left[\mid T_{+1}\rangle\langle T_{+1} \mid + \mid T_{-1}\rangle\langle T_{-1} \mid + \mid T_0\rangle\langle T_0 \mid -3 \mid s\rangle\langle s \mid\right]. \tag{A.6}$$

Finally the operator $\vec{S}_L \times \vec{S}_R$ acts like:

$$\begin{aligned}\vec{S}_L \times \vec{S}_R &= (S_L^y S_R^z - S_L^z S_R^y, -S_L^x S_R^z + S_L^z S_R^x, S_L^x S_R^y - S_L^y S_R^x) \\ &= \left(\frac{1}{2i}(S_L^+ S_R^z - S_L^- S_R^z - S_L^z S_R^+ + S_L^z S_R^-), \frac{1}{2}(-S_L^+ S_R^z - S_L^- S_R^z + S_L^z S_R^+ + S_L^z S_R^-),\right. \\ &\quad \left.\frac{1}{2i}(-S_L^+ S_R^- + S_L^- S_R^+)\right)\end{aligned}$$

and, when applied to the basis states, it gives:

$$(\vec{S}_L \times \vec{S}_R)^x \mid T_{+1}\rangle = \frac{1}{2i}\left(-\frac{1}{2}\mid\downarrow\uparrow\rangle + \frac{1}{2}\mid\uparrow\downarrow\rangle\right) = \frac{1}{i2\sqrt{2}} \mid s\rangle$$
$$(\vec{S}_L \times \vec{S}_R)^y \mid T_{+1}\rangle = \frac{1}{2}\left(-\frac{1}{2}\mid\downarrow\uparrow\rangle + \frac{1}{2}\mid\uparrow\downarrow\rangle\right) = \frac{1}{2\sqrt{2}} \mid s\rangle$$
$$(\vec{S}_L \times \vec{S}_R)^z \mid T_{+1}\rangle = 0$$
$$(\vec{S}_L \times \vec{S}_R)^x \mid T_{-1}\rangle = \frac{1}{2i}\left(-\frac{1}{2}\mid\uparrow\downarrow\rangle + \frac{1}{2}\mid\downarrow\uparrow\rangle\right) = -\frac{1}{i2\sqrt{2}} \mid s\rangle$$
$$(\vec{S}_L \times \vec{S}_R)^y \mid T_{-1}\rangle = \frac{1}{2}\left(\frac{1}{2}\mid\uparrow\downarrow\rangle - \frac{1}{2}\mid\downarrow\uparrow\rangle\right) = \frac{1}{2\sqrt{2}} \mid s\rangle$$
$$(\vec{S}_L \times \vec{S}_R)^z \mid T_{-1}\rangle = 0$$
$$(\vec{S}_L \times \vec{S}_R)^x \mid T_{0}\rangle = \frac{1}{i2\sqrt{2}}\left(\frac{1}{2}\mid\uparrow\uparrow\rangle + \frac{1}{2}\mid\downarrow\downarrow\rangle - \frac{1}{2}\mid\uparrow\uparrow\rangle - \frac{1}{2}\mid\downarrow\downarrow\rangle\right) = 0$$
$$(\vec{S}_L \times \vec{S}_R)^y \mid T_{0}\rangle = \frac{1}{2\sqrt{2}}\left(-\frac{1}{2}\mid\uparrow\uparrow\rangle + \frac{1}{2}\mid\downarrow\downarrow\rangle + \frac{1}{2}\mid\uparrow\uparrow\rangle - \frac{1}{2}\mid\downarrow\downarrow\rangle\right) = 0$$
$$(\vec{S}_L \times \vec{S}_R)^z \mid T_{0}\rangle = \frac{1}{i2\sqrt{2}}\left(-\mid\uparrow\downarrow\rangle + \mid\downarrow\uparrow\rangle\right) = -\frac{1}{i2} \mid s\rangle$$
$$(\vec{S}_L \times \vec{S}_R)^x \mid s\rangle = \frac{1}{i2\sqrt{2}}\left(-\mid\uparrow\uparrow\rangle + \mid\downarrow\downarrow\rangle\right) = \frac{1}{i2\sqrt{2}}\left(-\mid T_{+1}\rangle + \mid T_{-1}\rangle\right)$$
$$(\vec{S}_L \times \vec{S}_R)^y \mid s\rangle = \frac{1}{2\sqrt{2}}\left(\frac{1}{2}\mid\uparrow\uparrow\rangle + \frac{1}{2}\mid\downarrow\downarrow\rangle + \frac{1}{2}\mid\uparrow\uparrow\rangle + \frac{1}{2}\mid\downarrow\downarrow\rangle\right) = \frac{1}{2\sqrt{2}}\left(\mid T_{+1}\rangle + \mid T_{-1}\rangle\right)$$
$$(\vec{S}_L \times \vec{S}_R)^z \mid s\rangle = \frac{1}{i2\sqrt{2}}\left(\mid\uparrow\downarrow\rangle + \mid\downarrow\uparrow\rangle\right) = \frac{1}{i2} \mid T_0\rangle.$$

Introducing the following operator:

$$(\vec{S}_L \times \vec{S}_R)^{\pm} = (\vec{S}_L \times \vec{S}_R)^x \pm i(\vec{S}_L \times \vec{S}_R)^y \tag{A.7}$$

one gets:

$$\begin{aligned}
&(\vec{S}_L \times \vec{S}_R)^+ \mid T_{+1}\rangle = 0 \\
&(\vec{S}_L \times \vec{S}_R)^- \mid T_{+1}\rangle = -\frac{i}{\sqrt{2}} \mid s\rangle \\
&(\vec{S}_L \times \vec{S}_R)^+ \mid T_{-1}\rangle = \frac{i}{\sqrt{2}} \mid s\rangle \\
&(\vec{S}_L \times \vec{S}_R)^- \mid T_{-1}\rangle = 0 \\
&(\vec{S}_L \times \vec{S}_R)^+ \mid T_0\rangle = 0 \\
&(\vec{S}_L \times \vec{S}_R)^- \mid T_0\rangle = 0 \\
&(\vec{S}_L \times \vec{S}_R)^+ \mid s\rangle = \frac{i}{\sqrt{2}} \mid T_{+1}\rangle \\
&(\vec{S}_L \times \vec{S}_R)^- \mid s\rangle = -\frac{i}{\sqrt{2}} \mid T_{-1}\rangle.
\end{aligned}$$

The newly defined operators $(\vec{S}_L \times \vec{S}_R)^{\pm}$ can now be written like:

$$\begin{aligned}
(\vec{S}_L \times \vec{S}_R)^+ &= \frac{i}{\sqrt{2}} \mid T_{+1}\rangle\langle s \mid + \frac{i}{\sqrt{2}} \mid s\rangle\langle T_{-1} \mid \\
(\vec{S}_L \times \vec{S}_R)^- &= -\frac{i}{\sqrt{2}} \mid T_{-1}\rangle\langle s \mid - \frac{i}{\sqrt{2}} \mid s\rangle\langle T_{+1} \mid \\
(\vec{S}_L \times \vec{S}_R)^z &= \frac{i}{2} \mid s\rangle\langle 0 \mid - \frac{i}{2} \mid 0\rangle\langle s \mid .
\end{aligned}$$

All the previous definitions let us rewrite the coupling Hamiltonian in the following form:

$$\begin{aligned}
H'_{RL} = J_{RL} \Bigg[ &\left( -i(\vec{S}_L \times \vec{S}_R)^+ + \frac{1}{2}(\vec{S}_L + \vec{S}_R)^+ \right) c^\dagger_{R\downarrow} c_{L\uparrow} + \left( -i(\vec{S}_L \times \vec{S}_R)^- + \frac{1}{2}(\vec{S}_L + \vec{S}_R)^- \right) c^\dagger_{R\uparrow} c_{L\downarrow} \\
&+ \left( -i(\vec{S}_L \times \vec{S}_R)^z + \frac{1}{2}\left( 4(\vec{S}_L \cdot \vec{S}_R) + (\vec{S}_L + \vec{S}_R)^z + 2 \mid s\rangle\langle s \mid \right) \right) c^\dagger_{R\uparrow} c_{L\uparrow} \\
&+ \left( i(\vec{S}_L \times \vec{S}_R)^z + \frac{1}{2}\left( 4(\vec{S}_L \cdot \vec{S}_R) - (\vec{S}_L + \vec{S}_R)^z + 2 \mid s\rangle\langle s \mid \right) \right) c^\dagger_{R\downarrow} c_{L\downarrow} \Bigg] \\
= J_{RL} \Bigg[ &\left( -i(\vec{S}_L \times \vec{S}_R)^+ + \frac{1}{2}(\vec{S}_L + \vec{S}_R)^+ \right) c^\dagger_{R\downarrow} c_{L\uparrow} + \left( -i(\vec{S}_L \times \vec{S}_R)^- + \frac{1}{2}(\vec{S}_L + \vec{S}_R)^- \right) c^\dagger_{R\uparrow} c_{L\downarrow} \\
&+ \left( -i(\vec{S}_L \times \vec{S}_R)^z + \frac{1}{2}(\vec{S}_L + \vec{S}_R)^z \right) (c^\dagger_{R\uparrow} c_{L\uparrow} - c^\dagger_{R\downarrow} c_{L\downarrow}) \\
&+ \left( 2(\vec{S}_L \cdot \vec{S}_R) + \mid s\rangle\langle s \mid \right) (c^\dagger_{R\uparrow} c_{L\uparrow} + c^\dagger_{R\downarrow} c_{L\downarrow}) \Bigg] .
\end{aligned}$$

One can rewrite the Hamiltonian in a more compact form by defining the operator:

$$\vec{T} = (\vec{S}_L + \vec{S}_R) - 2i(\vec{S}_L \times \vec{S}_R) \tag{A.8}$$

and moreover if one notice that

$$2(\vec{S}_L \cdot \vec{S}_R) + \mid s\rangle\langle s \mid = \frac{1}{2}[\mid T_{+1}\rangle\langle T_{+1} \mid + \mid T_{-1}\rangle\langle T_{-1} \mid + \mid T_0\rangle\langle T_0 \mid + \mid s\rangle\langle s \mid -4 \mid s\rangle\langle s \mid] + \mid s\rangle\langle s \mid$$
$$= \frac{1}{4}\mathbf{I} + \vec{S}_L \cdot \vec{S}_R := \frac{P_0}{2} \tag{A.9}$$

we end up with:

$$H'_{RL} = J_{RL}\left[\frac{1}{2}\vec{T}\cdot\vec{s} + \left(\frac{1}{4}\mathbf{I} + \vec{S}_L \cdot \vec{S}_R\right)\sum_{\sigma=\uparrow,\downarrow} c_{L\sigma}c^{\dagger}_{R\sigma}\right] \tag{A.10}$$

where $\vec{s}$ refers to the coduction electron operators: $\vec{s} = \vec{\tau}_{\sigma\sigma'}c^{\dagger}_{R\sigma}c_{L\sigma'}$. Note that this result agrees with [?].
It is interesting to note that the potential scattering term of the Hamiltonian can also be rewritten in the following way:

$$H'^{pot}_{RL} = \vec{S}_L \cdot \vec{S}_R + \frac{1}{2}\left[(S^z_L)^2 + (S^z_R)^2\right] \tag{A.11}$$

once one have noticed how the combination $(S^z_L)^2 + (S^z_R)^2$ acts on the different states:

$$(S^z_L)^2 + (S^z_R)^2 \mid T_{+1}\rangle = \frac{1}{2} \mid T_{+1}\rangle$$
$$(S^z_L)^2 + (S^z_R)^2 \mid T_{-1}\rangle = \frac{1}{2} \mid T_{-1}\rangle$$
$$(S^z_L)^2 + (S^z_R)^2 \mid T_0\rangle = \frac{1}{2} \mid T_0\rangle$$
$$(S^z_L)^2 + (S^z_R)^2 \mid s\rangle = \frac{1}{2} \mid s\rangle.$$

and therefore it can be rewritten as:

$$(S^z_L)^2 + (S^z_R)^2 = \frac{1}{2}\left(\mid T_{+1}\rangle\langle T_{+1} \mid + \mid T_{-1}\rangle\langle T_{-1} \mid + \mid T_0\rangle\langle T_0 \mid + \mid s\rangle\langle s \mid\right). \tag{A.12}$$

Let us end by giving the complete expression for the Shrieffer-Wolff Hamiltonian for the lateral double-dot system:

$$H'_S = J_{12}\vec{S}_L \cdot \vec{S}_R + \frac{1}{2}J_L\vec{S}_L \cdot \vec{s}_L + \frac{1}{2}W_L\sum_{\sigma=\uparrow,\downarrow} c_{L\sigma}c^{\dagger}_{L\sigma} + \frac{1}{2}J_R\vec{S}_R \cdot \vec{s}_R + \frac{1}{2}W_R\sum_{\sigma=\uparrow,\downarrow} c_{R\sigma}c^{\dagger}_{R\sigma}$$
$$+ \frac{1}{2}J_{RL}\vec{T}_{RL} \cdot \vec{s}_{RL} + \frac{1}{2}W_{RL}P_0\sum_{\sigma=\uparrow,\downarrow} c_{L\sigma}c^{\dagger}_{R\sigma} + \frac{1}{2}J_{LR}\vec{T}_{LR} \cdot \vec{s}_{LR} + \frac{1}{2}W_{LR}P_0\sum_{\sigma=\uparrow,\downarrow} c_{R\sigma}c^{\dagger}_{L\sigma} \tag{A.13}$$

# B. Shrieffer-Wolff transformation for a three-dot lateral system

**Processes proportional to $c^\dagger_{R\downarrow}c_{L\uparrow}$**

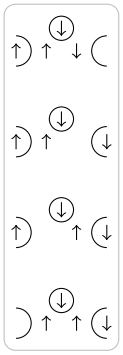

$$\propto J_H d^\dagger_{L\uparrow}d_{L\uparrow}d^\dagger_{R\uparrow}d_{R\downarrow}c^\dagger_{R\downarrow}c_{L\uparrow} := \hat{O}$$

$$\begin{cases}
\langle +q \mid \hat{O} \mid -q\rangle = \frac{1}{3}\left(\langle 0 \mid d_{R\uparrow}d_{C\downarrow}d_{L\uparrow} + \langle 0 \mid d_{R\downarrow}d_{C\uparrow}d_{L\uparrow}\right. \\
\qquad\qquad +\langle 0 \mid d_{R\uparrow}d_{C\uparrow}d_{L\downarrow}\rangle\, d^\dagger_{L\uparrow}d^\dagger_{R\uparrow}d^\dagger_{R\uparrow}d_{L\uparrow}d_{R\downarrow} \\
\qquad\qquad \left(d^\dagger_{L\uparrow}d^\dagger_{C\downarrow}d^\dagger_{R\downarrow} \mid 0\rangle + d^\dagger_{L\downarrow}d^\dagger_{C\downarrow}d^\dagger_{R\uparrow} \mid 0\rangle\right. \\
\qquad\qquad \left.+d^\dagger_{L\downarrow}d^\dagger_{C\uparrow}d^\dagger_{R\downarrow} \mid 0\rangle\right) c^\dagger_{R\downarrow}c_{L\uparrow} \\
\qquad\qquad = \frac{1}{3}\langle 0 \mid d_{R\uparrow}d_{C\downarrow}d_{L\uparrow}d^\dagger_{L\uparrow}d^\dagger_{R\uparrow}d_{L\uparrow}d_{R\downarrow}d^\dagger_{L\uparrow}d^\dagger_{C\downarrow}d^\dagger_{R\downarrow} \mid 0\rangle c^\dagger_{R\downarrow}c_{L\uparrow} \\
\qquad\qquad = \frac{1}{3}c^\dagger_{R\downarrow}c_{L\uparrow} \\
\langle +q \mid \hat{O} \mid -d\rangle = -\frac{1}{\sqrt{6}}c^\dagger_{R\downarrow}c_{L\uparrow} \\
\langle +q \mid \hat{O} \mid -d'\rangle = -\frac{1}{\sqrt{6}}c^\dagger_{R\downarrow}c_{L\uparrow} \\
\langle +d \mid \hat{O} \mid -q\rangle = -\frac{1}{\sqrt{6}}c^\dagger_{R\downarrow}c_{L\uparrow} \\
\langle +d \mid \hat{O} \mid -d\rangle = \frac{1}{2}c^\dagger_{R\downarrow}c_{L\uparrow} \\
\langle +d \mid \hat{O} \mid -d'\rangle = \frac{1}{2}c^\dagger_{R\downarrow}c_{L\uparrow} \\
\langle +d' \mid \hat{O} \mid -q\rangle = -\frac{1}{\sqrt{6}}c^\dagger_{R\downarrow}c_{L\uparrow} \\
\langle +d' \mid \hat{O} \mid -d\rangle = \frac{1}{2}c^\dagger_{R\downarrow}c_{L\uparrow} \\
\langle +d' \mid \hat{O} \mid -d'\rangle = \frac{1}{2}c^\dagger_{R\downarrow}c_{L\uparrow}
\end{cases}$$

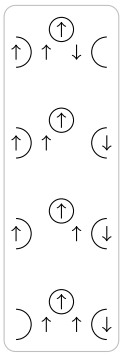

$$\propto J_H d^\dagger_{L\uparrow}d_{L\uparrow}d^\dagger_{R\uparrow}d_{R\downarrow}c^\dagger_{R\downarrow}c_{L\uparrow} := \hat{O}$$

$$\begin{cases}
\langle +\frac{3}{2} \mid \hat{O} \mid +q\rangle = \frac{1}{\sqrt{3}}c^\dagger_{R\downarrow}c_{L\uparrow} \\
\langle +\frac{3}{2} \mid \hat{O} \mid +d\rangle = 0 \\
\langle +\frac{3}{2} \mid \hat{O} \mid +d'\rangle = \frac{1}{\sqrt{2}}c^\dagger_{R\downarrow}c_{L\uparrow}
\end{cases}$$

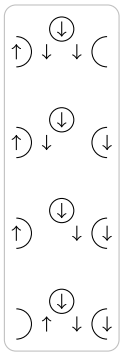

$$\propto J_H d^\dagger_{L\uparrow} d_{L\downarrow} d^\dagger_{R\downarrow} d_{R\downarrow} c^\dagger_{R\downarrow} c_{L\uparrow} := \hat{O}$$

$$\begin{cases} \langle -q \mid \hat{O} \mid -\frac{3}{2} \rangle = \frac{1}{\sqrt{3}} c^\dagger_{R\downarrow} c_{L\uparrow} \\ \langle -d \mid \hat{O} \mid -\frac{3}{2} \rangle = -\frac{1}{\sqrt{2}} c^\dagger_{R\downarrow} c_{L\uparrow} \\ \langle -d' \mid \hat{O} \mid -\frac{3}{2} \rangle = -\frac{1}{\sqrt{2}} c^\dagger_{R\downarrow} c_{L\uparrow} \end{cases}$$

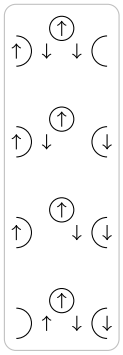

$$\propto J_H d^\dagger_{L\uparrow} d_{L\downarrow} d^\dagger_{R\downarrow} d_{R\downarrow} c^\dagger_{R\downarrow} c_{L\uparrow} := \hat{O}$$

$$\begin{cases} \langle +q \mid \hat{O} \mid -q \rangle = \frac{1}{3} c^\dagger_{R\downarrow} c_{L\uparrow} \\ \langle +q \mid \hat{O} \mid -d \rangle = \frac{1}{\sqrt{6}} c^\dagger_{R\downarrow} c_{L\uparrow} \\ \langle +q \mid \hat{O} \mid -d' \rangle = 0 \\ \langle +d \mid \hat{O} \mid -q \rangle = 0 \\ \langle +d \mid \hat{O} \mid -d \rangle = 0 \\ \langle +d \mid \hat{O} \mid -d' \rangle = 0 \\ \langle +d' \mid \hat{O} \mid -q \rangle = \frac{1}{\sqrt{6}} c^\dagger_{R\downarrow} c_{L\uparrow} \\ \langle +d' \mid \hat{O} \mid -d \rangle = \frac{1}{2} c^\dagger_{R\downarrow} c_{L\uparrow} \\ \langle +d' \mid \hat{O} \mid -d' \rangle = 0 \end{cases}$$

## Processes proportional to $c^\dagger_{R\uparrow}c_{L\downarrow}$

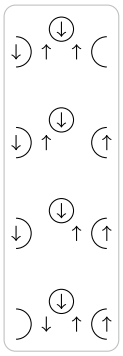

$$\propto J_H d^\dagger_{L\downarrow} d_{L\uparrow} d^\dagger_{R\uparrow} d_{R\uparrow} c^\dagger_{R\uparrow} c_{L\downarrow} := \hat{O}$$

$$\begin{cases} \langle -q \mid \hat{O} \mid +q \rangle = \frac{1}{3} c^\dagger_{R\uparrow} c_{L\downarrow} \\ \langle -q \mid \hat{O} \mid +d \rangle = -\frac{1}{\sqrt{6}} c^\dagger_{R\uparrow} c_{L\downarrow} \\ \langle -q \mid \hat{O} \mid +d' \rangle = -\frac{1}{\sqrt{6}} c^\dagger_{R\uparrow} c_{L\downarrow} \\ \langle -d \mid \hat{O} \mid +q \rangle = 0 \\ \langle -d \mid \hat{O} \mid +d \rangle = 0 \\ \langle -d \mid \hat{O} \mid +d' \rangle = 0 \\ \langle -d' \mid \hat{O} \mid +q \rangle = \frac{1}{\sqrt{6}} c^\dagger_{R\uparrow} c_{L\downarrow} \\ \langle -d' \mid \hat{O} \mid +d \rangle = -\frac{1}{2} c^\dagger_{R\uparrow} c_{L\downarrow} \\ \langle -d' \mid \hat{O} \mid +d' \rangle = -\frac{1}{2} c^\dagger_{R\uparrow} c_{L\downarrow} \end{cases}$$

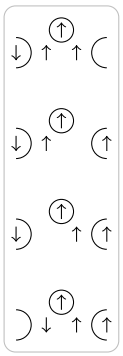

$$\propto J_H d^\dagger_{L\downarrow} d_{L\uparrow} d^\dagger_{R\uparrow} d_{R\uparrow} c^\dagger_{R\uparrow} c_{L\downarrow} := \hat{O}$$

$$\begin{cases} \langle +q \mid \hat{O} \mid +\frac{3}{2} \rangle = \frac{1}{\sqrt{3}} c^\dagger_{R\uparrow} c_{L\downarrow} \\ \langle +d \mid \hat{O} \mid +\frac{3}{2} \rangle = \frac{1}{\sqrt{2}} c^\dagger_{R\uparrow} c_{L\downarrow} \\ \langle +d' \mid \hat{O} \mid +\frac{3}{2} \rangle = 0 \end{cases}$$

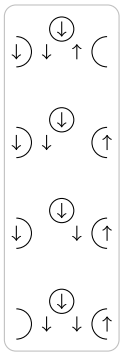

$$\propto J_H d^\dagger_{L\downarrow} d_{L\downarrow} d^\dagger_{R\downarrow} d_{R\uparrow} c^\dagger_{R\uparrow} c_{L\downarrow} := \hat{O}$$

$$\begin{cases} \langle -\frac{3}{2} \mid \hat{O} \mid -q \rangle = \frac{1}{\sqrt{3}} c^\dagger_{R\uparrow} c_{L\downarrow} \\ \langle -\frac{3}{2} \mid \hat{O} \mid -d \rangle = 0 \\ \langle -\frac{3}{2} \mid \hat{O} \mid -d' \rangle = \frac{1}{\sqrt{2}} c^\dagger_{R\uparrow} c_{L\downarrow} \end{cases}$$

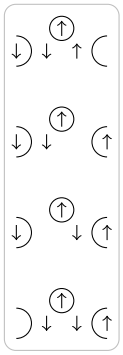

$$\propto J_H d^\dagger_{L\downarrow} d_{L\downarrow} d^\dagger_{R\downarrow} d_{R\uparrow} c^\dagger_{R\uparrow} c_{L\downarrow} := \hat{O}$$

$$\begin{cases} \langle -q \mid \hat{O} \mid +q \rangle = \frac{1}{3} c^\dagger_{R\uparrow} c_{L\downarrow} \\ \langle -q \mid \hat{O} \mid +d \rangle = \frac{1}{\sqrt{6}} c^\dagger_{R\uparrow} c_{L\downarrow} \\ \langle -q \mid \hat{O} \mid +d' \rangle = 0 \\ \langle -d \mid \hat{O} \mid +q \rangle = \frac{1}{\sqrt{6}} c^\dagger_{R\uparrow} c_{L\downarrow} \\ \langle -d \mid \hat{O} \mid +d \rangle = \frac{1}{2} c^\dagger_{R\uparrow} c_{L\downarrow} \\ \langle -d \mid \hat{O} \mid +d' \rangle = 0 \\ \langle -d' \mid \hat{O} \mid +q \rangle = 0 \\ \langle -d' \mid \hat{O} \mid +d \rangle = 0 \\ \langle -d' \mid \hat{O} \mid +d' \rangle = 0 \end{cases}$$

## Processes proportional to $c^\dagger_{R\uparrow}c_{L\uparrow}$

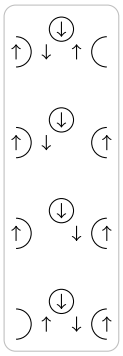

$$\propto J_H d^\dagger_{L\uparrow} d_{L\downarrow} d^\dagger_{R\downarrow} d_{R\uparrow} c^\dagger_{R\uparrow} c_{L\uparrow} := \hat{O}$$

$$\begin{cases} \langle -q \mid \hat{O} \mid -q \rangle = \frac{1}{3} c^\dagger_{R\uparrow} c_{L\uparrow} \\ \langle -q \mid \hat{O} \mid -d \rangle = 0 \\ \langle -q \mid \hat{O} \mid -d' \rangle = \frac{1}{\sqrt{6}} c^\dagger_{R\uparrow} c_{L\uparrow} \\ \langle -d \mid \hat{O} \mid -q \rangle = -\frac{1}{\sqrt{6}} c^\dagger_{R\uparrow} c_{L\uparrow} \\ \langle -d \mid \hat{O} \mid -d \rangle = 0 \\ \langle -d \mid \hat{O} \mid -d' \rangle = -\frac{1}{2} c^\dagger_{R\uparrow} c_{L\uparrow} \\ \langle -d' \mid \hat{O} \mid -q \rangle = -\frac{1}{\sqrt{6}} c^\dagger_{R\uparrow} c_{L\uparrow} \\ \langle -d' \mid \hat{O} \mid -d \rangle = 0 \\ \langle -d' \mid \hat{O} \mid -d' \rangle = -\frac{1}{2} c^\dagger_{R\uparrow} c_{L\uparrow} \end{cases}$$

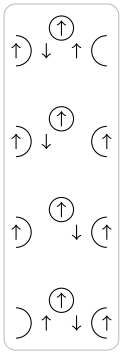

$$\propto J_H d^\dagger_{L\uparrow} d_{L\downarrow} d^\dagger_{R\downarrow} d_{R\uparrow} c^\dagger_{R\uparrow} c_{L\uparrow} := \hat{O}$$

$$\begin{cases} \langle +q \mid \hat{O} \mid +q \rangle = \frac{1}{3} c^\dagger_{R\uparrow} c_{L\uparrow} \\ \langle +q \mid \hat{O} \mid +d \rangle = -\frac{1}{\sqrt{6}} c^\dagger_{R\uparrow} c_{L\uparrow} \\ \langle +q \mid \hat{O} \mid +d' \rangle = 0 \\ \langle +d \mid \hat{O} \mid +q \rangle = 0 \\ \langle +d \mid \hat{O} \mid +d \rangle = 0 \\ \langle +d \mid \hat{O} \mid +d' \rangle = 0 \\ \langle +d' \mid \hat{O} \mid +q \rangle = \frac{1}{\sqrt{6}} c^\dagger_{R\uparrow} c_{L\uparrow} \\ \langle +d' \mid \hat{O} \mid +d \rangle = \frac{1}{2} c^\dagger_{R\uparrow} c_{L\uparrow} \\ \langle +d' \mid \hat{O} \mid +d' \rangle = 0 \end{cases}$$

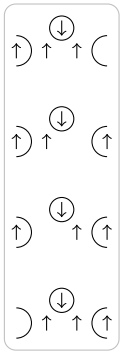

$$\propto J_H d^\dagger_{L\uparrow} d_{L\uparrow} d^\dagger_{R\uparrow} d_{R\uparrow} c^\dagger_{R\uparrow} c_{L\uparrow} := \hat{O}$$

$$\begin{cases} \langle +q \mid \hat{O} \mid +q \rangle = \frac{1}{3} c^\dagger_{R\uparrow} c_{L\uparrow} \\ \langle +q \mid \hat{O} \mid +d \rangle = -\frac{1}{\sqrt{6}} c^\dagger_{R\uparrow} c_{L\uparrow} \\ \langle +q \mid \hat{O} \mid +d' \rangle = -\frac{1}{\sqrt{6}} c^\dagger_{R\uparrow} c_{L\uparrow} \\ \langle +d \mid \hat{O} \mid +q \rangle = -\frac{1}{\sqrt{6}} c^\dagger_{R\uparrow} c_{L\uparrow} \\ \langle +d \mid \hat{O} \mid +d \rangle = \frac{1}{2} c^\dagger_{R\uparrow} c_{L\uparrow} \\ \langle +d \mid \hat{O} \mid +d' \rangle = \frac{1}{2} c^\dagger_{R\uparrow} c_{L\uparrow} \\ \langle +d' \mid \hat{O} \mid +q \rangle = -\frac{1}{\sqrt{6}} c^\dagger_{R\uparrow} c_{L\uparrow} \\ \langle +d' \mid \hat{O} \mid +d \rangle = \frac{1}{2} c^\dagger_{R\uparrow} c_{L\uparrow} \\ \langle +d' \mid \hat{O} \mid +d' \rangle = \frac{1}{2} c^\dagger_{R\uparrow} c_{L\uparrow} \end{cases}$$

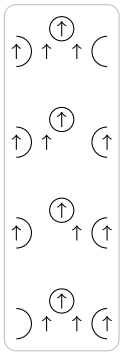

$$\propto J_H d^\dagger_{L\uparrow} d_{L\uparrow} d^\dagger_{R\uparrow} d_{R\uparrow} c^\dagger_{R\uparrow} c_{L\uparrow} := \hat{O}$$

$$\left\{ \quad \langle +\tfrac{3}{2} \mid \hat{O} \mid +\tfrac{3}{2} \rangle = c^\dagger_{R\uparrow} c_{L\uparrow} \right.$$

## Processes proportional to $c^\dagger_{R\downarrow}c_{L\downarrow}$

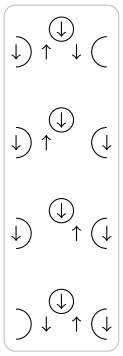

$$\propto J_H d^\dagger_{L\downarrow}d_{L\uparrow}d^\dagger_{R\uparrow}d_{R\downarrow}c^\dagger_{R\downarrow}c_{L\downarrow} := \hat{O}$$

$$\begin{cases} \langle -q \mid \hat{O} \mid -q\rangle = \frac{1}{3}c^\dagger_{R\downarrow}c_{L\downarrow} \\ \langle -q \mid \hat{O} \mid -d\rangle = -\frac{1}{\sqrt{6}}c^\dagger_{R\downarrow}c_{L\downarrow} \\ \langle -q \mid \hat{O} \mid -d'\rangle = -\frac{1}{\sqrt{6}}c^\dagger_{R\downarrow}c_{L\downarrow} \\ \langle -d \mid \hat{O} \mid -q\rangle = 0 \\ \langle -d \mid \hat{O} \mid -d\rangle = 0 \\ \langle -d \mid \hat{O} \mid -d'\rangle = 0 \\ \langle -d' \mid \hat{O} \mid -q\rangle = \frac{1}{\sqrt{6}}c^\dagger_{R\downarrow}c_{L\downarrow} \\ \langle -d' \mid \hat{O} \mid -d\rangle = -\frac{1}{2}c^\dagger_{R\downarrow}c_{L\downarrow} \\ \langle -d' \mid \hat{O} \mid -d'\rangle = -\frac{1}{2}c^\dagger_{R\downarrow}c_{L\downarrow} \end{cases}$$

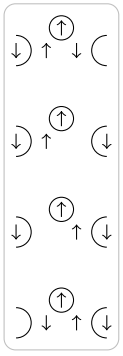

$$\propto J_H d^\dagger_{L\downarrow}d_{L\uparrow}d^\dagger_{R\uparrow}d_{R\downarrow}c^\dagger_{R\downarrow}c_{L\downarrow} := \hat{O}$$

$$\begin{cases} \langle +q \mid \hat{O} \mid +q\rangle = \frac{1}{3}c^\dagger_{R\downarrow}c_{L\downarrow} \\ \langle +q \mid \hat{O} \mid +d\rangle = 0 \\ \langle +q \mid \hat{O} \mid +d'\rangle = \frac{1}{\sqrt{6}}c^\dagger_{R\downarrow}c_{L\downarrow} \\ \langle +d \mid \hat{O} \mid +q\rangle = \frac{1}{\sqrt{6}}c^\dagger_{R\downarrow}c_{L\downarrow} \\ \langle +d \mid \hat{O} \mid +d\rangle = 0 \\ \langle +d \mid \hat{O} \mid +d'\rangle = \frac{1}{2}c^\dagger_{R\downarrow}c_{L\downarrow} \\ \langle +d' \mid \hat{O} \mid +q\rangle = 0 \\ \langle +d' \mid \hat{O} \mid +d\rangle = 0 \\ \langle +d' \mid \hat{O} \mid +d'\rangle = 0 \end{cases}$$

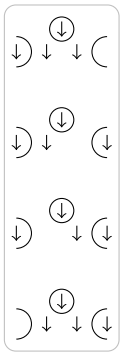

$$\propto J_H d^\dagger_{L\downarrow} d_{L\downarrow} d^\dagger_{R\downarrow} d_{R\downarrow} c^\dagger_{R\downarrow} c_{L\downarrow} := \hat{O}$$

$$\left\{ \quad \langle -\tfrac{3}{2} \mid \hat{O} \mid -\tfrac{3}{2} \rangle = 1 c^\dagger_{R\downarrow} c_{L\downarrow} \right.$$

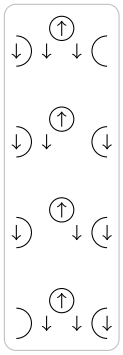

$$\propto J_H d^\dagger_{L\downarrow} d_{L\downarrow} d^\dagger_{R\downarrow} d_{R\downarrow} c^\dagger_{R\downarrow} c_{L\downarrow} := \hat{O}$$

$$\left\{ \begin{array}{l} \langle -q \mid \hat{O} \mid -q \rangle = \frac{1}{3} c^\dagger_{R\downarrow} c_{L\downarrow} \\ \langle -q \mid \hat{O} \mid -d \rangle = \frac{1}{\sqrt{6}} c^\dagger_{R\downarrow} c_{L\downarrow} \\ \langle -q \mid \hat{O} \mid -d' \rangle = 0 \\ \langle -d \mid \hat{O} \mid -q \rangle = \frac{1}{\sqrt{6}} c^\dagger_{R\downarrow} c_{L\downarrow} \\ \langle -d \mid \hat{O} \mid -d \rangle = \frac{1}{2} c^\dagger_{R\downarrow} c_{L\downarrow} \\ \langle -d \mid \hat{O} \mid -d' \rangle = 0 \\ \langle -d' \mid \hat{O} \mid -q \rangle = 0 \\ \langle -d' \mid \hat{O} \mid -d \rangle = 0 \\ \langle -d' \mid \hat{O} \mid -d' \rangle = 0 \end{array} \right.$$

The interacting Hamiltonian for the processes described above can then be written in the following form:

$$
\begin{aligned}
H'_{RL} = \Bigg[ & \frac{1}{\sqrt{3}} \mid +\frac{3}{2}\rangle\langle +q \mid + \frac{2}{3} \mid +q\rangle\langle -q \mid + \frac{1}{\sqrt{3}} \mid -q\rangle\langle -\frac{3}{2} \mid - \frac{1}{\sqrt{6}} \mid +q\rangle\langle -d' \mid - \frac{1}{\sqrt{2}} \mid -d'\rangle\langle -\frac{3}{2} \mid \\
& + \frac{1}{\sqrt{2}} \mid +\frac{3}{2}\rangle\langle +d' \mid - \frac{1}{\sqrt{6}} \mid +d\rangle\langle -q \mid - \frac{1}{\sqrt{2}} \mid -d\rangle\langle -\frac{3}{2} \mid + \frac{1}{2} \mid +d\rangle\langle -d \mid \\
& + \frac{1}{2} \mid +d'\rangle\langle -d' \mid + \frac{1}{2} \mid +d\rangle\langle -d' \mid + \mid +d'\rangle\langle -d \mid \Bigg] c^{\dagger}_{R\downarrow} c_{L\uparrow} + \\
+ \Bigg[ & \frac{1}{\sqrt{3}} \mid +q\rangle\langle +\frac{3}{2} \mid + \frac{2}{3} \mid -q\rangle\langle +q \mid + \frac{1}{\sqrt{3}} \mid -\frac{3}{2}\rangle\langle -q \mid - \frac{1}{\sqrt{6}} \mid -q\rangle\langle +d' \mid + \frac{1}{\sqrt{6}} \mid -d'\rangle\langle +q \mid \\
& - \frac{1}{2} \mid -d'\rangle\langle +d \mid - \frac{1}{2} \mid -d'\rangle\langle +d' \mid + \frac{1}{\sqrt{2}} \mid +d\rangle\langle +\frac{3}{2} \mid + \frac{1}{\sqrt{2}} \mid -\frac{3}{2}\rangle\langle -d' \mid \\
& + \frac{1}{\sqrt{6}} \mid -d\rangle\langle +q \mid + \frac{1}{2} \mid -d\rangle\langle +d \mid \Bigg] c^{\dagger}_{R\uparrow} c_{L\downarrow} + \\
+ \Bigg[ & \frac{1}{3} \mid -q\rangle\langle -q \mid + \frac{1}{\sqrt{6}} \mid -q\rangle\langle -d' \mid - \frac{1}{\sqrt{6}} \mid -d\rangle\langle -q \mid - \frac{1}{2} \mid -d\rangle\langle -d' \mid \\
& - \frac{1}{\sqrt{6}} \mid -d'\rangle\langle -q \mid - \frac{1}{2} \mid -d'\rangle\langle -d' \mid + \frac{2}{3} \mid +q\rangle\langle +q \mid + \mid +d'\rangle\langle +d \mid \\
& - \sqrt{6} \mid +q\rangle\langle +d' \mid - \frac{1}{\sqrt{6}} \mid +d\rangle\langle +q \mid + \frac{1}{2} \mid +d\rangle\langle +d \mid + \frac{1}{2} \mid +d\rangle\langle +d' \mid \\
& + \frac{1}{2} \mid +d'\rangle\langle +d' \mid + \mid +\frac{3}{2}\rangle\langle +\frac{3}{2} \mid \Bigg] c_{L\uparrow} c^{\dagger}_{R\uparrow} + \\
+ \Bigg[ & \frac{2}{3} \mid -q\rangle\langle -q \mid - \frac{1}{\sqrt{6}} \mid -q\rangle\langle -d' \mid + \frac{1}{\sqrt{6}} \mid -d'\rangle\langle -q \mid - \frac{1}{2} \mid -d'\rangle\langle -d \mid \\
& - \frac{1}{2} \mid -d'\rangle\langle -d' \mid + \frac{1}{3} \mid +q\rangle\langle +q \mid + \frac{1}{\sqrt{6}} \mid +q\rangle\langle +d' \mid + \frac{1}{\sqrt{6}} \mid +d\rangle\langle +q \mid \\
& + \frac{1}{2} \mid +d\rangle\langle +d' \mid + \mid -\frac{3}{2}\rangle\langle -\frac{3}{2} \mid + \frac{1}{\sqrt{6}} \mid -d\rangle\langle -q \mid \\
& + \frac{1}{2} \mid -d\rangle\langle -d \mid \Bigg] c_{L\downarrow} c^{\dagger}_{R\downarrow}
\end{aligned}
$$

Notice that in the Hamiltonian the sum of the term proportional to $c^{\dagger}_{R\uparrow} c_{L\uparrow}$ and that proportional to $c^{\dagger}_{R\downarrow} c_{L\downarrow}$ can be rewritten in the following way:

$$
a c^{\dagger}_{R\uparrow} c_{L\uparrow} + b c^{\dagger}_{R\downarrow} c_{L\downarrow} = \left[ \frac{1}{2} a \left( \tau^z + \tau^0 \right)_{\sigma\sigma'} + \frac{1}{2} b \left( \tau^0 - \tau^z \right)_{\sigma\sigma'} \right] c^{\dagger}_{R\sigma} c_{L\sigma'} = \left[ \frac{a+b}{2} \tau^0_{\sigma\sigma'} + \frac{a-b}{2} \tau^z_{\sigma\sigma'} \right] c^{\dagger}_{R\sigma} c_{L\sigma'} \tag{B.1}
$$

where $a$ and $b$ are the coefficients of the term proportional to $c^{\dagger}_{R\uparrow} c_{L\uparrow}$ and $c^{\dagger}_{R\downarrow} c_{L\downarrow}$ respectively and $\{\tau^x, \tau^y, \tau^z, \tau^0\}$ are the Pauli matrices and the identity matrix. Let us use this trick to rewrite

the Hamiltonian:

$$
\begin{aligned}
H'_{RL} = &\Bigg[\frac{1}{\sqrt{3}} \mid +\frac{3}{2}\rangle\langle +q \mid +\frac{2}{3} \mid +q\rangle\langle -q \mid +\frac{1}{\sqrt{3}} \mid -q\rangle\langle -\frac{3}{2} \mid -\frac{1}{\sqrt{6}} \mid +q\rangle\langle -d' \mid -\frac{1}{\sqrt{2}} \mid -d'\rangle\langle -\frac{3}{2} \mid \\
&+ \frac{1}{\sqrt{2}} \mid +\frac{3}{2}\rangle\langle +d' \mid -\frac{1}{\sqrt{6}} \mid +d\rangle\langle -q \mid -\frac{1}{\sqrt{2}} \mid -d\rangle\langle -\frac{3}{2} \mid +\frac{1}{2} \mid +d\rangle\langle -d \mid \\
&+\frac{1}{2} \mid +d'\rangle\langle -d' \mid +\frac{1}{2} \mid +d\rangle\langle -d' \mid + \mid +d'\rangle\langle -d \mid\Bigg] c^{\dagger}_{R\downarrow} c_{L\uparrow} + \\
+ &\Bigg[\frac{1}{\sqrt{3}} \mid +q\rangle\langle +\frac{3}{2} \mid +\frac{2}{3} \mid -q\rangle\langle +q \mid +\frac{1}{\sqrt{3}} \mid -\frac{3}{2}\rangle\langle -q \mid -\frac{1}{\sqrt{6}} \mid -q\rangle\langle +d' \mid +\frac{1}{\sqrt{6}} \mid -d'\rangle\langle +q \mid \\
&- \frac{1}{2} \mid -d'\rangle\langle +d \mid -\frac{1}{2} \mid -d'\rangle\langle +d' \mid +\frac{1}{\sqrt{2}} \mid +d\rangle\langle +\frac{3}{2} \mid +\frac{1}{\sqrt{2}} \mid -\frac{3}{2}\rangle\langle -d' \mid \\
&+\frac{1}{\sqrt{6}} \mid -d\rangle\langle +q \mid +\frac{1}{2} \mid -d\rangle\langle +d \mid\Bigg] c^{\dagger}_{R\uparrow} c_{L\downarrow} + \\
+ &\frac{1}{2}\Bigg[-\frac{1}{3} \mid -q\rangle\langle -q \mid +\frac{1}{3} \mid +q\rangle\langle +q \mid + \mid +\frac{3}{2}\rangle\langle +\frac{3}{2} \mid - \mid -\frac{3}{2}\rangle\langle -\frac{3}{2} \mid +\frac{2}{\sqrt{6}} \mid -q\rangle\langle -d' \mid \\
&- \frac{2}{\sqrt{6}} \mid -d'\rangle\langle -q \mid -\frac{2}{\sqrt{6}} \mid +q\rangle\langle +d' \mid -\frac{2}{\sqrt{6}} \mid -d\rangle\langle -q \mid -\frac{2}{\sqrt{6}} \mid +d\rangle\langle +q \mid + \mid +d'\rangle\langle +d \mid \\
&+ \frac{1}{2} \mid -d'\rangle\langle -d \mid +\frac{1}{2} \mid +d\rangle\langle +d \mid +\frac{1}{2} \mid +d'\rangle\langle +d' \mid -\frac{1}{2} \mid -d\rangle\langle -d \mid \\
&-\frac{1}{2} \mid -d\rangle\langle -d' \mid\Bigg] \tau^{z} c^{\dagger}_{R\sigma} c_{L\sigma'} + \\
+ &\frac{1}{2}\Bigg[\mid -q\rangle\langle -q \mid + \mid +q\rangle\langle +q \mid + \mid +\frac{3}{2}\rangle\langle +\frac{3}{2} \mid + \mid -\frac{3}{2}\rangle\langle -\frac{3}{2} \mid - \mid -d'\rangle\langle -d' \mid +\frac{1}{2} \mid +d'\rangle\langle +d' \mid \\
&-\frac{1}{2} \mid -d\rangle\langle -d' \mid + \mid +d'\rangle\langle +d \mid + \mid +d\rangle\langle +d' \mid -\frac{1}{2} \mid -d'\rangle\langle -d \mid +\frac{1}{2} \mid -d\rangle\langle -d \mid +\frac{1}{2} \mid +d\rangle\langle +d \mid\Bigg] \tau^{0} c^{\dagger}_{R\sigma} c_{L\sigma'}
\end{aligned}
$$

It is useful to define the following two-spin operators:

$$
\begin{aligned}
\vec{S}_{sum} &= \vec{S}_L + \vec{S}_R \\
\vec{S}_{dif} &= \vec{S}_L - \vec{S}_R \\
\vec{S}_{prod} &= \vec{S}_L \times \vec{S}_R \\
\vec{S}_{dot} &= \vec{S}_L \cdot \vec{S}_R
\end{aligned}
$$

wich can be rewritten in our basis:

$$
\begin{aligned}
(S_L+S_R)^+ &= \frac{2}{\sqrt{3}}\mid +\frac{3}{2}\rangle\langle +q\mid +\frac{4}{3}\mid +q\rangle\langle -q\mid -\frac{1}{\sqrt{6}}\mid +d\rangle\langle -q\mid -\frac{1}{\sqrt{6}}\mid +d'\rangle\langle -q\mid \\
&+\frac{2}{\sqrt{3}}\mid -q\rangle\langle -\frac{3}{2}\mid -\frac{1}{\sqrt{2}}\mid -d\rangle\langle -\frac{3}{2}\mid +\frac{1}{\sqrt{2}}\mid +\frac{3}{2}\rangle\langle +d\mid +\frac{1}{\sqrt{6}}\mid +q\rangle\langle -d\mid \\
&+\mid +d\rangle\langle -d\mid +\mid +d'\rangle\langle -d\mid +\frac{1}{\sqrt{2}}\mid +\frac{3}{2}\rangle\langle +d'\mid \\
(S_L+S_R)^- &= \frac{2}{\sqrt{3}}\mid +q\rangle\langle +\frac{3}{2}\mid +\frac{4}{3}\mid -q\rangle\langle +q\mid -\frac{1}{\sqrt{6}}\mid -q\rangle\langle +d\mid -\frac{1}{\sqrt{6}}\mid -q\rangle\langle +d'\mid \\
&+\frac{2}{\sqrt{3}}\mid -\frac{3}{2}\rangle\langle -q\mid -\frac{1}{\sqrt{2}}\mid -\frac{3}{2}\rangle\langle -d\mid +\frac{1}{\sqrt{2}}\mid +d\rangle\langle +\frac{3}{2}\mid +\frac{1}{\sqrt{6}}\mid -d\rangle\langle +q\mid \\
&+\mid -d\rangle\langle +d\mid +\mid -d\rangle\langle +d'\mid +\frac{1}{\sqrt{2}}\mid +d'\rangle\langle +\frac{3}{2}\mid \\
(S_L+S_R)^z &=\mid +\frac{3}{2}\rangle\langle +\frac{3}{2}\mid +\frac{1}{3}\mid +q\rangle\langle +q\mid -\frac{1}{3}\mid -q\rangle\langle -q\mid -\mid -\frac{3}{2}\rangle\langle -\frac{3}{2}\mid \\
&-\frac{1}{\sqrt{6}}\mid +d\rangle\langle +q\mid -\frac{1}{\sqrt{6}}\mid +d'\rangle\langle +q\mid -\frac{1}{\sqrt{6}}\mid -d\rangle\langle -q\mid -\frac{1}{\sqrt{6}}\mid +q\rangle\langle +d\mid \\
&+\frac{1}{2}\mid +d\rangle\langle +d\mid +\frac{1}{2}\mid +d'\rangle\langle +d'\mid -\frac{1}{\sqrt{6}}\mid -q\rangle\langle -d\mid -\frac{1}{2}\mid -d\rangle\langle -d\mid \\
&-\frac{1}{\sqrt{6}}\mid +q\rangle\langle +d'\mid +\frac{1}{2}\mid +d\rangle\langle +d'\mid +\frac{1}{2}\mid +d'\rangle\langle +d\mid \\
(S_L\times S_R)^+ &= -\frac{i}{2\sqrt{6}}\mid +d\rangle\langle -q\mid +\frac{i}{2\sqrt{6}}\mid +d'\rangle\langle -q\mid -\frac{i}{2\sqrt{2}}\mid -d\rangle\langle -\frac{3}{2}\mid -\frac{i}{\sqrt{2}}\mid -d'\rangle\langle -\frac{3}{2}\mid \\
&-\frac{i}{2\sqrt{2}}\mid +\frac{3}{2}\rangle\langle +d\mid -\frac{i}{2\sqrt{6}}\mid +q\rangle\langle -d\mid +\frac{i}{2}\mid +d'\rangle\langle -d\mid +\frac{i}{2\sqrt{2}}\mid +\frac{3}{2}\rangle\mid +d'\rangle \\
&-\frac{i}{\sqrt{6}}\mid +q\rangle\langle -d'\mid +\frac{i}{2}\mid +d\rangle\langle -d'\mid +\frac{i}{2}\mid +d'\rangle\langle -d'\mid \\
(S_L\times S_R)^- &= \frac{i}{2\sqrt{2}}\mid +d\rangle\langle +\frac{3}{2}\mid -\frac{i}{2\sqrt{2}}\mid +d'\rangle\langle +\frac{3}{2}\mid +\frac{i}{2\sqrt{6}}\mid -d\rangle\langle +q\mid +\frac{i}{\sqrt{6}}\mid -d'\rangle\langle +q\mid \\
&+\frac{i}{2\sqrt{6}}\mid -q\rangle\langle +d\mid -\frac{i}{2}\mid -d'\rangle\langle +d\mid +\frac{i}{2\sqrt{2}}\mid -\frac{3}{2}\rangle\langle -d\mid -\frac{i}{2\sqrt{6}}\mid -q\rangle\langle +d'\mid \\
&-\frac{i}{2}\mid -d'\rangle\langle +d'\mid -\frac{i}{2}\mid -d'\rangle\langle +d'\mid +\frac{i}{\sqrt{2}}\mid -\frac{3}{2}\rangle\langle -d'\mid \\
(S_L\times S_R)^z &= -\frac{i}{2\sqrt{6}}\mid +d\rangle\langle +q\mid +\frac{i}{2\sqrt{6}}\mid +d'\rangle\langle +q\mid -\frac{i}{2\sqrt{6}}\mid -d\rangle\langle -q\mid -\frac{i}{\sqrt{6}}\mid -d'\rangle\langle -q\mid \\
&+\frac{i}{2\sqrt{6}}\mid +q\rangle\langle +d\mid +\frac{i}{4}\mid +d'\rangle\langle +d\mid +\frac{i}{2\sqrt{6}}\mid -q\rangle\langle -d\mid +\frac{i}{4}\mid -d'\rangle\langle -d\mid \\
&-\frac{i}{2\sqrt{6}}\mid +q\rangle\langle +d'\mid -\frac{i}{4}\mid +d\rangle\langle +d'\mid +\frac{i}{\sqrt{6}}\mid -q\rangle\langle -d'\mid -\frac{i}{4}\mid -d\rangle\langle -d'\mid \\
\vec{S_L}\cdot\vec{S_R} &= \frac{1}{4}\mid +\frac{3}{2}\rangle\langle +\frac{3}{2}\mid +\frac{1}{4}\mid +q\rangle\langle +q\mid +\frac{1}{4}\mid -q\rangle\langle -q\mid +\frac{1}{4}\mid -\frac{3}{2}\rangle\langle -\frac{3}{2}\mid \\
&-\frac{3}{4}\mid -d'\rangle\langle -d'\mid +\frac{3}{8}\mid +d'\rangle\langle +d\mid +\frac{3}{8}\mid +d\rangle\langle +d'\mid -\frac{3}{8}\mid -d'\rangle\langle -d\mid -\frac{3}{8}\mid -d\rangle\langle -d'\mid .
\end{aligned}
$$

Notice the following combination of the above operators:

$$\begin{aligned}
\frac{1}{2}[(S_L+S_R)-2i(S_L\times S_R)]^{+} &= -\frac{1}{\sqrt{6}}\mid +d\rangle\langle -q\mid -\frac{1}{\sqrt{2}}\mid -d\rangle\langle -\frac{3}{2}\mid -\frac{1}{\sqrt{2}}\mid -d'\rangle\langle -\frac{3}{2}\mid +\mid +d'\rangle\langle -d\mid \\
&+\frac{1}{\sqrt{2}}\mid +\frac{3}{2}\rangle\langle +d'\mid -\frac{1}{\sqrt{6}}\mid +q\rangle\langle -d'\mid +\frac{1}{2}\mid +d\rangle\langle -d'\mid +\frac{1}{2}\mid +d'\rangle\langle -d'\mid \\
&+\frac{1}{\sqrt{3}}\mid +\frac{3}{2}\rangle\langle +q\mid +\frac{2}{3}\mid +q\rangle\langle -q\mid +\frac{1}{\sqrt{3}}\mid -q\rangle\langle -\frac{3}{2}\mid +\frac{1}{2}\mid +d\rangle\langle -d\mid \\
\frac{1}{2}[(S_L+S_R)-2i(S_L\times S_R)]^{-} &= \frac{1}{\sqrt{2}}\mid +d\rangle\langle +\frac{3}{2}\mid +\frac{1}{\sqrt{6}}\mid -d\rangle\langle +q\mid +\frac{1}{\sqrt{6}}\mid -d'\rangle\langle +d\mid \\
&-\frac{1}{\sqrt{6}}\mid -q\rangle\langle +d'\mid -\frac{1}{2}\mid -d'\rangle\langle +d'\mid +\frac{1}{\sqrt{2}}\mid -\frac{3}{2}\rangle\langle -d'\mid +\frac{1}{\sqrt{3}}\mid +q\rangle\langle +\frac{3}{2}\mid \\
&+\frac{2}{3}\mid -q\rangle\langle +q\mid +\frac{1}{\sqrt{3}}\mid -\frac{3}{2}\rangle\langle -q\mid +\frac{1}{2}\mid -d\rangle\langle +d\mid \\
\frac{1}{2}[(S_L+S_R)-2i(S_L\times S_R)]^{z} &= -\frac{1}{\sqrt{6}}\mid +d\rangle\langle +q\mid -\frac{1}{\sqrt{6}}\mid -d\rangle\langle -q\mid -\frac{1}{\sqrt{6}}\mid -d'\rangle\langle -q\mid \\
&+\frac{1}{2}\mid +d'\rangle\langle +d\mid +\frac{1}{4}\mid -d'\rangle\langle -d\mid -\frac{1}{\sqrt{6}}\mid +q\rangle\langle +d'\mid +\frac{1}{\sqrt{6}}\mid -q\rangle\langle -d'\mid \\
&-\frac{1}{4}\mid -d\rangle\langle -d'\mid +\frac{1}{2}\mid +\frac{3}{2}\rangle\langle +\frac{3}{2}\mid +\frac{1}{6}\mid +q\rangle\langle +q\mid -\frac{1}{6}\mid -q\rangle\langle -q\mid \\
&-\frac{1}{2}\mid -\frac{3}{2}\rangle\langle -\frac{3}{2}\mid +\frac{1}{4}\mid +d\rangle\langle +d\mid -\frac{1}{4}\mid -d\rangle\langle -d\mid +\frac{1}{4}\mid +d'\rangle\langle +d'\mid
\end{aligned}$$

With the definitions above and introducing the conduction electron operator $\vec{s}=\vec{\tau}_{\sigma\sigma'}c^{\dagger}_{R\sigma}c_{L\sigma'}$ and the identity operator in the spin Hilber space $\tau^{0}_{\sigma\sigma'}=\delta_{\sigma\sigma'}$ the Hamiltonian becomes:

$$\begin{aligned}
H'_{RL} = &\frac{1}{2}\left[-i2(S_L\times S_R)+(S_L+S_R)\right]^{+}c^{\dagger}_{R\downarrow}c_{L\uparrow}+\frac{1}{2}\left[-i2(S_L\times S_R)+(S_L+S_R)\right]^{-}c^{\dagger}_{R\uparrow}c_{L\downarrow}+ \\
&\frac{1}{2}\left[-i2(S_L\times S_R)+(S_L+S_R)\right]^{z}\tau^{z}_{\sigma\sigma'}c^{\dagger}_{R\sigma}c_{L\sigma'}+\left[\vec{S_L}\cdot\vec{S_R}+\frac{1}{2}\left((S^{z}_{L})^2+(S^{z}_{R})^2\right)\right]\tau^{0}_{\sigma\sigma'}c^{\dagger}_{R\sigma}c_{L\sigma'}
\end{aligned} \tag{B.2}$$

Note that the combination $\vec{S_L}\cdot\vec{S_R}+\frac{1}{2}\left((S^{z}_{L})^2+(S^{z}_{R})^2\right)$ is an operator that replace the left spin by the right one and viceversa. Let us define an "exchange"operator $P$ in the following way:$P=2\left[\vec{S_L}\cdot\vec{S_R}+\frac{1}{2}\left((S^{z}_{L})^2+(S^{z}_{R})^2\right)\right]$ and an exchange operator $\vec{T}=-i2(\vec{S}_L\times\vec{S}_R)+(\vec{S}_L+\vec{S}_R)$ so

that we can rewrite the Hamiltonian:

$$\begin{aligned}
H'_{RL} &= \frac{1}{2}T^+c^\dagger_{R\downarrow}c_{L\uparrow} + \frac{1}{2}T^-c^\dagger_{R\uparrow}c_{L\downarrow} + \frac{1}{2}T^z\tau^z_{\sigma\sigma'}c^\dagger_{R\sigma}c_{L\sigma'} + \frac{1}{2}P\tau^0_{\sigma\sigma'}c^\dagger_{R\sigma}c_{L\sigma'} \\
&= \frac{1}{2}(T^x + iT^y)c^\dagger_{R\downarrow}c_{L\uparrow} + \frac{1}{2}(T^x - iT^y)c^\dagger_{R\uparrow}c_{L\downarrow} + \frac{1}{2}T^z\tau^z_{\sigma\sigma'}c^\dagger_{R\sigma}c_{L\sigma'} + \frac{1}{2}P\tau^0_{\sigma\sigma'}c^\dagger_{R\sigma}c_{L\sigma'} \\
&= \frac{1}{2}T^x\frac{\tau^+_{\sigma\sigma'}c^\dagger_{R\sigma}c_{L\sigma'} + \tau^-_{\sigma\sigma'}c^\dagger_{R\sigma}c_{L\sigma'}}{2} + \frac{1}{2}T^y\frac{\tau^+_{\sigma\sigma'}c^\dagger_{R\sigma}c_{L\sigma'} - \tau^-_{\sigma\sigma'}c^\dagger_{R\sigma}c_{L\sigma'}}{2i} + \frac{1}{2}T^z\tau^z_{\sigma\sigma'}c^\dagger_{R\sigma}c_{L\sigma'} + \frac{1}{2}P\tau^0_{\sigma\sigma'}c^\dagger_{R\sigma}c_{L\sigma'} \\
&= \frac{1}{2}T^x\tau^x_{\sigma\sigma'}c^\dagger_{R\sigma}c_{L\sigma'} + \frac{1}{2}T^y\tau^y_{\sigma\sigma'}c^\dagger_{R\sigma}c_{L\sigma'} + \frac{1}{2}T^z\tau^z_{\sigma\sigma'}c^\dagger_{R\sigma}c_{L\sigma'} + \frac{1}{2}P\tau^0_{\sigma\sigma'}c^\dagger_{R\sigma}c_{L\sigma'} \\
&= \frac{1}{2}\vec{T}\cdot\vec{s} + \frac{1}{2}P\tau^0_{\sigma\sigma'}c^\dagger_{R\sigma}c_{L\sigma'} \\
&= \frac{1}{2}\left[-i2(\vec{S}_L\times\vec{S}_R) + (\vec{S}_L + \vec{S}_R)\right]\cdot\vec{s} + \left[\vec{S}_L\cdot\vec{S}_R + \frac{1}{2}\left((S^z_L)^2 + (S^z_R)^2\right)\right]\tau^0_{\sigma\sigma'}c^\dagger_{R\sigma}c_{L\sigma'}. \quad \text{(B.3)}
\end{aligned}$$

Observe that we call $\vec{S}_\alpha$ some real spins, while we are calling $\vec{s}_{\alpha\beta}$ the conduction electron operators, with the following convention: $\vec{s}_{\alpha\beta} = \vec{\tau}_{\sigma\sigma'}c^\dagger_{\alpha\sigma}c_{\beta\sigma'}$, which differs from the usual convention for a factor 1/2.
Note that this Hamiltonian looks exactly the same as the one for the two-spin case. This result is reasonable since the transport process involves just two of the spins.

All together we can write a transport Hamiltonian that looks this way:

$$\begin{aligned}
H = &\sum_{\alpha k\sigma}\xi_{\alpha k}c^\dagger_{\alpha k\sigma}c_{\alpha k\sigma} + \frac{J_L}{2}\vec{S}_L\cdot\vec{s}_L + \frac{J_R}{2}\vec{S}_R\cdot\vec{s}_R + J_{12}\vec{S}_L\cdot\vec{S}_C + J_{23}\vec{S}_C\cdot\vec{S}_R + J_{13}\vec{S}_L\cdot\vec{S}_R \\
&\underbrace{+\frac{1}{2}J_H(\vec{S}_L + \vec{S}_R - 2i\vec{S}_L\times\vec{S}_R)\cdot\vec{s}_{RL} + \frac{1}{2}P\sum_\sigma c^\dagger_{R\sigma}c_{L\sigma}}_{h_{RL}} + h_{LR}
\end{aligned}$$

where $h_{LR}$ is the term describing transport from the right to the left lead. This term turns out to be the same as $h_{RL}$, in fact if one analyzes all the possible processes, as we did above, one would get, e.g. for the terms proportional to $c^\dagger_{L\uparrow}c_{R\downarrow}$:

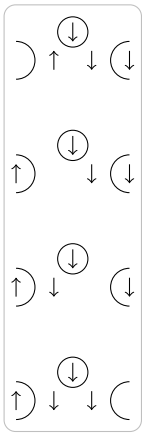

$$\propto J^*_H d^\dagger_{R\downarrow}d_{R\uparrow}d^\dagger_{L\uparrow}d_{L\uparrow}c^\dagger_{L\uparrow}c_{R\downarrow} := (\hat{O})^\dagger$$

which is exactly the process one obtains by taking the third process proportional to $c^\dagger_{R\downarrow}c_{L\uparrow}$ and looking at it from the last to the first picture, i.e. it's the inverse process.
Moreover the matrix elements are easily seen to be the the complex conjugates of the ones considered in the the previous process (proportional to $c^\dagger_{R\downarrow}c_{L\uparrow}$). In fact the previous final states becomes the initial state here and viceversa and the operator is the Hermitian conjugate of the one considered earlier: $\langle i \mid \hat{O}^\dagger \mid f\rangle = (\langle f \mid \hat{O} \mid i\rangle)^*$

One can therefore easily understand that $h_{LR}$ will be given by:

$$\begin{aligned}
h_{LR} &= \frac{1}{2}\left((S_L+S_R)-2i(S_L\times S_R)\right)^{+}c^{\dagger}_{L\uparrow}c_{R\downarrow}+\frac{1}{2}\left((S_L+S_R)-2i(S_L\times S_R)\right)^{-}c^{\dagger}_{L\downarrow}c_{R\uparrow}\\
&\quad+\frac{1}{2}\left((S_L+S_R)-2i(S_L\times S_R)\right)^{z}\tau^{z}_{\sigma\sigma'}c^{\dagger}_{L\sigma}c_{R\sigma'}+\frac{1}{2}\mid -q\rangle\langle -q\mid+\mid +q\rangle\langle +q\mid+\mid +\frac{3}{2}\rangle\langle +\frac{3}{2}\mid\\
&\quad+\mid -\frac{3}{2}\rangle\langle -\frac{3}{2}\mid-\mid -d'\rangle\langle -d'\mid+\frac{1}{2}\mid +d'\rangle\langle +d'\mid\\
&\quad-\frac{1}{2}\mid -d\rangle\langle -d'\mid+\mid +d'\rangle\langle +d\mid+\mid +d\rangle\langle +d'\mid-\frac{1}{2}\mid -d'\rangle\langle -d\mid+\frac{1}{2}\mid -d\rangle\langle -d\mid\tau^{0}_{\sigma\sigma'}c^{\dagger}_{L\sigma}c_{R\sigma'}\\
&=\frac{1}{2}\left((S_L+S_R)-2i(S_R\times S_L)\right)^{-}\frac{\tau^{+}_{\sigma\sigma'}}{2}c^{\dagger}_{L\sigma'}c_{R\sigma}+\frac{1}{2}\left((S_L+S_R)-2i(S_R\times S_L)\right)^{+}\frac{1}{2}\tau^{-}_{\sigma\sigma'}c^{\dagger}_{L\sigma'}c_{R\sigma}\\
&\quad+\frac{1}{2}\left((S_L+S_R)-2i(S_R\times S_L)\right)^{z}\tau^{z}_{\sigma\sigma'}c^{\dagger}_{L\sigma'}c_{R\sigma}+\text{potential scattering term }\tau^{0}_{\sigma\sigma'}c^{\dagger}_{L\sigma'}c_{R\sigma}\\
&=\frac{1}{2}(\vec{S}_L+\vec{S}_R-2i\vec{S}_R\times\vec{S}_L)\cdot\vec{s}_{LR}+\frac{1}{2}P\sum_{\sigma}c^{\dagger}_{L\sigma}c_{R\sigma}
\end{aligned}$$

where I used $P^{\dagger}=P$ The final total Hamiltonian then looks as follows:

$$\begin{aligned}
H &= \sum_{\alpha k\sigma}\xi_{\alpha k}c^{\dagger}_{\alpha k\sigma}c_{\alpha k\sigma}+\frac{J_L}{2}\vec{S}_L\cdot\vec{s}_L+\frac{J_R}{2}\vec{S}_R\cdot\vec{s}_R+J_{12}\vec{S}_L\cdot\vec{S}_C+J_{23}\vec{S}_C\cdot\vec{S}_R+J_{13}\vec{S}_L\cdot\vec{S}_R\\
&\quad-\vec{B}\cdot(\vec{S}_L+\vec{S}_C+\vec{S}_R)+\underbrace{\frac{1}{2}J_H\vec{T}\cdot\vec{s}_{RL}+\frac{1}{2}W_HP\sum_{\sigma}c^{\dagger}_{R\sigma}c_{L\sigma}}_{h_{RL}}+\underbrace{\frac{1}{2}J^{*}_H\vec{T}\cdot\vec{s}_{LR}+\frac{1}{2}W^{*}_HP\sum_{\sigma}c^{\dagger}_{L\sigma}c_{R\sigma}}_{h_{LR}}\\
&=\sum_{\alpha k\sigma}\xi_{\alpha k}c^{\dagger}_{\alpha k\sigma}c_{\alpha k\sigma}+\frac{J_L}{2}\vec{S}_L\cdot\vec{s}_L+\frac{J_R}{2}\vec{S}_R\cdot\vec{s}_R+J_{12}\vec{S}_L\cdot\vec{S}_C+J_{23}\vec{S}_C\cdot\vec{S}_R+J_{13}\vec{S}_L\cdot\vec{S}_R\\
&\quad-\vec{B}\cdot(\vec{S}_L+\vec{S}_C+\vec{S}_R)+\underbrace{\frac{1}{2}J^{RL}_H\vec{T}\cdot\vec{s}_{RL}+\frac{1}{2}W^{RL}_HP\sum_{\sigma}c^{\dagger}_{R\sigma}c_{L\sigma}}_{h_{RL}}+\underbrace{\frac{1}{2}J^{LR}_H\vec{T}\cdot\vec{s}_{LR}+\frac{1}{2}W^{LR}_HP\sum_{\sigma}c^{\dagger}_{L\sigma}c_{R\sigma}}_{h_{LR}}
\end{aligned}$$

where $\vec{T}=\vec{S}_L+\vec{S}_R-2i\vec{S}_L\times\vec{S}_R$, $\vec{\tilde{T}}=\vec{S}_L+\vec{S}_R-2i\vec{S}_R\times\vec{S}_L$ and the conduction electron operators are: $\vec{s}_{RL}=\vec{\tau}_{\sigma\sigma'}c^{\dagger}_{Rk\sigma}c_{Lk'\sigma'}$ and $\vec{s}_{LR}=\vec{\tau}_{\sigma\sigma'}c^{\dagger}_{Lk\sigma}c_{Rk'\sigma'}$ Let us know have a look at the commutation relations for the operators defined above. One finds:

- $[S^i_{sum},S^j_{sum}]=i\varepsilon_{ijk}S^k_{sum}$
- $[S^i_{dif},S^j_{dif}]=i\varepsilon_{ijk}S^k_{sum}$
- $[S^i_{sum},S^j_{dif}]=i\varepsilon_{ijk}S^k_{dif}$
- $[S^i_{prod},S^j_{prod}]=\frac{i}{4}\varepsilon_{ijk}S^k_{sum}$
- $[S^i_{prod},S^j_{sum}]=i\varepsilon_{ijk}S^k_{prod}$

Moreover, one also find the following:

- $[S^i_{sum},T^j]=i\varepsilon_{ijk}T^k$
- $[S^i_{sum},\tilde{T}^j]=i\varepsilon_{ijk}\tilde{T}^k$

- $[T^i, T^j] = 4\varepsilon_{ijk} S^k_{prod}$
- $[\tilde{T}^i, \tilde{T}^j] = -4\varepsilon_{ijk} S^k_{prod}$
- $[T^i, \tilde{T}^j] = 2i\varepsilon_{ijk} S^k_{plus}$
- $[P, P] = 0$
- $[P, T^i] = -2S^i_{minus}$
- $[P, \tilde{T}^i] = 2S^i_{minus}$

# C. Coefficients of the low-energy Hamiltonians

## C.1. Coefficients of the low-energy Hamiltonian for $B > 0$

$$A = \frac{1}{\sqrt{\left|\frac{-J_{12}+J_{23}+\sqrt{J_{12}^2-J_{23}J_{12}+J_{23}^2+J_{31}^2-(J_{12}+J_{23})J_{31}}}{J_{12}-J_{31}}\right|^2+\left|\frac{J_{23}-J_{31}+\sqrt{J_{12}^2-J_{23}J_{12}+J_{23}^2+J_{31}^2-(J_{12}+J_{23})J_{31}}}{J_{12}-J_{31}}\right|^2+1}}$$

$$B1 = \frac{1}{2}$$

$$B2 = \frac{-J_{12}\left(\sqrt{J_{12}^2-J_{31}(J_{12}+J_{23})-J_{12}J_{23}+J_{23}^2+J_{31}^2}+2J_{23}\right)+J_{31}\left(J_{31}-\sqrt{J_{12}^2-J_{31}(J_{12}+J_{23})-J_{12}J_{23}+J_{23}^2+J_{31}^2}\right)+2J_{23}\left(\sqrt{J_{12}^2-J_{31}(J_{12}+J_{23})-J_{12}J_{23}+J_{23}^2+J_{31}^2}-J_{31}\right)+J_{12}^2+2J_{23}^2}{(J_{12}-J_{31})^2\left(\left|\frac{-J_{12}+J_{23}+\sqrt{J_{12}^2-J_{23}J_{12}+J_{23}^2+J_{31}^2-(J_{12}+J_{23})J_{31}}}{J_{12}-J_{31}}\right|^2+\left|\frac{J_{23}-J_{31}+\sqrt{J_{12}^2-J_{23}J_{12}+J_{23}^2+J_{31}^2-(J_{12}+J_{23})J_{31}}}{J_{12}-J_{31}}\right|^2+1\right)}$$

$$C = \frac{\sqrt{J_{12}^2-J_{31}(J_{12}+J_{23})-J_{12}J_{23}+J_{23}^2+J_{31}^2}-J_{12}+J_{23}}{(J_{12}-J_{31})\sqrt{\left|\frac{-J_{12}+J_{23}+\sqrt{J_{12}^2-J_{23}J_{12}+J_{23}^2+J_{31}^2-(J_{12}+J_{23})J_{31}}}{J_{12}-J_{31}}\right|^2+\left|\frac{J_{23}-J_{31}+\sqrt{J_{12}^2-J_{23}J_{12}+J_{23}^2+J_{31}^2-(J_{12}+J_{23})J_{31}}}{J_{12}-J_{31}}\right|^2+1}}$$

$$D1 = \frac{1}{2}$$

$$D2 = \frac{\sqrt{J_{12}^2-J_{31}(J_{12}+J_{23})-J_{12}J_{23}+J_{23}^2+J_{31}^2}+J_{23}-J_{31}}{(J_{12}-J_{31})\left(\left|\frac{-J_{12}+J_{23}+\sqrt{J_{12}^2-J_{23}J_{12}+J_{23}^2+J_{31}^2-(J_{12}+J_{23})J_{31}}}{J_{12}-J_{31}}\right|^2+\left|\frac{J_{23}-J_{31}+\sqrt{J_{12}^2-J_{23}J_{12}+J_{23}^2+J_{31}^2-(J_{12}+J_{23})J_{31}}}{J_{12}-J_{31}}\right|^2+1\right)}$$

$$E = \frac{2\left(\sqrt{J_{12}^2-J_{31}(J_{12}+J_{23})-J_{12}J_{23}+J_{23}^2+J_{31}^2}-J_{12}+J_{23}\right)}{(J_{12}-J_{31})\sqrt{\left|\frac{-J_{12}+J_{23}+\sqrt{J_{12}^2-J_{23}J_{12}+J_{23}^2+J_{31}^2-(J_{12}+J_{23})J_{31}}}{J_{12}-J_{31}}\right|^2+\left|\frac{J_{23}-J_{31}+\sqrt{J_{12}^2-J_{23}J_{12}+J_{23}^2+J_{31}^2-(J_{12}+J_{23})J_{31}}}{J_{12}-J_{31}}\right|^2+1}} \quad (C.1)$$

$$
\begin{aligned}
F &= \frac{2}{\sqrt{\left|\frac{-J_{12}+J_{23}+\sqrt{J_{12}^2-J_{23}J_{12}+J_{23}^2+J_{31}^2-(J_{12}+J_{23})J_{31}}}{J_{12}-J_{31}}\right|^2+\left|\frac{J_{23}-J_{31}+\sqrt{J_{12}^2-J_{23}J_{12}+J_{23}^2+J_{31}^2-(J_{12}+J_{23})J_{31}}}{J_{12}-J_{31}}\right|^2+1}} \\
G1 &= 1 \\
G2 &= \frac{2J_{31}\left(J_{31}-\sqrt{J_{12}^2-J_{31}(J_{12}+J_{23})-J_{12}J_{23}+J_{23}^2+J_{31}^2}\right)+J_{23}\left(2\sqrt{J_{12}^2-J_{31}(J_{12}+J_{23})-J_{12}J_{23}+J_{23}^2+J_{31}^2}-3J_{31}\right)+J_{12}^2-J_{12}(J_{23}+J_{31})+2J_{23}^2}{(J_{12}-J_{31})^2\left(\left|\frac{-J_{12}+J_{23}+\sqrt{J_{12}^2-J_{23}J_{12}+J_{23}^2+J_{31}^2-(J_{12}+J_{23})J_{31}}}{J_{12}-J_{31}}\right|^2+\left|\frac{J_{23}-J_{31}+\sqrt{J_{12}^2-J_{23}J_{12}+J_{23}^2+J_{31}^2-(J_{12}+J_{23})J_{31}}}{J_{12}-J_{31}}\right|^2+1\right)} \\
H1 &= 1 \\
H2 &= -\frac{(J_{12}+J_{23}-2J_{31})\left(-2\sqrt{J_{12}^2-J_{31}(J_{12}+J_{23})-J_{12}J_{23}+J_{23}^2+J_{31}^2}+J_{12}-2J_{23}+J_{31}\right)}{(J_{12}-J_{31})^2\left(\left|\frac{-J_{12}+J_{23}+\sqrt{J_{12}^2-J_{23}J_{12}+J_{23}^2+J_{31}^2-(J_{12}+J_{23})J_{31}}}{J_{12}-J_{31}}\right|^2+\left|\frac{J_{23}-J_{31}+\sqrt{J_{12}^2-J_{23}J_{12}+J_{23}^2+J_{31}^2-(J_{12}+J_{23})J_{31}}}{J_{12}-J_{31}}\right|^2+1\right)}
\end{aligned}
\tag{C.2}
$$

Rewriting the low-energy Hamiltonian (4.4) as in (4.7), i.e.

$$
\begin{aligned}
H = \sum_{\alpha,\alpha',k,k'} \Big[ & J^{+}_{\alpha'\alpha}\tau^{+}c^{\dagger}_{\alpha'k'\downarrow}c_{\alpha k\uparrow} + J^{-}_{\alpha'\alpha}\tau^{-}c^{\dagger}_{\alpha'k'\uparrow}c_{\alpha k\downarrow} + J^{z\uparrow}_{\alpha'\alpha}\tau^{z}c^{\dagger}_{\alpha'k'\uparrow}c_{\alpha k\uparrow} + J^{z\downarrow}_{\alpha'\alpha}\tau^{z}c^{\dagger}_{\alpha'k'\downarrow}c_{\alpha k\downarrow} \\
& + J^{0\uparrow}_{\alpha'\alpha}\tau^{0}c^{\dagger}_{\alpha'k'\uparrow}c_{\alpha k\uparrow} + J^{0\downarrow}_{\alpha'\alpha}\tau^{0}c^{\dagger}_{\alpha'k'\downarrow}c_{\alpha k\downarrow} \Big],
\end{aligned}
\tag{C.3}
$$

the following constants have implicitly been defined:

$$
\begin{aligned}
J^{z\uparrow}_{LL}(\ln(D_0)) &= \frac{J_L(1/2-B)}{2}\\
J^{0\uparrow}_{LL}(\ln(D_0)) &= \frac{J_L(1/2+B)}{2}+\frac{W_L}{2}\\
J^{+}_{LL}(\ln(D_0)) &= \frac{J_L A}{2}\\
J^{-}_{LL}(\ln(D_0)) &= \frac{J_L A}{2}\\
J^{z\downarrow}_{LL}(\ln(D_0)) &= \frac{J_L(B-1/2)}{2}\\
J^{0\downarrow}_{LL}(\ln(D_0)) &= -\frac{J_L(1/2+B)}{2}+\frac{W_L}{2}\\
J^{z\uparrow}_{RR}(\ln(D_0)) &= \frac{J_R(1/2-D)}{2}\\
J^{0\uparrow}_{RR}(\ln(D_0)) &= \frac{J_R(1/2+D)}{2}+\frac{W_R}{2}\\
J^{+}_{RR}(\ln(D_0)) &= \frac{J_R C}{2}\\
J^{-}_{RR}(\ln(D_0)) &= \frac{J_R C}{2}\\
J^{z\downarrow}_{RR}(\ln(D_0)) &= \frac{J_R(D-1/2)}{2}\\
J^{0\downarrow}_{RR}(\ln(D_0)) &= -\frac{J_R(1/2+D)}{2}+\frac{W_R}{2}\\
J^{z\uparrow}_{RL}(\ln(D_0)) &= \frac{J_{RL}(1-G)+W_{RL}(1-H)}{4}\\
J^{0\uparrow}_{RL}(\ln(D_0)) &= \frac{J_{RL}(1+G)+W_{RL}(1+H)}{4}\\
J^{+}_{RL}(\ln(D_0)) &= \frac{J_{RL} E}{4}\\
J^{-}_{RL}(\ln(D_0)) &= \frac{J_{RL} F}{4}\\
J^{z\downarrow}_{RL}(\ln(D_0)) &= \frac{-J_{RL}(1-G)+W_{RL}(1-H)}{4}\\
J^{0\downarrow}_{RL}(\ln(D_0)) &= \frac{-J_{RL}(1+G)+W_{RL}(1+H)}{4}\\
J^{z\uparrow}_{LR}(\ln(D_0)) &= \frac{J_{LR}(1-G)+W_{LR}(1-H)}{4}\\
J^{0\uparrow}_{LR}(\ln(D_0)) &= \frac{J_{LR}(1+G)+W_{LR}(1+H)}{4}\\
J^{+}_{LR}(\ln(D_0)) &= \frac{J_{LR} F}{4}\\
J^{-}_{LR}(\ln(D_0)) &= \frac{J_{LR} E}{4}\\
J^{z\downarrow}_{LR}(\ln(D_0)) &= \frac{-J_{LR}(1-G)+W_{LR}(1-H)}{4}\\
J^{0\downarrow}_{LR}(\ln(D_0)) &= \frac{-J_{LR}(1+G)+W_{LR}(1+H)}{4}
\end{aligned}
\tag{C.4}
$$

## C.2. Coefficients of the low-energy Hamiltonian for $B = 0$

$$
\begin{aligned}
A = {} & \Big(2\Big(J_{12}^3(J_{23}-J_{31}) + J_{12}^2\Big(J_{23}\Big(\sqrt{J_{12}^2 - J_{31}(J_{12}+J_{23}) - J_{12}J_{23} + J_{23}^2 + J_{31}^2} - J_{31}\Big) - J_{31}\sqrt{J_{12}^2 - J_{31}(J_{12}+J_{23}) - J_{12}J_{23} + J_{23}^2 + J_{31}^2}\Big) \\
& + J_{12}J_{23}\Big(J_{23}\Big(\sqrt{J_{12}^2 - J_{31}(J_{12}+J_{23}) - J_{12}J_{23} + J_{23}^2 + J_{31}^2} - J_{31}\Big) + J_{23}^2 + 2J_{31}^2\Big) \\
& - J_{23}^2 J_{31}\Big(\sqrt{J_{12}^2 - J_{31}(J_{12}+J_{23}) - J_{12}J_{23} + J_{23}^2 + J_{31}^2} + J_{23}\Big)\Big)\Big) \Big/ \Big(\Big(J_{23}J_{31} - J_{12}\Big(\sqrt{J_{12}^2 - J_{12}(J_{23}+J_{31}) + J_{23}^2 - J_{23}J_{31} + J_{31}^2} + J_{12}\Big)\Big)^2 \\
& \surd\Bigg(\Bigg(\Bigg|\frac{-J_{12}+J_{23}+\sqrt{J_{12}^2 - J_{23}J_{12} + J_{23}^2 + J_{31}^2 - (J_{12}+J_{23})J_{31}}}{J_{12}-J_{31}}\Bigg|^2 + \Bigg|\frac{J_{23}-J_{31}+\sqrt{J_{12}^2 - J_{23}J_{12} + J_{23}^2 + J_{31}^2 - (J_{12}+J_{23})J_{31}}}{J_{12}-J_{31}}\Bigg|^2 + 1\Bigg) \\
& \Bigg(\Bigg|\frac{-J_{12}+J_{31}+\sqrt{J_{12}^2 - J_{23}J_{12} + J_{23}^2 + J_{31}^2 - (J_{12}+J_{23})J_{31}}}{J_{12}-J_{23}}\Bigg|^2 + \Bigg|\frac{-J_{23}+J_{31}+\sqrt{J_{12}^2 - J_{23}J_{12} + J_{23}^2 + J_{31}^2 - (J_{12}+J_{23})J_{31}}}{J_{12}-J_{23}}\Bigg|^2 + 1\Bigg)\Bigg)\Bigg)
\end{aligned}
$$

$$
B1 = \frac{-J_{12}\Big(\sqrt{J_{12}^2 - J_{31}(J_{12}+J_{23}) - J_{12}J_{23} + J_{23}^2 + J_{31}^2} + 2J_{23}\Big) + J_{31}\Big(J_{31} - \sqrt{J_{12}^2 - J_{31}(J_{12}+J_{23}) - J_{12}J_{23} + J_{23}^2 + J_{31}^2}\Big) + 2J_{23}\Big(\sqrt{J_{12}^2 - J_{31}(J_{12}+J_{23}) - J_{12}J_{23} + J_{23}^2 + J_{31}^2} - J_{31}\Big) + J_{12}^2 + 2J_{23}^2}{(J_{12}-J_{31})^2\Bigg(\Bigg|\frac{-J_{12}+J_{23}+\sqrt{J_{12}^2 - J_{23}J_{12} + J_{23}^2 + J_{31}^2 - (J_{12}+J_{23})J_{31}}}{J_{12}-J_{31}}\Bigg|^2 + \Bigg|\frac{J_{23}-J_{31}+\sqrt{J_{12}^2 - J_{23}J_{12} + J_{23}^2 + J_{31}^2 - (J_{12}+J_{23})J_{31}}}{J_{12}-J_{31}}\Bigg|^2 + 1\Bigg)}
$$

$$
B2 = \frac{\sqrt{J_{12}^2 - J_{31}(J_{12}+J_{23}) - J_{12}J_{23} + J_{23}^2 + J_{31}^2} - J_{12} + J_{31}}{(J_{12}-J_{23})\Bigg(\Bigg|\frac{-J_{12}+J_{31}+\sqrt{J_{12}^2 - J_{23}J_{12} + J_{23}^2 + J_{31}^2 - (J_{12}+J_{23})J_{31}}}{J_{12}-J_{23}}\Bigg|^2 + \Bigg|\frac{-J_{23}+J_{31}+\sqrt{J_{12}^2 - J_{23}J_{12} + J_{23}^2 + J_{31}^2 - (J_{12}+J_{23})J_{31}}}{J_{12}-J_{23}}\Bigg|^2 + 1\Bigg)}
$$

$$
\begin{aligned}
C = 2/ & \Bigg[\surd\Bigg(\Bigg(\Bigg|\frac{-J_{12}+J_{23}+\sqrt{J_{12}^2 - J_{23}J_{12} + J_{23}^2 + J_{31}^2 - (J_{12}+J_{23})J_{31}}}{J_{12}-J_{31}}\Bigg|^2 + \Bigg|\frac{J_{23}-J_{31}+\sqrt{J_{12}^2 - J_{23}J_{12} + J_{23}^2 + J_{31}^2 - (J_{12}+J_{23})J_{31}}}{J_{12}-J_{31}}\Bigg|^2 + 1\Bigg) \\
& \Bigg(\Bigg|\frac{-J_{12}+J_{31}+\sqrt{J_{12}^2 - J_{23}J_{12} + J_{23}^2 + J_{31}^2 - (J_{12}+J_{23})J_{31}}}{J_{12}-J_{23}}\Bigg|^2 + \Bigg|\frac{-J_{23}+J_{31}+\sqrt{J_{12}^2 - J_{23}J_{12} + J_{23}^2 + J_{31}^2 - (J_{12}+J_{23})J_{31}}}{J_{12}-J_{23}}\Bigg|^2 + 1\Bigg)\Bigg)\Bigg]
\end{aligned}
$$

$$
D1 = \frac{\sqrt{J_{12}^2 - J_{31}(J_{12}+J_{23}) - J_{12}J_{23} + J_{23}^2 + J_{31}^2} + J_{23} - J_{31}}{(J_{12}-J_{31})\Bigg(\Bigg|\frac{-J_{12}+J_{23}+\sqrt{J_{12}^2 - J_{23}J_{12} + J_{23}^2 + J_{31}^2 - (J_{12}+J_{23})J_{31}}}{J_{12}-J_{31}}\Bigg|^2 + \Bigg|\frac{J_{23}-J_{31}+\sqrt{J_{12}^2 - J_{23}J_{12} + J_{23}^2 + J_{31}^2 - (J_{12}+J_{23})J_{31}}}{J_{12}-J_{31}}\Bigg|^2 + 1\Bigg)}
$$

$$
D2 = -\frac{\sqrt{J_{12}^2 - J_{31}(J_{12}+J_{23}) - J_{12}J_{23} + J_{23}^2 + J_{31}^2} - J_{23} + J_{31}}{(J_{12}-J_{23})\Bigg(\Bigg|\frac{-J_{12}+J_{31}+\sqrt{J_{12}^2 - J_{23}J_{12} + J_{23}^2 + J_{31}^2 - (J_{12}+J_{23})J_{31}}}{J_{12}-J_{23}}\Bigg|^2 + \Bigg|\frac{-J_{23}+J_{31}+\sqrt{J_{12}^2 - J_{23}J_{12} + J_{23}^2 + J_{31}^2 - (J_{12}+J_{23})J_{31}}}{J_{12}-J_{23}}\Bigg|^2 + 1\Bigg)}
$$

$$
\begin{aligned}
E = {} & \Big(2\Big(2J_{12}^4 + J_{12}^2\Big(J_{23}\Big(\sqrt{J_{12}^2 - J_{31}(J_{12}+J_{23}) - J_{12}J_{23} + J_{23}^2 + J_{31}^2} - 4J_{31}\Big) + J_{31}\Big(J_{31} - \sqrt{J_{12}^2 - J_{31}(J_{12}+J_{23}) - J_{12}J_{23} + J_{23}^2 + J_{31}^2}\Big) + J_{23}^2\Big) \\
& + J_{12}J_{23}\Big(J_{23}\Big(\sqrt{J_{12}^2 - J_{31}(J_{12}+J_{23}) - J_{12}J_{23} + J_{23}^2 + J_{31}^2} - J_{31}\Big) + 2J_{31}\Big(J_{31} - \sqrt{J_{12}^2 - J_{31}(J_{12}+J_{23}) - J_{12}J_{23} + J_{23}^2 + J_{31}^2}\Big) + J_{23}^2\Big) \\
& - J_{23}^2 J_{31}\Big(\sqrt{J_{12}^2 - J_{31}(J_{12}+J_{23}) - J_{12}J_{23} + J_{23}^2 + J_{31}^2} + J_{23} - J_{31}\Big) + 2J_{12}^3\Big(\sqrt{J_{12}^2 - J_{31}(J_{12}+J_{23}) - J_{12}J_{23} + J_{23}^2 + J_{31}^2} - J_{31}\Big)\Big)\Big) \\
& \Big/\Big(\Big(J_{23}J_{31} - J_{12}\Big(\sqrt{J_{12}^2 - J_{12}(J_{23}+J_{31}) + J_{23}^2 - J_{23}J_{31} + J_{31}^2} + J_{12}\Big)\Big)^2 \\
& \surd\Bigg(\Bigg(\Bigg|\frac{-J_{12}+J_{23}+\sqrt{J_{12}^2 - J_{23}J_{12} + J_{23}^2 + J_{31}^2 - (J_{12}+J_{23})J_{31}}}{J_{12}-J_{31}}\Bigg|^2 + \Bigg|\frac{J_{23}-J_{31}+\sqrt{J_{12}^2 - J_{23}J_{12} + J_{23}^2 + J_{31}^2 - (J_{12}+J_{23})J_{31}}}{J_{12}-J_{31}}\Bigg|^2 + 1\Bigg) \\
& \Bigg(\Bigg|\frac{-J_{12}+J_{31}+\sqrt{J_{12}^2 - J_{23}J_{12} + J_{23}^2 + J_{31}^2 - (J_{12}+J_{23})J_{31}}}{J_{12}-J_{23}}\Bigg|^2 + \Bigg|\frac{-J_{23}+J_{31}+\sqrt{J_{12}^2 - J_{23}J_{12} + J_{23}^2 + J_{31}^2 - (J_{12}+J_{23})J_{31}}}{J_{12}-J_{23}}\Bigg|^2 + 1\Bigg)\Bigg)\Bigg)
\end{aligned}
$$

$$
\begin{aligned}
F &= E \\
G1 &= \frac{2J_{31}\left(J_{31}-\sqrt{J_{12}^2-J_{31}(J_{12}+J_{23})-J_{12}J_{23}+J_{23}^2+J_{31}^2}\right)+J_{23}\left(2\sqrt{J_{12}^2-J_{31}(J_{12}+J_{23})-J_{12}J_{23}+J_{23}^2+J_{31}^2}-3J_{31}\right)+J_{12}^2-J_{12}(J_{23}+J_{31})+2J_{23}^2}{(J_{12}-J_{31})^2\left(\left|\frac{-J_{12}+J_{23}+\sqrt{J_{12}^2-J_{23}J_{12}+J_{23}^2+J_{31}^2-(J_{12}+J_{23})J_{31}}}{J_{12}-J_{31}}\right|^2+\left|\frac{J_{23}-J_{31}+\sqrt{J_{12}^2-J_{23}J_{12}+J_{23}^2+J_{31}^2-(J_{12}+J_{23})J_{31}}}{J_{12}-J_{31}}\right|^2+1\right)} \\
G2 &= -\frac{1}{\left|\frac{-J_{12}+J_{31}+\sqrt{J_{12}^2-J_{23}J_{12}+J_{23}^2+J_{31}^2-(J_{12}+J_{23})J_{31}}}{J_{12}-J_{23}}\right|^2+\left|\frac{-J_{23}+J_{31}+\sqrt{J_{12}^2-J_{23}J_{12}+J_{23}^2+J_{31}^2-(J_{12}+J_{23})J_{31}}}{J_{12}-J_{23}}\right|^2+1} \\
H1 &= -\frac{(J_{12}+J_{23}-2J_{31})\left(-2\sqrt{J_{12}^2-J_{31}(J_{12}+J_{23})-J_{12}J_{23}+J_{23}^2+J_{31}^2}+J_{12}-2J_{23}+J_{31}\right)}{(J_{12}-J_{31})^2\left(\left|\frac{-J_{12}+J_{23}+\sqrt{J_{12}^2-J_{23}J_{12}+J_{23}^2+J_{31}^2-(J_{12}+J_{23})J_{31}}}{J_{12}-J_{31}}\right|^2+\left|\frac{J_{23}-J_{31}+\sqrt{J_{12}^2-J_{23}J_{12}+J_{23}^2+J_{31}^2-(J_{12}+J_{23})J_{31}}}{J_{12}-J_{31}}\right|^2+1\right)} \\
H2 &= -\frac{(J_{12}+J_{23}-2J_{31})\left(-2\left(\sqrt{J_{12}^2-J_{31}(J_{12}+J_{23})-J_{12}J_{23}+J_{23}^2+J_{31}^2}+J_{31}\right)+J_{12}+J_{23}\right)}{(J_{12}-J_{23})^2\left(\left|\frac{-J_{12}+J_{31}+\sqrt{J_{12}^2-J_{23}J_{12}+J_{23}^2+J_{31}^2-(J_{12}+J_{23})J_{31}}}{J_{12}-J_{23}}\right|^2+\left|\frac{-J_{23}+J_{31}+\sqrt{J_{12}^2-J_{23}J_{12}+J_{23}^2+J_{31}^2-(J_{12}+J_{23})J_{31}}}{J_{12}-J_{23}}\right|^2+1\right)}
\end{aligned}
\tag{C.5}
$$

Rewriting the low-energy Hamiltonian (??) as in (4.7), i.e.

$$
\begin{aligned}
H = \sum_{\alpha,\alpha',k,k'} \Big[ & J^{+}_{\alpha'\alpha}\tau^{+}c^{\dagger}_{\alpha'k'\downarrow}c_{\alpha k\uparrow} + J^{-}_{\alpha'\alpha}\tau^{-}c^{\dagger}_{\alpha'k'\uparrow}c_{\alpha k\downarrow} + J^{z\uparrow}_{\alpha'\alpha}\tau^{z}c^{\dagger}_{\alpha'k'\uparrow}c_{\alpha k\uparrow} + J^{z\downarrow}_{\alpha'\alpha}\tau^{z}c^{\dagger}_{\alpha'k'\downarrow}c_{\alpha k\downarrow} \\
& + J^{0\uparrow}_{\alpha'\alpha}\tau^{0}c^{\dagger}_{\alpha'k'\uparrow}c_{\alpha k\uparrow} + J^{0\downarrow}_{\alpha'\alpha}\tau^{0}c^{\dagger}_{\alpha'k'\downarrow}c_{\alpha k\downarrow}\Big],
\end{aligned}
\tag{C.6}
$$

the following constants have implicitly been defined:

$$
\begin{aligned}
J^{z\uparrow}_{LL}(\ln(D_0)) &= \frac{J_L(B1-B2)}{2}\\
J^{0\uparrow}_{LL}(\ln(D_0)) &= \frac{J_L(B1+B2)}{2}+\frac{W_L}{2}\\
J^{+}_{LL}(\ln(D_0)) &= \frac{J_L A}{2}\\
J^{-}_{LL}(\ln(D_0)) &= \frac{J_L A}{2}\\
J^{z\downarrow}_{LL}(\ln(D_0)) &= \frac{J_L(B2-B1)}{2}\\
J^{0\downarrow}_{LL}(\ln(D_0)) &= -\frac{J_L(B1+B2)}{2}+\frac{W_L}{2}\\
J^{z\uparrow}_{RR}(\ln(D_0)) &= \frac{J_R(D1-D2)}{2}\\
J^{0\uparrow}_{RR}(\ln(D_0)) &= \frac{J_R(D1+D2)}{2}+\frac{W_R}{2}\\
J^{+}_{RR}(\ln(D_0)) &= \frac{J_R C}{2}\\
J^{-}_{RR}(\ln(D_0)) &= \frac{J_R C}{2}\\
J^{z\downarrow}_{RR}(\ln(D_0)) &= \frac{J_R(D2-D1)}{2}\\
J^{0\downarrow}_{RR}(\ln(D_0)) &= -\frac{J_R(D1+D2)}{2}+\frac{W_R}{2}\\
J^{z\uparrow}_{RL}(\ln(D_0)) &= \frac{J_{RL}(G1-G2)+W_{RL}(H1-H2)}{4}\\
J^{0\uparrow}_{RL}(\ln(D_0)) &= \frac{J_{RL}(G1+G2)+W_{RL}(H1+H2)}{4}\\
J^{+}_{RL}(\ln(D_0)) &= \frac{J_{RL}E}{4}\\
J^{-}_{RL}(\ln(D_0)) &= \frac{J_{RL}F}{4}\\
J^{z\downarrow}_{RL}(\ln(D_0)) &= \frac{-J_{RL}(G1-G2)+W_{RL}(H1-H2)}{4}\\
J^{0\downarrow}_{RL}(\ln(D_0)) &= \frac{-J_{RL}(G1+G2)+W_{RL}(H1+H2)}{4}\\
J^{z\uparrow}_{LR}(\ln(D_0)) &= \frac{J_{LR}(G1-G2)+W_{LR}(H1-H2)}{4}\\
J^{0\uparrow}_{LR}(\ln(D_0)) &= \frac{J_{LR}(G1+G2)+W_{LR}(H1+H2)}{4}\\
J^{+}_{LR}(\ln(D_0)) &= \frac{J_{LR}F}{4}\\
J^{-}_{LR}(\ln(D_0)) &= \frac{J_{LR}E}{4}\\
J^{z\downarrow}_{LR}(\ln(D_0)) &= \frac{-J_{LR}(G1-G2)+W_{LR}(H1-H2)}{4}\\
J^{0\downarrow}_{LR}(\ln(D_0)) &= \frac{-J_{LR}(G1+G2)+W_{LR}(H1+H2)}{4}
\end{aligned}
\tag{C.7}
$$

# D. Calculations regarding the Poor man's scaling equations for the completely anisotropic Kondo model

In this appendix we write in detail the steps needed to go from (4.17) to the scaling equations (D.4).
We use the following relations:

$$\begin{aligned}
&\tau^+\tau^- = 2(\tau^0 + \tau^z)\\
&\tau^-\tau^+ = 2(\tau^0 - \tau^z)\\
&\tau^+\tau^z = -\tau^z\tau^+ = -\tau^+\\
&\tau^-\tau^z = -\tau^z\tau^- = \tau^-\\
&\tau^z\tau^z = \tau^0
\end{aligned} \tag{D.1}$$

in order to rewrite the terms appearing in (4.17), which thus look as follows:

$$\begin{aligned}
&H_{10}(E-H_{00})^{-1}H_{01} =\\
&\quad\sum_{\beta q\sigma}\{\left[\left(2J^+_{\alpha'\beta}J^-_{\beta\alpha} + J^{z\uparrow}_{\alpha'\beta}J^{0\uparrow}_{\beta\alpha} + J^{0\uparrow}_{\alpha'\beta}J^{z\uparrow}_{\beta\alpha}\right)\tau^z + \left(2J^+_{\alpha'\beta}J^-_{\beta\alpha} + J^{z\uparrow}_{\alpha'\beta}J^{z\uparrow}_{\beta\alpha} + J^{0\uparrow}_{\alpha'\beta}J^{0\uparrow}_{\beta\alpha}\right)\tau^0\right]c_{\alpha'k'\uparrow}c^\dagger_{\alpha k\uparrow}\\
&\quad+\left[-J^+_{\alpha'\beta}J^{z\downarrow}_{\beta\alpha} + J^+_{\alpha'\beta}J^{0\downarrow}_{\beta\alpha} + J^{z\uparrow}_{\alpha'\beta}J^+_{\beta\alpha} + J^{0\uparrow}_{\alpha'\beta}J^+_{\beta\alpha}\right]\tau^+c_{\alpha'k'\uparrow}c^\dagger_{\alpha k\downarrow}\\
&\quad+\left[J^-_{\alpha'\beta}J^{z\uparrow}_{\beta\alpha} + J^-_{\alpha'\beta}J^{0\uparrow}_{\beta\alpha} - J^{z\downarrow}_{\alpha'\beta}J^-_{\beta\alpha} + J^{0\downarrow}_{\alpha'\beta}J^-_{\beta\alpha}\right]\tau^-c_{\alpha'k'\downarrow}c^\dagger_{\alpha k\uparrow}\\
&\quad+\left[\left(-2J^-_{\alpha'\beta}J^+_{\beta\alpha} + J^{0\downarrow}_{\alpha'\beta}J^{z\downarrow}_{\beta\alpha} + J^{0\downarrow}_{\alpha'\beta}J^{z\uparrow}_{\beta\alpha}\right)\tau^z + \left(2J^-_{\alpha'\beta}J^+_{\beta\alpha} + J^{z\downarrow}_{\alpha'\beta}J^{z\downarrow}_{\beta\alpha} + J^{0\downarrow}_{\alpha'\beta}J^{0\downarrow}_{\beta\alpha}\right)\tau^0\right]c_{\alpha'k'\downarrow}c^\dagger_{\alpha k\downarrow}\\
&\quad\}n_{\beta q\sigma}(E-D+\varepsilon_{k'})^{-1}\\
&H_{12}(E-H_{22})^{-1}H_{21} =\\
&\quad\sum_{\beta q\sigma}\{\left[\left(-2J^-_{\alpha'\beta}J^+_{\beta\alpha} + J^{z\uparrow}_{\alpha'\beta}J^{0\uparrow}_{\beta\alpha} + J^{0\uparrow}_{\alpha'\beta}J^{z\uparrow}_{\beta\alpha}\right)\tau^z + \left(2J^-_{\alpha'\beta}J^+_{\beta\alpha} + J^{z\uparrow}_{\alpha'\beta}J^{z\uparrow}_{\beta\alpha} + J^{0\uparrow}_{\alpha'\beta}J^{0\uparrow}_{\beta\alpha}\right)\tau^0\right]c^\dagger_{\alpha'k'\uparrow}c_{\alpha k\uparrow}\\
&\quad+\left[-J^+_{\alpha'\beta}J^{z\uparrow}_{\beta\alpha} + J^+_{\alpha'\beta}J^{0\uparrow}_{\beta\alpha} + J^{z\downarrow}_{\alpha'\beta}J^+_{\beta\alpha} + J^{0\downarrow}_{\alpha'\beta}J^+_{\beta\alpha}\right]\tau^+c^\dagger_{\alpha'k'\downarrow}c_{\alpha k\uparrow}\\
&\quad+\left[J^-_{\alpha'\beta}J^{z\downarrow}_{\beta\alpha} + J^-_{\alpha'\beta}J^{0\downarrow}_{\beta\alpha} - J^{z\uparrow}_{\alpha'\beta}J^-_{\beta\alpha} + J^{0\uparrow}_{\alpha'\beta}J^-_{\beta\alpha}\right]\tau^-c^\dagger_{\alpha'k'\uparrow}c_{\alpha k\uparrow}\\
&\quad+\left[\left(2J^+_{\alpha'\beta}J^-_{\beta\alpha} + J^{0\downarrow}_{\alpha'\beta}J^{z\downarrow}_{\beta\alpha} + J^{z\downarrow}_{\alpha'\beta}J^{0\downarrow}_{\beta\alpha}\right)\tau^z + \left(2J^+_{\alpha'\beta}J^-_{\beta\alpha} + J^{z\downarrow}_{\alpha'\beta}J^{z\downarrow}_{\beta\alpha} + J^{0\downarrow}_{\alpha'\beta}J^{0\downarrow}_{\beta\alpha}\right)\tau^0\right]c^\dagger_{\alpha'k'\downarrow}c_{\alpha k\downarrow}\\
&\quad\}(1-n_{\beta q\sigma})(E-D-\varepsilon_k)^{-1}.
\end{aligned} \tag{D.2}$$

Plugging these expressions into (4.17), one obtains an Hamiltonian that looks just like (4.13) but has renormalized couplings $J \to J + \delta J$ where $\delta J$ is given by:

$$\begin{aligned}
\delta J^{z\uparrow}_{\alpha'\alpha} &= \Bigg[-2J^{+}_{\alpha'\beta}J^{-}_{\beta\alpha}\left(\frac{1}{E-D+\varepsilon_{k'}}+\frac{1}{E-D-\varepsilon_k}\right)\\
&\quad+\left(J^{z\uparrow}_{\alpha'\beta}J^{0\uparrow}_{\beta\alpha}+J^{0\uparrow}_{\alpha'\beta}J^{z\uparrow}_{\beta\alpha}\right)\left(-\frac{1}{E-D+\varepsilon_{k'}}+\frac{1}{E-D-\varepsilon_k}\right)\Bigg]\rho_0|\delta D|\\
\delta J^{0\uparrow}_{\alpha'\alpha} &= \left[\left(-2J^{+}_{\alpha'\beta}J^{-}_{\beta\alpha}+J^{z\uparrow}_{\alpha'\beta}J^{z\uparrow}_{\beta\alpha}+J^{0\uparrow}_{\alpha'\beta}J^{0\uparrow}_{\beta\alpha}\right)\left(-\frac{1}{E-D+\varepsilon_{k'}}+\frac{1}{E-D-\varepsilon_k}\right)\right]\rho_0|\delta D|\\
\delta J^{+}_{\alpha'\alpha} &= \Bigg[\left(-J^{z\uparrow}_{\alpha'\beta}J^{+}_{\beta\alpha}+J^{+}_{\alpha'\beta}J^{z\downarrow}_{\beta\alpha}\right)\left(\frac{1}{E-D+\varepsilon_{k'}}+\frac{1}{E-D-\varepsilon_k}\right)\\
&\quad+\left(J^{+}_{\alpha'\beta}J^{0\downarrow}_{\beta\alpha}+J^{0\uparrow}_{\alpha'\beta}J^{+}_{\beta\alpha}\right)\left(-\frac{1}{E-D+\varepsilon_{k'}}+\frac{1}{E-D-\varepsilon_k}\right)\Bigg]\rho_0|\delta D|\\
\delta J^{-}_{\alpha'\alpha} &= \Bigg[\left(J^{z\downarrow}_{\alpha'\beta}J^{-}_{\beta\alpha}-J^{-}_{\alpha'\beta}J^{z\uparrow}_{\beta\alpha}\right)\left(\frac{1}{E-D+\varepsilon_{k'}}+\frac{1}{E-D-\varepsilon_k}\right)\\
&\quad+\left(J^{-}_{\alpha'\beta}J^{0\uparrow}_{\beta\alpha}+J^{0\downarrow}_{\alpha'\beta}J^{-}_{\beta\alpha}\right)\left(-\frac{1}{E-D+\varepsilon_{k'}}+\frac{1}{E-D-\varepsilon_k}\right)\Bigg]\rho_0|\delta D|\\
\delta J^{z\downarrow}_{\alpha'\alpha} &= \Bigg[2J^{-}_{\alpha'\beta}J^{+}_{\beta\alpha}\left(\frac{1}{E-D+\varepsilon_{k'}}+\frac{1}{E-D-\varepsilon_k}\right)\\
&\quad+\left(J^{z\downarrow}_{\alpha'\beta}J^{0\downarrow}_{\beta\alpha}+J^{0\downarrow}_{\alpha'\beta}J^{z\downarrow}_{\beta\alpha}\right)\left(-\frac{1}{E-D+\varepsilon_{k'}}+\frac{1}{E-D-\varepsilon_k}\right)\Bigg]\rho_0|\delta D|\\
\delta J^{0\uparrow}_{\alpha'\alpha} &= \left[\left(2J^{-}_{\alpha'\beta}J^{+}_{\beta\alpha}+J^{z\downarrow}_{\alpha'\beta}J^{z\downarrow}_{\beta\alpha}+J^{0\downarrow}_{\alpha'\beta}J^{0\downarrow}_{\beta\alpha}\right)\left(-\frac{1}{E-D+\varepsilon_{k'}}+\frac{1}{E-D-\varepsilon_k}\right)\right]\rho_0|\delta D|. \qquad \text{(D.3)}
\end{aligned}$$

By gradually eliminating virtual transitions to states at the edges of the bandwidth of the leads, our model Hamiltonian can be rewritten in the same form (4.13), but the coupling coefficients are scaled depending on the width of the elimated band edges.
When dropping $E, \varepsilon_k, \varepsilon_{k'}$ (which can be assumed to be small), (D.3) give the following scaling equations:

$$\begin{aligned}
\frac{dJ^{z\uparrow}_{\alpha'\alpha}}{d\ln D} &= -4J^{+}_{\alpha'\beta}J^{-}_{\beta\alpha}\rho_0\\
\frac{dJ^{0\uparrow}_{\alpha'\alpha}}{d\ln D} &= 0\\
\frac{dJ^{+}_{\alpha'\alpha}}{d\ln D} &= 2\left(-J^{z\uparrow}_{\alpha'\beta}J^{+}_{\beta\alpha}+J^{+}_{\alpha'\beta}J^{z\downarrow}_{\beta\alpha}\right)\rho_0\\
\frac{dJ^{-}_{\alpha'\alpha}}{d\ln D} &= 2\left(J^{z\downarrow}_{\alpha'\beta}J^{-}_{\beta\alpha}-J^{-}_{\alpha'\beta}J^{z\uparrow}_{\beta\alpha}\right)\rho_0\\
\frac{dJ^{z\downarrow}_{\alpha'\alpha}}{d\ln D} &= 4J^{-}_{\alpha'\beta}J^{+}_{\beta\alpha}\rho_0\\
\frac{dJ^{0\uparrow}_{\alpha'\alpha}}{d\ln D} &= 0. \qquad \text{(D.4)}
\end{aligned}$$

# Bibliography


[1] G. Begemann, S. Koller, M. Grifoni and J. Paaske, Phys. Rev. B **82**, 045316 (2010)

[2] A. C. Hewson, *The Kondo problem to heavy Fermions* (Cambridge University Press, Cambridge, 1993)

[3] A. Messiah, *Quantum Mechanics* (North-Holland publishing company, Amsterdam, 1961)

[4] R. Winkler, *Spin-orbit Coupling Effects in Two-Dimensional Electron and Hole Systems*(Springer Tracts in Modern Physics, Heidelberg, 2003)

[5] E. A. Osorio, K. Moth-Poulsen, H. S. J. van der Zant, J. Paaske, P. Hedegård, F. Flensberg, J. Bendix and T. Bjørnholm, Nano Letters **10**, 105 (2010)

[6] E. A. Osorio, K. O'Neill, M. Wegewijs, N. Stuhr-Hansen, J. Paaske, T. Bjørnholm and H. S. J. van der Zant, Nano Letters **7**, 3336 (2007)

[7] J. Paaske, A. Rosch, P. Wölfle, N. Mason, C. M. Marcus and J. Nygård, Nature Physics **2**, 460 (2006)

[8] E. Lörtscher, J. W. Ciszek, J. Tour, H. Riel, Small **2**, 973 (2006)

[9] C. Joachim, J. K. Gimzewski and A. Aviram, Nature **408**, 541 (2000)

[10] A. Nitzan and M. A. Ratner, Science **300**, 1384 (2003)

[11] H. B. Heersche, Z. de Groot, J. A. Folk, H. S. J. van der Zant, C. Romeike, M. R. Wegewijs, L. Zobbi, D. Barreca, E. Tondello and A. Cornia, Phys. Rev. Lett. **96**, 206801 (2006)

[12] M. H. Jo, J. E. Grose, K. Baheti, M. M. Deshmukh, J. J. Sokol, E. M. Rumberger, D. N. Hendrickson, J. R. Long, H. Park, D. C. Ralph, Nano Letters **6**, 2014 (2006)

[13] J. R. Schrieffer and P. A. Wolff, Phys. Rev. **149**, 491 (1966)

[14] Martin Leijnse, *Transport spectroscopy and control of molecular quantum dots* (PhD dissertetion, RWTH Aachen University, 2009)

[15] Verena Köerting, *Non-equilibrium electron transport through a double quantum dot system, study of two exchange coupled quantum dots in a 4-terminal geometry* (PhD dissertetion, Fakultät für Physik der Universität Karlsruhe, 2007)

[16] Kim Georg Lind Pedersen, *Poor man's scaling for the nonequilibrium Kondo problem and antiferromagnetic correlations in optical lattices*, (MSc thesis, København Universitet, 2009)

[17] Jens Paaske, *Cotunneling and Kondo effect in quantum dots* (lecture notes from the DPG Physics School 2010, Physikzentrum Bad Honnef, Germany)

[18] R.M. Potok, I.G. Rau, H. Shtrikman, Y. Oreg and D. Goldhaber-Gordon, Nature **446**, 167 (2007)